Investigation of the Thermophysical Properties of Building Enveloping Materials – Theoretical Approach and Experimental Implementation (Thermobox)

Master Thesis

Syed Adeeb Ahmed

At the

Albert-Ludwigs-Universität Freiburg

Submitted master thesis in accordance with the provisions of the examination regulations of the Albert-Ludwigs-University of Freiburg for the Master of Science (M.Sc.) degree in Sustainable Systems Engineering.

Thesis Duration

09.10.2019 – 14.05.2020

Examiners

Dr. Stefan Hess

Prof. Dr.-Ing. Jens Pfafferott

Supervisor

Beatrice Rodenbücher, M.Sc.

Declaration

I hereby declare that I am the sole author and composer of my thesis and that no other sources or learning aids, other than those listed have been used. Furthermore, I declare that I have acknowledged the work of others by providing detailed references to said work.

I hereby also declare that my thesis has not been prepared for another examination or assignment, either wholly or excerpts thereof.

Place, Date

Signature

Abstract

To achieve a climate-neutral building sector, it is imperative to improve the energy efficiency of buildings. To that extent, it becomes important to understand the thermophysical properties of building construction materials, especially building enveloping materials. In this thesis, a novel experimental setup (the Thermobox) is used to experimentally determine different thermophysical properties of seven measurement samples, constructed from four different building enveloping materials. To improve the thermal performance of the Thermobox, several modifications are performed on the device and their effects are observed. To improve the stability of the temperature inside the Thermobox, a PID controller is also developed and implemented. Steady-state measurements are performed on the measurement samples to experimentally calculate the thermal conductance and the thermal transmittance. The calculations are performed with the temperature method, and a heat flux sensor is later installed to develop an alternate steady-state calculation method. Further dynamic experiments are performed with the Thermobox on three selected measurement samples to determine the time lag and the decrement factor. From the time lags and the decrement factors of the samples, the thermal diffusivity, the specific heat capacity at constant pressure, and the thermal mass are calculated. The measurement results are then compared to the literature values. The results show that the estimation of the thermal conductance and the thermal transmittance from the steady-state measurements is quite accurate for MDF, MDF+PUR, UHPC and single glass. The results for UHPC+PUR are closer to the reference with the heat flux method than the temperature method. On the contrary, neither the temperature method nor the heat flux method is able to accurately estimate the thermal conductance of the samples with double glazing. The dynamic measurement results of MDF, UHPC and single glass have high deviations from the reference values and thus are considered unsatisfactory. In conclusion, the Thermobox can be used in the laboratory as a teaching tool on the experimental determination of several thermophysical properties of different building enveloping materials.

Acknowledgements

I would like to take this opportunity to show my gratitude to all the people who helped and supported me during this research work. I would like to cordially thank Dr. Stefan Hess and Prof. Dr.-Ing. Jens Pfafferott for taking the time to examine this thesis. I would also express my thanks to my supervisor Ms Beatrice Rodenbücher, who supervised my work during this thesis and guided me through all the steps with her valuable advice. I would also thank Mr Thomas Schmidt (exergia) for designing and manufacturing the Thermobox and for constantly helping me with his knowledge during this thesis. I am further grateful to Dr. Tilmann Kuhn (Fraunhofer ISE) for his important suggestions on the Thermobox modifications, Dr.-Ing. Bilal Khatri (INATECH) for his help with the installation of the heat flux sensor, and Mr Peter Wissmann for his assistance with the density measurements. I would also thank my colleague Jonaed for his help and support during this thesis.

Table of Contents

List of Figures

List of Tables

Nomenclature

Latin Characters

Symbol	Designation	Unit
ΔT	Temperature rise	K
A	Area	m^2
$A_{\mathrm{box,o}}$	Outside surface area	m^2
a_{i}	Amplitude of the wave at the inside surface	°C
a_0	Amplitude of the wave at the outside surface	°C
c	Calibration coefficient of heat flux sensor	$W/m^2.mV$
c_{p}	Specific heat capacity of the sample at constant pressure	J/kg.K
$c_{\mathrm{p,s}}$	Specific heat capacity of sample material at constant pressure	J/kgK
d	Thickness	m
d_{s}	Thickness of the sample	m
$d_{\mathrm{s,tot}}$	Total thickness of a composite sample	m
e	Control error	-
E_{stored}	Energy stored by a material when heated	J
f	Decrement factor	-
$h_{\mathrm{a,c}}$	Convective heat transfer coefficient at the cold side of the wall	$W/m^2.K$
$h_{\mathrm{a,h}}$	Convective heat transfer coefficient at the hot side of the wall	$W/m^2.K$
h_{c}	Convective heat transfer coefficient	$W/m^2.K$
h_{i}	Convective and radiative hear transfer coefficient at inner surface of the sample	$W/m^2.K$
h_{o}	Convective and radiative hear transfer coefficient at outer surface of the sample	$W/m^2.K$
H_{per}	Percentage of heating power required to increase T_{box} from 50 °C to 70 °C	%
k	Thermal conductance	W/m.K
K_{p}	Proportional gain	-

k_{s}	Thermal conductance of the sample	W/m.K
$\bar{k}_{\mathrm{s}}$	Mean value of the experimental thermal conductance	W/mK
$k_{\mathrm{s,tot}}$	Combined thermal conductance of a composite sample	W/mK
m	Mass	Kg
M_{th}	Thermal mass	J/m^3.K
$M_{\mathrm{th,s}}$	Thermal mass of a sample	kJ/m^{3}K
N	Number of data in the dataset	-
P	Period of wave propagation	s
P_{s}	Period of wave propagation for a sample	s
Q	Heat flow	J
$\dot{Q}$	Heat flow rate	W
$\dot{q}$	Heat flux	W/m^2
$\dot{Q}_{\mathrm{box}}$	Power supplied by the regular heater	W
$\dot{q}_{\mathrm{cond}}$	Heat flux due to conduction	W/m^2
$\dot{q}_{\mathrm{conv,c}}$	Heat flux due to convection from colder wall surface to air	W/m^2
$\dot{q}_{\mathrm{conv,h}}$	Heat flux due to convection from air to hotter wall surface	W/m^2
$\dot{q}_{\mathrm{i}}$	Heat flux between air inside the box and inner surface of the sample	W/m^2
$\dot{q}_{\mathrm{o}}$	Heat flux between outer surface of the sample and ambient air	W/m^2
$\dot{q}_{\mathrm{s}}$	Heat flux due to conduction	W/m^2
$\dot{q}_{\mathrm{tot}}$	Total heat flux	W/m^2
R_{cond}	Thermal resistance due to conduction	m^2.K/W
r_{cond}	Thermal resistance due to conduction through a unit area	W/mK
$r_{\mathrm{cond,tot}}$	Total thermal resistance due to conduction through a unit area of a composite sample	W/mK
R_{conv}	Thermal resistance due to convection	m^2.K/W
R_{tot}	Overall thermal resistance	m^2.K/W
r_{tot}	Overall thermal resistance of unit area	m^2.K/W

SD	Standard deviation	-
SD_{k_s}	Standard deviation of the experimental thermal conductance	W/mK
SD_{U_s}	Standard deviation of the experimental thermal transmittance	W/m^{2}K
T	Temperature	°C
t	Time	s
$T_{a,c}$	Air temperature at the cold side of the wall	°C
$T_{a,h}$	Air temperature at the hot side of the wall	°C
T_{box}	Temperature inside the Thermobox	°C
t_{cool}	Time required for cooling the heating chamber of the Thermobox	s
t_d	Derivative time	min
T_f	Fluid temperature	°C
t_{heat}	Time required for heating the heating chamber of the Thermobox	s
t_i	Integral time	min
$T_{i,max}$	Maximum inside surface temperature	°C
$t_{i,max}$	Time when inside surface temperature is maximum	s
$T_{i,min}$	Minimum inside surface temperature	°C
T_o	Initial temperature	K
$T_{o,max}$	Maximum outside surface temperature	°C
$t_{o,max}$	Time when outside surface temperature is maximum	s
$T_{o,min}$	Minimum outside surface temperature	°C
T_{room}	Room temperature	°C
T_w	Surface temperature of a body	°C
$T_{w,c}$	Surface temperature at the cold side of the wall	°C
$T_{w,h}$	Surface temperature at the hot side of the wall	°C
$T_{w,i}$	Inside surface temperature of the sample	°C
$T_{w,o}$	Outside surface temperature of the sample	°C

U	Thermal transmittance	W/m^2.K
u	Control variable of a control process	-
u_{o}	Nominal value of the control variable	-
U_{s}	Thermal transmittance of the sample	W/m^2.K
$\overline{U}_{\mathrm{s}}$	Mean value of the experimental thermal transmittance	W/m^{2}K
v	Disturbance of a control process	-
V_{th}	Voltage output of heat flux sensor	mV
X	One data in a dataset	-
x	Distance	m
$\bar{X}$	Mean of a dataset	-
y	Process variable of a control process	-
y_{SP}	Set point of a control process	-

Greek Characters

Symbol	**Designation**	**Unit**
α	Thermal diffusivity	m^2/s
α_{s}	Thermal diffusivity of the sample	m^2/s
λ_{i}	Peak-to-peak amplitude of the wave at inner surface	°C
λ_{o}	Peak-to-peak amplitude of the wave at outer surface	°C
ρ	Density	kg/m^3
ρ_{s}	Density of sample material	kg/m^3
σ	Stefan-Boltzmann constant	W/m^2.K^4
τ	Time lag	s
ω	Angular frequency of the propagated wave	rad/s
ϵ	Emissivity of a radiating body	-

1 Introduction

This chapter gives a brief description of the motivation behind this thesis and the objective of this research work.

1.1 Motivation

The responsibility of a building is to provide safety and comfort to its occupants (thermal, visual and acoustic) (Oral et al. 2004, p. 281). For that purpose, a building generally has an interface called the building envelope, which separates its indoor environment from the outdoor environment (Balaji et al. 2019, p. 373). As explained by Ahmad et al. (2014, p. 132), an envelope may comprise several elements, such as external walls, windows, roof, underground slabs, and foundation. These elements are constructed from different opaque and transparent materials, with varying physical and thermal properties, discussed elaborately by Oral et al. (2004). The heat flow through such an envelope influences the heating/cooling load of a building substantially. This flow of heat is characterized by the thermophysical properties of different elements of the envelope, thus influencing the thermal comfort of the building's indoor environment (Jin et al. 2012, p. 369).

The growing demand for thermal comfort throughout the world results in increased consumption of energy in buildings, escalating the emission of greenhouse gases. According to the Climate Action in Figures: Facts, Trends and Incentives for German Climate Policy (2019), the building sector contributes to 14 % of the total greenhouse gas emission in Germany, which is equivalent to 117 million tonnes of CO_2. The target is to reduce this emission by 2030 to 66-67 %, compared to the emission in 1990. Also, by 2050, the German building stock is expected to become nearly climate neutral, which can be achievable by incorporating renewable energy, combined with efficient energy systems. To achieve that, the energy-efficiency of the building sector needs to be improved. The energy-efficiency of a building is greatly influenced by the thermal performance of different enveloping materials, which leads to the study of their thermophysical properties (Zhang et al. 2006, pp. 1164–1165).

The thermophysical properties of building enveloping materials can be analysed under either steady-state conditions or dynamic conditions. In steady-state calculations, stable conditions are assumed (e.g. stable inside and outside temperatures). Dynamic calculations, on the other hand, evaluate the thermal performance of different enveloping materials under changing conditions, as discussed by Mohammad & Shea (2013, pp. 674–677). They explained that the thermal transmittance or U-value, which is determined through steady-state calculations, considers the radiative and convective heat transfer at the surface as well as the thermal conductance of a wall, but ignores the effect of heat storage capacity. The heat storage capacity of a building is also known as the building thermal mass (Reilly and Kinnane 2017, pp. 108–109). When a heatwave propagates through a building envelope, the envelope itself stores some of the heat until reaching thermal equilibrium and releases that heat later. The time delay of this released heatwave is called the time lag, and the amplitude damping of the released heatwave is called the decrement factor. These two parameters are of great importance for the dynamic assessment of building enveloping materials (Asan 2000, p. 197). To properly analyse the thermal performance of building envelopes, it is necessary to evaluate their dynamic behaviour in addition to their steady-state behaviour (Aste et al. 2009, p. 1181).

1.2 Research Objective

The main objective of this thesis is to determine the different thermal properties of several building enveloping materials experimentally. In order to perform these measurements, an experimental setup was developed, which was named as the Thermobox. In this thesis, the Thermobox is further modified, so that proper and reliable steady-state measurements and dynamic measurements can be performed. Such modifications include reduction of the thermal bridge effects, improvement of the thermal radiation effects inside the Thermobox, adjustment of the air circulation inside the Thermobox to ensure uniform heating of the measurement samples, implementation of temperature control strategies by using a PID controller, and integration of a heat flux sensor to the electronic unit of the Thermobox for an alternative approach to the steady-state measurements.

Steady-state measurements are then performed for calculating the thermal conductance, k, and the thermal transmittance, U, of the samples, along with their heat transfer coefficients. Two different methods, i.e. the temperature method and the heat flux method, are used for calculating the steady-state parameters. The values obtained by the two different methods are afterwards compared to each other, as well as to the literature values in order to assess the better calculation procedure.

Dynamic measurements are also performed by using the Thermobox to obtain the time lag, τ, and the decrement factor, f, of the measurement samples. Subsequently, τ and f can be used to calculate the specific heat capacity, the thermal diffusivity and the thermal mass of the samples. Finally, all the obtained and calculated values are evaluated and compared to the literature values to determine the reliability of the performed measurements, and thus the accuracy of the Thermobox.

2 Theoretical Framework

This chapter presents a detailed discussion of the theoretical knowledge relevant to this thesis. The first section gives an overview of basic heat transfer and briefly explains different heat transfer processes, as well as discusses thermal bridges. In the second section, the steady-state and the dynamic thermal properties are defined and the theories behind them are discussed. Subsequently, in the following sections, the control theory is briefly introduced and the theory behind a heat flux sensor is presented. The final section provides a discussion on the calculation of standard deviation.

2.1 Heat Transfer and Heat Transfer Processes

Heat transfer, Q, is the transfer of energy across the boundary of a thermodynamic system due to a temperature difference between the system and its surroundings, and always occurs from higher to lower temperatures. The heat flow rate, $\dot{Q}$, is defined as the heat transfer per unit of time, as shown in Equation 2.1. The heat flux, $\dot{q}$, is defined as the heat flow rate through a unit area perpendicular to the direction of heat flow, and is given by Equation 2.2 (VDI-Gesellschaft Verfahrenstechnik und Chemieingenieurwesen 2010, p. 17).

$$\dot{Q} = \frac{dQ}{dt} \tag{2.1}$$

$$\dot{q} = \frac{d\dot{Q}}{dA} \tag{2.2}$$

Where t is the duration of the heat transfer process, and A is the heat transfer area, perpendicular to the direction of heat flow.

Heat transfer through a medium, in general, can occur by three processes, which are conduction, convection and radiation (VDI-Gesellschaft Verfahrenstechnik und Chemieingenieurwesen 2010, pp. 17–18). All three types of heat transfer processes are relevant for the measurements with the Thermobox.

2.1.1 Conduction

Heat conduction is the heat transfer process that transports heat from a higher temperature to a lower temperature through molecular interactions, either within the same body or between two bodies that are in physical contact with each other. In such a heat flow, the heat flux is directly proportional to the temperature gradient, as shown in Equation 2.3 (Rohsenow et al. 1998, 1.1).

$$\dot{q} = -k\frac{dT}{dx} \tag{2.3}$$

The proportionality constant, k, is known as the thermal conductance. It is a materialistic property, which describes the heat conduction through a material. The negative sign in Equation 2.3 indicates a heat flow towards a lower temperature.

If we consider an infinitely large wall in stationary conditions, as shown in Figure 2.1, and a one-dimensional heat flow along the direction of its thickness, then the heat conduction equation through this wall, shown in Equation 2.4, can be derived from Equation 2.3 (Rohsenow et al. 1998, 1.2).

$$\dot{q} = \frac{k}{d}(T_1 - T_2) \tag{2.4}$$

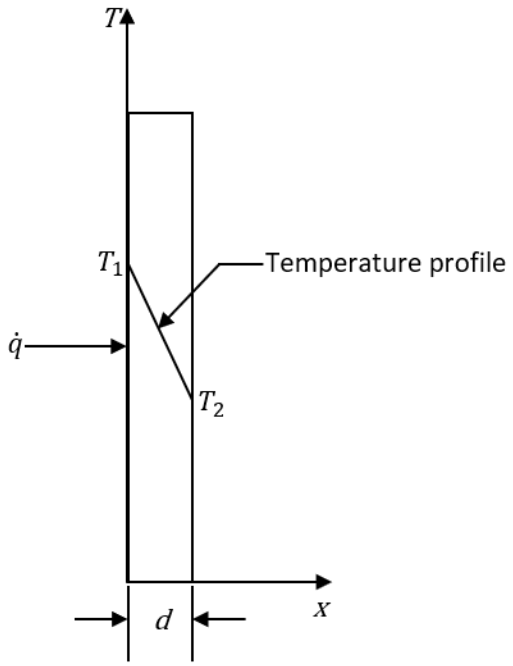

Figure 2.1: Heat conduction through a wall as adapted from Rohsenow et al. (1998, 1.2). Here, d is the thickness of the wall and T_2 and T_1 are the temperatures across the wall, where $T_1 > T_2$.

Thermal resistance for conduction, R_{cond}, can be defined by Equation 2.5 (VDI-Gesellschaft Verfahrenstechnik und Chemieingenieurwesen 2010, p. 21).

$$R_{\mathrm{cond}} = \frac{d}{kA} \tag{2.5}$$

2.1.2 Convection

Convection is the transfer of heat from the surface of a body to a fluid in motion or the transfer of heat within the fluid across its flow plane. The equation of the heat flux due to convection can be derived from Newton's law of cooling and is expressed by Equation 2.6 (Rohsenow et al. 1998, 1.4).

$$\dot{q} = h_{\mathrm{c}}(T_{\mathrm{w}} - T_{\mathrm{f}}) \tag{2.6}$$

Where T_{w} is the surface temperature of the body, T_{f} is the fluid temperature, and h_{c} is the convective heat transfer coefficient.

Thermal resistance for conduction, R_{conv}, can then be defined by Equation 2.7 (VDI-Gesellschaft Verfahrenstechnik und Chemieingenieurwesen 2010, p. 21).

$$R_{\mathrm{conv}} = \frac{1}{h_{\mathrm{c}} A} \tag{2.7}$$

2.1.3 Radiation

Radiation or thermal radiation is the heat emission of a body due to its temperature. Unlike conduction and convection, radiation does not require a material medium to transfer heat. The equation of the heat flux from a body due to thermal radiation can be derived from the Stefan-Boltzmann law and can be expressed by Equation 2.8 (Rohsenow et al. 1998, p. 1.3).

$$\dot{q} = \epsilon \sigma T^4 \tag{2.8}$$

Where σ is the Stefan-Boltzmann constant and ϵ is the emissivity of the body with $0 \leq \varepsilon \leq 1$. According to Haynes (2017, p. 2-51), emissivity can be defined as the radiation of a body with respect to the radiation of a blackbody.

2.1.4 Thermal Bridge

Thermal bridge is an important topic when the thermal performance of a building envelope is considered. A thermal bridge is an area on the envelope where a two or three-dimensional heat transfer occurs. Thermal bridges can be of two types, geometric thermal bridges and structural thermal bridges (Hens 2012).

Geometric Thermal Bridges

Geometric thermal bridges occur due to the geometry of an envelope, for example at angles and corners (Hens 2012). A geometric thermal bridge is presented in Figure 2.2. Due to the geometry of the wall, as shown in the figure, the outside surface has a bigger area than the inside surface, which results in additional heat loss.

If the temperature at point B drops below the dew point, then the water vapour present in the air inside the room will condensate at point B. This can lead to mould formation, which can deteriorate the painting and plaster of walls and cause a severe health hazard.

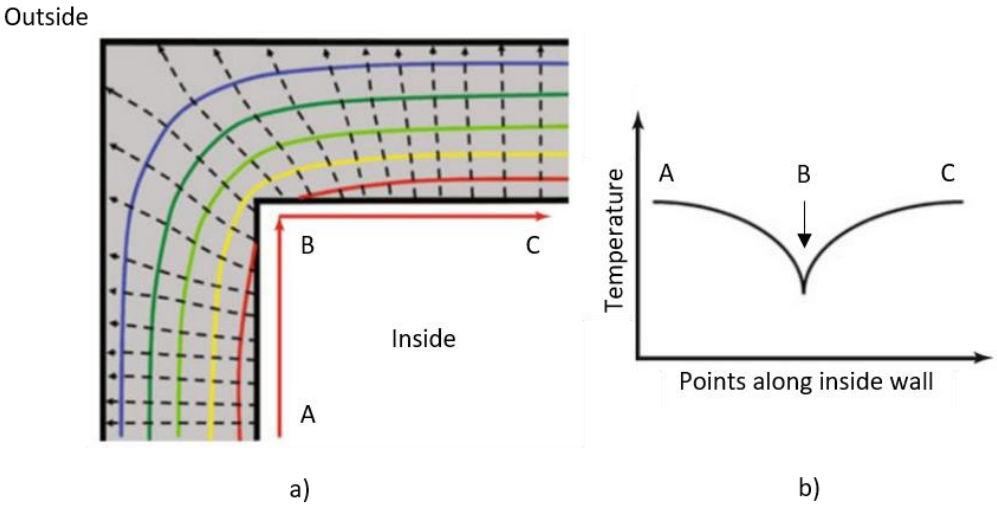

Figure 2.2: A geometric thermal bridge at the corner of a wall, adapted from Vollmer & Möllmann (2010, p. 501). The inside temperature is higher than the outside temperature. a) The coloured lines represent constant temperature lines inside the wall, with blue being lowest and red being highest. The dashed lines show the heat flux across the wall. b) Temperatures at different points along the inside wall. The temperature at B is lower than the temperatures at A and C. This can lead to condensation of water vapour at B.

Structural Thermal Bridges

Structural thermal bridges are formed due to the construction of the envelope. For example, the penetration of a beam into the envelope causes the formation of a thermal bridge (Hens 2012), as shown in Figure 2.3.

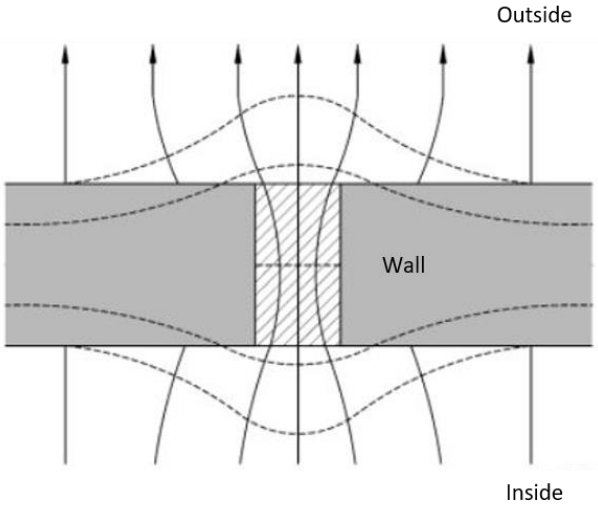

Figure 2.3: A structural thermal bridge, where there is an inclusion of an object into the wall. This penetration results in a discontinuation of the insulation, causing additional heat losses. The solid lines represent constant temperature lines and the dashed lines represent the heat flux across the wall.

Most common areas at where thermal bridges can occur are corners, overhangs, wall and roof or ceiling interfaces, and perimeters of doors and windows. Thermal bridges result in increased energy consumption by the building. Thermal bridges can further compromise the overall thermal comfort of the building (Kreith and Chhabra 2017).

2.2 Steady-state Heat Transmission and Dynamic Heat Transmission

One of the main focuses of this thesis is the determination of the steady-state parameters and the dynamic parameters of different building enveloping materials with the Thermobox. To obtain these parameters, steady-state measurements and dynamic measurements are performed. To understand these measurements, it is important to have a clear knowledge of the theories behind them. In this section, the theories of steady-state heat transmission and dynamic heat transmission are therefore briefly discussed.

2.2.1 Steady-state Heat Transmission

When two sides of a plane wall are at two different temperatures, then heat is transmitted through the wall from the hot side to the cold side. For steady-state heat transmission, the heat source, which is responsible for the said temperature difference, needs to generate a uniform temperature profile. This means that the temperature on the hot side of the wall is always at a constant level. With time, more and more heat transmit through the wall, and consequently, the temperature on the cold side of the wall gradually increases. Eventually, the cold side also reaches a constant temperature level. This is when the system attains steady-state conditions.

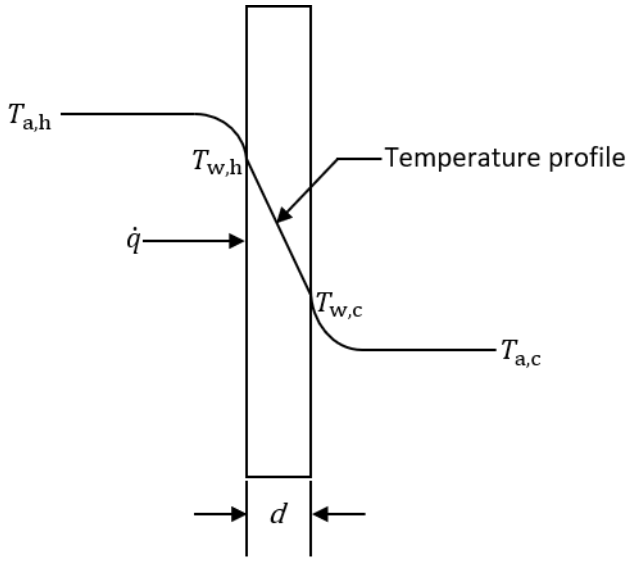

Figure 2.4: Heat transmission through a plane wall (VDI-Gesellschaft Verfahrenstechnik und Chemieingenieurwesen 2010, p. 21). Here, d is the thickness of the wall, $T_{a,h}$ and $T_{a,c}$ are the air temperatures at the hot side and the cold side respectively, $T_{w,h}$ is the wall surface temperature at the hot side, and $T_{w,c}$ is the wall surface temperature at the cold side.

If there is a heat transfer fluid, e.g. air, between the heat source and the hot side of the wall, then the heat will transfer from the air to the hotter wall surface by convection, from the hot side to the cold side of the wall by conduction, and finally, from the colder wall surface to the air by convection (VDI-Gesellschaft

Verfahrenstechnik und Chemieingenieurwesen 2010, p. 21). The heat transmission through the wall is a combination of all the heat transfer processes, as shown in Figure 2.4.

From Equations 2.4 and 2.6, the relevant equations of the heat transfer processes, presented in Figure 2.4, can be derived.

From Equation 2.4, the conductive heat flux for steady-state heat transmission, $\dot{q}_{\mathrm{cond}}$, can be given as Equation 2.9.

$$\dot{q}_{\mathrm{cond}} = \frac{k}{d}(T_{\mathrm{w,h}} - T_{\mathrm{w,c}}) \tag{2.9}$$

The convective heat fluxes for steady-state heat transmission can be expressed from Equation 2.6 by Equations 2.10 and 2.11.

$$\dot{q}_{\mathrm{conv,h}} = h_{\mathrm{a,h}}(T_{\mathrm{a,h}} - T_{\mathrm{w,h}}) \tag{2.10}$$

$$\dot{q}_{\mathrm{conv,c}} = h_{a,\mathrm{c}}(T_{\mathrm{w,c}} - T_{\mathrm{a,c}}) \tag{2.11}$$

Where $\dot{q}_{\mathrm{conv,h}}$ is the heat flux from air to the hotter wall surface, $\dot{q}_{\mathrm{conv,c}}$ is the heat flux from the colder wall surface to air, $h_{\mathrm{a,h}}$ is the convective heat transfer coefficient at the hot side, and $h_{\mathrm{a,c}}$ is the convective heat transfer coefficient at the cold side. It should be noted that these heat transfer coefficients only account for convective heat transfer, neglecting the radiation part. The transfer of heat by radiation can be included in the heat transfer coefficients, resulting in combined heat transfer coefficients due to convection and radiation. The combined heat transfer coefficients can be taken from standards or can be determined experimentally, which is discussed later in the thesis.

At steady-state conditions, the heat fluxes $\dot{q}_{\mathrm{cond}}$, $\dot{q}_{\mathrm{conv,h}}$ and $\dot{q}_{\mathrm{conv,c}}$ become equal, and can be replaced by the total heat flux through the system, i.e. from the air at the hot side to the air at the cold side. This is shown in Equation 2.12.

$$\dot{q}_{\mathrm{tot}} = \dot{q}_{\mathrm{cond}} = \dot{q}_{\mathrm{conv,h}} = \dot{q}_{\mathrm{conv,c}} \tag{2.12}$$

Where $\dot{q}_{\mathrm{tot}}$ is the total heat flux, which can be expressed by Equation 2.13 (VDI-Gesellschaft Verfahrenstechnik und Chemieingenieurwesen 2010, p. 21).

$$\dot{q}_{\mathrm{tot}} = U(T_{\mathrm{a,h}} - T_{\mathrm{a,c}}) \tag{2.13}$$

Where U is the overall heat transfer coefficient or the thermal transmittance. The thermal transmittance can be defined as the heat flow through a unit area of a structure per unit time for a unit difference in temperature. It is the property of a material that describes the heat transmission through the structure under steady-state conditions (Snow 2002, p. 30/5).

For one-dimensional heat transfer, the thermal resistances of the above-mentioned heat transfer scenarios can be considered to be in series. Then the overall thermal resistance, R_{tot}, can be derived from Equations 2.5 and 2.7 and Figure 2.4 (VDI-Gesellschaft Verfahrenstechnik und Chemieingenieurwesen 2010, p. 21), and is given in Equation 2.14.

$$R_{\mathrm{tot}} = \frac{1}{h_{\mathrm{a,h}} A} + \frac{d}{kA} + \frac{1}{h_{\mathrm{a,c}} A} \tag{2.14}$$

or,

$$r_{\mathrm{tot}} = \frac{1}{h_{\mathrm{a,h}}} + \frac{d}{k} + \frac{1}{h_{\mathrm{a,c}}} \tag{2.15}$$

r_{tot}, which is presented in Equation 2.15, is the overall thermal resistance of a unit area, and is the reciprocal of the thermal transmittance of the system as shown in Equation 2.16 (VDI-Gesellschaft Verfahrenstechnik und Chemieingenieurwesen 2010, p. 21).

$$r_{\mathrm{tot}} = \frac{1}{U} = \frac{1}{h_{\mathrm{a,h}}} + \frac{d}{k} + \frac{1}{h_{\mathrm{a,c}}} \tag{2.16}$$

Alternatively, U can be measured from Equation 2.13, as shown in Equation 2.17.

$$U = \frac{\dot{q}_{\mathrm{tot}}}{(T_{\mathrm{a,h}} - T_{\mathrm{a,c}})} \tag{2.17}$$

The thermal transmittance can be determined from steady-state heat transmission, using either Equation 2.16 or Equation 2.17. Thus, this method can be used for measuring the thermal transmittance of different building enveloping materials.

2.2.2 Dynamic Heat Transmission

For a real building, the outer walls of the building envelope experience different temperature profile during one day, which consequently affects the inside walls of the building. These profiles depend on the inside and outside temperatures of the building and the material of the enveloping wall. During this transient state, a sinus heatwave is considered to be applied on the outer wall surface, and it propagates through the wall. The amplitude of this wave indicates the temperature and the wavelength of this wave indicates the duration of the propagation of the heatwave. When the wave propagates through the wall, the wall itself stores the heat passing through it due to its thermal mass. The wave eventually reaches the inner surface of the wall with a time delay and a smaller amplitude. The time, required for the heatwave to reach the inner surface from the outer surface, is known as the time lag, τ (Equation 2.18), and the ratio of the wave amplitude at the inside surface to the wave amplitude at the outside surface is known as the decrement factor, f (Equation 2.19).

The dynamic heat transmission through a wall is presented schematically in Figure 2.5. The time lag and the decrement factor can be calculated from Figure 2.5 by using Equations 2.18 and 2.19 (Asan 2006, pp. 615–616).

$$\tau = \begin{cases} t_{\mathrm{i,max}} - t_{\mathrm{o,max}}; when\ t_{\mathrm{i,max}} > t_{\mathrm{o,max}} \\ t_{\mathrm{i,max}} - t_{\mathrm{o,max}} + P; when\ t_{\mathrm{i,max}} < t_{\mathrm{o,max}} \\ P; when\ t_{\mathrm{i,max}} = t_{\mathrm{o,max}} \end{cases} \tag{2.18}$$

$$f = \frac{\lambda_{\mathrm{i}}}{\lambda_{\mathrm{o}}} = \frac{T_{\mathrm{i,max}} - T_{\mathrm{i,min}}}{T_{\mathrm{o,max}} - T_{\mathrm{o,min}}} \tag{2.19}$$

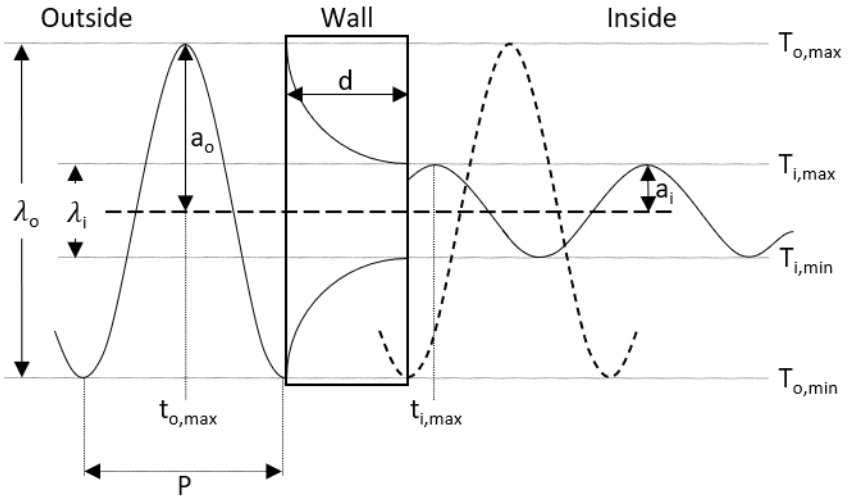

Figure 2.5: Dynamic heat transmission through a plane wall (Asan 2006, p. 616). The heatwave is propagating from the higher outside temperature to the lower inside temperature. Here a_{o} is the amplitude of the wave at the outer surface of the wall, and a_{i} is the amplitude of the wave leaving the inside surface of the wall. $T_{\mathrm{o,max}}$ and $T_{\mathrm{o,min}}$ are respectively the maximum and the minimum outside surface temperatures, $T_{\mathrm{i,max}}$ and $T_{\mathrm{i,min}}$ are respectively the maximum and the minimum inside surface temperatures. $t_{\mathrm{o,max}}$ is the time when the outside surface temperature is $T_{\mathrm{o,max}}$, $t_{\mathrm{i,max}}$ is the time when the inside surface temperature is $T_{\mathrm{i,max}}$, and P is the period of wave propagation. λ_{o} and λ_{i} are the peak-to-peak amplitude of the propagating wave at the outer surface and the inner surface respectively, where $\lambda_{\mathrm{o}} = 2a_{\mathrm{o}}$ and $\lambda_{\mathrm{i}} = 2a_{\mathrm{i}}$.

The time lag and the decrement factor are parameters that are strongly dependent on the thickness of the material. As a result, comparing these values to literature proves to be difficult. Further material-specific parameters can be calculated from the measured time lag and decrement factor. These parameters are thermal diffusivity, specific heat capacity and thermal mass.

Thermal diffusivity, specific heat capacity and thermal mass can be calculated from the time lag and the decrement factor by using the equations of the propagated heatwave.

Equations of the Propagated Heatwave

When periodic heating, as shown in Figure 2.5, is applied to a material, the temperature profile of the material, $T(x,t)$, can be described by Equation 2.20 (Bodas et al. 1998, p. 529).

$$T(x,t) = \frac{4T_o}{\pi} e^{-x\sqrt{\frac{\omega}{2\alpha}}} \sin(\omega t - x\sqrt{\frac{\omega}{2\alpha}}) \quad (2.20)$$

Where T_o is the initial temperature of the material, ω is the angular frequency of the propagated wave, and α is the thermal diffusivity of the material. The angular frequency can be calculated by Equation 2.21 (Thomas et al. 2006, p. 6898).

$$\omega = \frac{2\pi}{P} \quad (2.21)$$

Where P is the time-period of the propagated wave.

From Equation 2.20, the time lag and the decrement factor can be written as shown in Equations 2.22 and 2.23 (Thomas et al. 2006, p. 6898).

$$\tau = x\sqrt{\frac{1}{2\alpha\omega}} \quad (2.22)$$

$$f = e^{-x\sqrt{\frac{\omega}{2\alpha}}} \quad (2.23)$$

From Equations 2.22 and 2.23, it is evident that the time lag and the decrement factor of a material depend not only on the thickness of the material but also on the thermal diffusivity, which is, as discussed below, obtained from the thermal conductance, the density and the specific heat capacity of the material.

Thermal Diffusivity

Thermal diffusivity of a material describes the speed of heat propagation through the material over time during changes in its temperature. It measures the temperature change in a unit volume of a material due to the amount of heat that flows through a unit area of a unit thickness of the material in unit time, having unit temperature difference between its two faces (Salazar 2003, p. 352). It is the ratio of a material's thermal conductance and volumetric heat capacity at constant pressure. The equation to define the thermal diffusivity of a material, α, can be found in Equation 2.24 (Dante 2016).

$$\alpha = \frac{k}{\rho c_p} \quad (2.24)$$

Where k is the thermal conductance, ρ is the density, and c_p is the specific heat capacity at constant pressure of a material.

Thermal diffusivity can also be expressed in terms of time lag and decrement factor by using Equations 2.22 and 2.23 and is shown in Equations 2.25 and 2.26 (Thomas et al. 2006, p. 6898).

$$\alpha = \frac{1}{2\omega} . \left(\frac{x}{\tau}\right)^2 \tag{2.25}$$

$$\alpha = \frac{\omega}{2} \left(\frac{x}{\ln f}\right)^2 \tag{2.26}$$

Specific Heat Capacity

Specific heat capacity is a materialistic parameter that describes a material's ability to store heat (Holzner 2009, p. 215). When the temperature of one kg of material is raised by one K, the amount of heat stored by the material is defined as its specific heat capacity (Kaviany 2002, p. 175). Under constant pressure, this specific heat capacity is called the specific heat capacity at constant pressure and is denoted with c_p (Mark 2007, p. 145). c_p can be expressed by Equation 2.27 (Breithaupt 2001, pp. 57–58).

$$c_\mathrm{p} = \frac{E_\mathrm{stored}}{m\ x\ \Delta T} \tag{2.27}$$

Where E_stored is the energy stored by the material when heated, m is the mass of the material, and ΔT is the rise in temperature of the material.

c_p can also be calculated from thermal diffusivity by obtaining Equation 2.28 from Equation 2.24.

$$c_\mathrm{p} = \frac{k}{\rho\alpha} \tag{2.28}$$

Thermal Mass

The thermal mass of a structure, M_th, refers to its heat storage ability, and is a function of the density and the specific heat capacity of the structure material (Gregory et al. 2008, p. 459). It can be measured from the volumetric heat capacity of the structure material, as presented in Equation 2.29 (Baggs and Mortensen 2006). The 10^{-3} in the equation is for changing the unit from J/m^{3}K to kJ/m^{3}K.

$$M_\mathrm{th} = \rho c_\mathrm{p} \times 10^{-3} \tag{2.29}$$

2.3 Control Theory

Control theory is important for technical systems, which have parameters that change over time. Constant regulation of the controlled parameters is necessary for the system to function properly, and a suitable controller allows the system to automatically correct its behaviour by regulating the parameters (Haugen 2004, p. 1).

In control theory, a system is generally named as a process, as presented in Figure 2.6. A process has a control variable, u, which is used to control the process, and a process output variable, y, which needs to be close to the setpoint. The setpoint, y_SP, is the specified or desired value of the process output variable.

The disturbance, v, is a non-controlled input variable affecting the process output variable. Lastly, the control error, e, is the difference between the setpoint and the process output variable, as shown by Equation 2.30 (Haugen 2004, pp. 11–13).

$$e = y_{\mathrm{SP}} - y \tag{2.30}$$

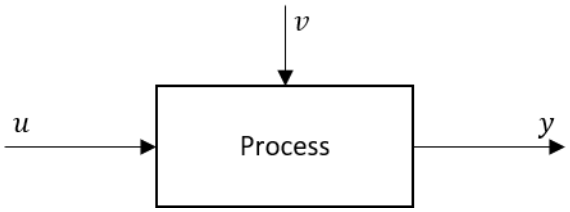

Figure 2.6: Block diagram of a control process with different variables from Haugen (2004, p. 12)

The control problem, as defined by Haugen (2004, p. 13), is the manipulation of the control variable, u, so that the control error, e, is within acceptable limits. To solve the control problem, Haugen (2004, p. 14) described two methods. One is using a constant control signal and the other is using a continuously adjusting control signal, based on the change in control error.

2.3.1 Controlling with a Constant Control Signal

In this method, a process is controlled by a constant control signal. A process with a constant control signal is presented in Figure 2.7.

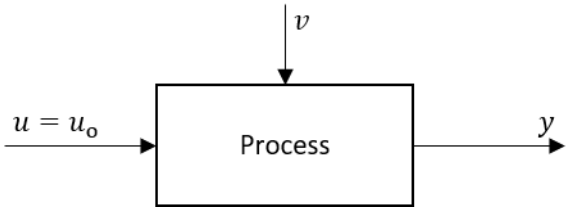

Figure 2.7: Block diagram of a control process with a constant control signal (Haugen 2004, p. 15). Here u_{o} is the constant control signal, such as $u_{\mathrm{o}} = u = constant$.

The value of u_{o} can be determined either experimentally or from mathematical models. The problem with controlling with a constant control signal is that if the setpoint or the disturbance changes, the control variable cannot be adjusted accordingly, which results in a high control error. The control variable of an error-based control signal, on the other hand, can be adjusted with the fluctuation of the setpoint or the disturbance (Haugen 2004, p. 16).

2.3.2 Controlling with an Error-based Control Signal

In this method, the control variable is continuously calculated and adjusted as a function of the error. This method of control is also known as the feedback control, as there is a feedback from the process output to the input, as shown in Figure 2.8.

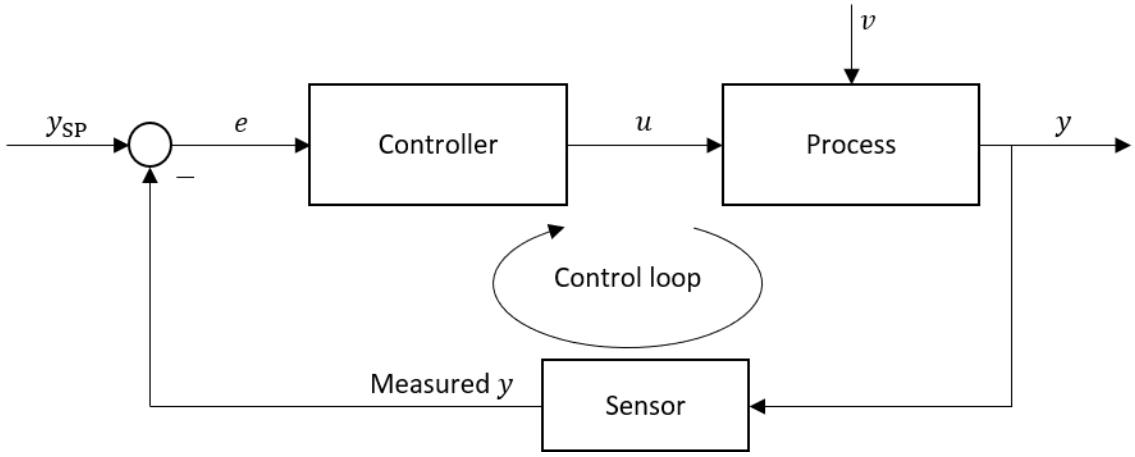

Figure 2.8: Block diagram of a feedback control process from Haugen (2004, p. 17)

With feedback control, the control error is smaller compared to control with a constant control signal (Haugen 2004, p. 19). Thus, feedback control is the most widely used control method in practice. One of the most common feedback controllers is the proportional-integral-derivative controller or the PID controller.

2.3.3 PID Controller

A PID controller consists of three terms, the proportional or P-term, the integral or I-term, and the derivative or D-term. Equation 2.31 describes such a PID controller.

$$u = u_{\mathrm{o}} + K_{\mathrm{p}} e + \frac{K_{\mathrm{p}}}{t_{\mathrm{i}}} \int_0^t e dt + K_{\mathrm{p}} t_{\mathrm{d}} \frac{de}{dt} \tag{2.31}$$

Where u_{o} is the nominal value of the control variable, K_{p} is the proportional gain, t_{i} is the integral time and t_{d} is the derivative time. $K_{\mathrm{p}} e$ is the P-term, $\frac{K_{\mathrm{p}}}{t_{\mathrm{i}}} \int_0^t e dt$ is the I-term and $K_{\mathrm{p}} t_{\mathrm{d}} \frac{de}{dt}$ is the D-term (Haugen 2004, p. 33).

While selecting a controller, the PID controller is generally the first choice, as it has quicker control and no static control error. But other controllers are also used depending on the application, such as the P controller or the PI controller or the PD controller, which can be derived from the PID controller. The P controller is used when the process has a pure integrator. The PI controller can be considered when the process has fast dynamics, or the process is of the first order. For processes with high measurement noise, a PI controller can be applied. The PD controller can be used in electrical servomechanisms having sufficiently small steady-state control error (Haugen 2004, p. 73).

Selecting a suitable controller is important to get the desired outcome of different applications. For this research work, a PID controller is considered.

2.3.4 Parameterization of the Controller

Determining the optimal values of the control parameters, K_p, T_i and T_d, is important so that a stable control loop can be achieved. Different tuning methods are used in practice for controller parameterization. One such method, the Chien-Hrones-Reswick (CHR) method, is used in this thesis for calculating the optimal values of the control parameters.

Chien-Hrones-Reswick (CHR) Method

The CHR tuning method is a modification of the open-loop Ziegler-Nichols method (Shahrokhi and Zomorrodi 2003, p. 3). The step response of the output variable is observed with a step-change in the input variable, as shown in Figure 2.9. A tangent can be drawn on the step response curve at the inflexion point (Xue et al. 2007, p. 188), and the parameters K_m, τ_m and d_m can be determined (Shahrokhi and Zomorrodi 2003, p. 8). These parameters are then used to calculate the PID control parameters, K_p, T_i and T_d, by using the formulas, presented in Table 1.

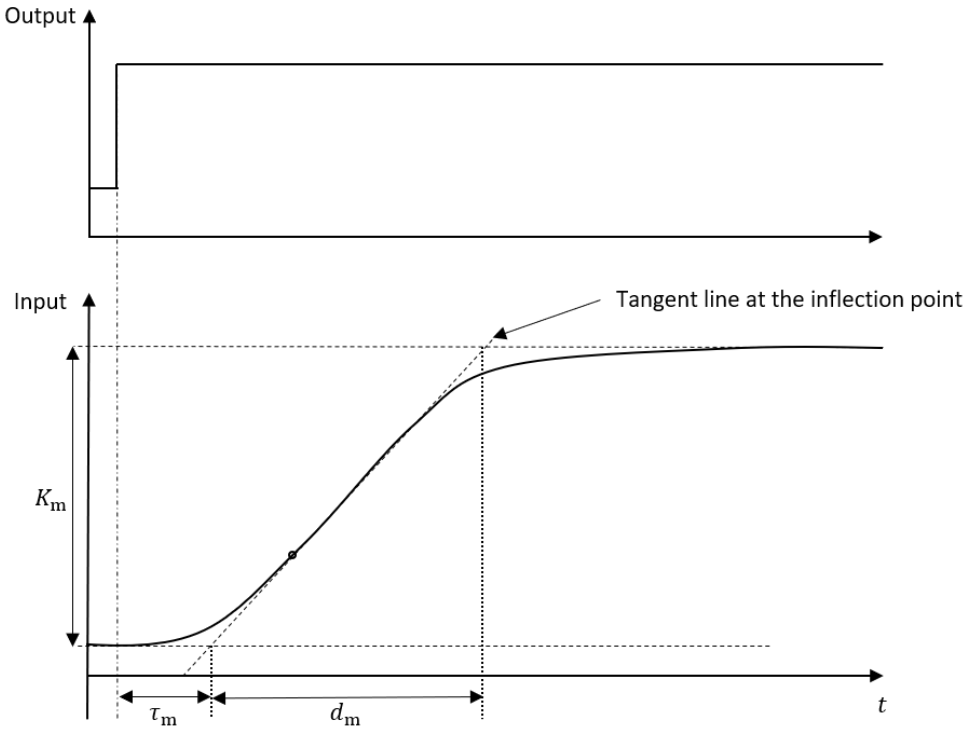

Figure 2.9: Step response curve (Xue et al. 2007, p. 188)

Table 1: Calculation of control parameters by CHR method (Xue et al. 2007, p. 199)

Control parameters	Formula
K_p	$\frac{0.6}{K_\mathrm{m}}\frac{\tau_\mathrm{m}}{d_\mathrm{m}}$
t_i	τ_m
t_d	$0.5\tau_\mathrm{m}$

2.4 Theory of Heat Flux Sensor

The heat flux sensor, as shown in Figure 2.10, measures heat flux by a thermopile, which is a series connection of several hundred thermocouple junctions (Cu and CuNi44). This series of thermocouples are embedded in a filling material (typically a plastic), which is then placed between a hot and a cold side. Due to the temperature difference between the two sides, a thermovoltage is generated by each thermocouple, which is proportional to the temperature difference between the Cu-CuNi44 joint and the CuNi44-Cu joint. The total voltage output of the series of thermocouples, and consequently the heat flux sensor, V_{th}, is proportional to the heat flux through the filling material, $\dot{q}$, which is same as the heat flux through the sample (Azar 2009, p. 24).

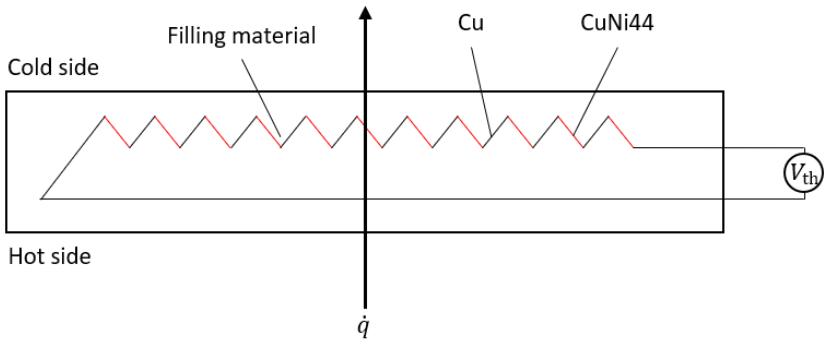

Figure 2.10: Schematic diagram of the working principle of a basic heat flux sensor (Phymeas 2020b). Here $\dot{q}$ is the heat flux through the sensor and V_{th} is the voltage output of the sensor.

The heat flux, $\dot{q}$, can be expressed in Equation 2.32 (Phymeas 2020b).

$$\dot{q} = c.V_{\text{th}} \tag{2.32}$$

Where c is the calibration coefficient of the heat flux sensor, which is defined as the heat flux required to generate a voltage of 1 mV. The value of c for the heat flux sensor used in this thesis is given by the manufacturer as 8.05 W/m^2.mV.

2.5 Standard Deviation

Standard deviation is used in mathematics for determining the variation among the data in a dataset with respect to the mean of the dataset. It is a measure of how the data are spread out from the mean (Christmann 2012, p. 35). The standard deviation of an entire dataset can be denoted by SD and expressed by Equation 2.33 (Barlow 2013, p. 9).

$$SD = \sqrt{\frac{\sum(X - \bar{X})^2}{N}} \tag{2.33}$$

Where X is a data in the dataset, $\bar{X}$ is the mean of the data set, and N is the number of data in the dataset. A low value of standard deviation indicates that most of the data in the set are closer to the average. A high value of standard deviation indicates that the data in the set are more spread out from the mean.

3 Experimental Setup

In this chapter, the devices used for different measurements in this thesis are introduced. The primary experimental setup for this thesis is the Thermobox. A detailed description of the Thermobox and its components is provided in this chapter. Some additional devices were used for evaluating the performance of the Thermobox. These devices include a thermal imaging camera and an emissiometer. These devices are also discussed in this chapter. The detail description of the heat flux sensor used in this thesis is also presented in this chapter.

3.1 Description of the Thermobox

The Thermobox is the primary experimental setup that was used for different measurements in this thesis. The detailed construction of the Thermobox, its different components, the measurement samples, the electronic unit and the software interface are discussed in the following sections.

3.1.1 Introduction of the Thermobox

The Thermobox was designed by Thomas Schmidt from exergia - The Invention Company. The company constructed three identical Thermoboxes. The Thermoboxes each has a dedicated laptop, which controls the heating of the respective Thermobox, as well as collect and store data. One laptop holds the main LabVIEW programme, where the control mechanism of the Thermoboxes was programmed by exergia. This Thermobox is labelled as the main Thermobox. The other laptops, consequently the Thermoboxes, use a copy of the main programme. To maintain consistency of the measurements performed in this thesis, all the experiments are performed using the main Thermobox. This also allows for direct adjustment of the LabVIEW programme if necessary. Any adjustments made to the main programme during this thesis is also copied to the other laptops so that all three of the Thermoboxes have the same control mechanism.

3.1.2 Construction of the Thermobox

The Thermobox, which is presented schematically in Figure 3.1, is mainly constructed from MDF or Medium-density Fibreboard. MDF is a type of engineered wood. It is manufactured from residuals of hardwood or softwood, breaking it into fibres and combining with wax, resin and other materials (Spence 2006, p. 114).

The device consists of an insulated chamber, which represents the inside of a room. This chamber has five fixed walls, which have inside insulation of polyurethane (PUR) foam. Each wall is 56 mm thick, comprising 16 mm wood of and 40 mm of insulation. The chamber is called the heating chamber. The front face of the chamber is not fixed, and different measurement samples can be set up there for experimentation.

The inside dimension of the heating chamber of the Thermobox is 340 mm x 340 mm x 310 mm. The volume is then calculated as 0.0358 m^3 and the inside surface area is calculated as 0.653 m^2. The outside dimensioning of the Thermobox, on the other hand, is complicated, due to the presence of extended surfaces. But the outside surface area is a necessary parameter for proper evaluation of the heat transfer on the outside surface of the Thermobox. Thus, the outside surface area needs to be determined.

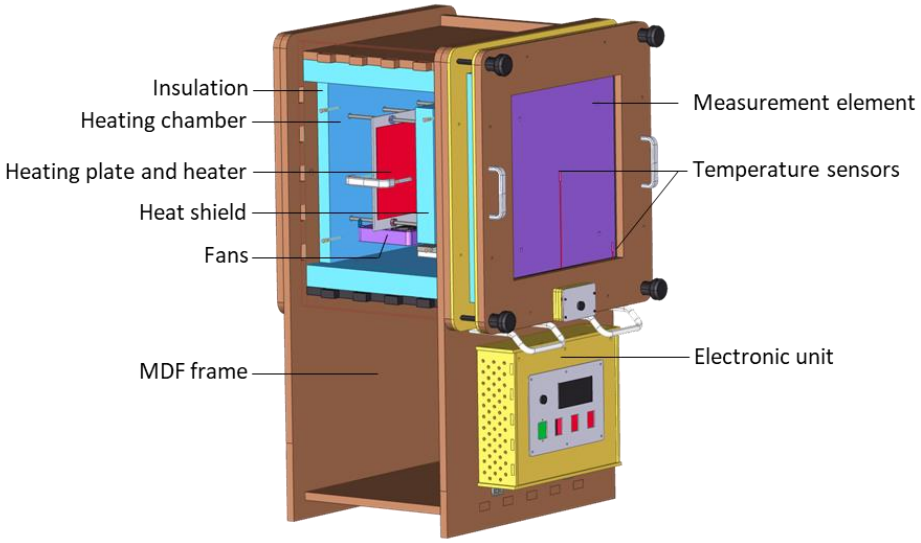

Figure 3.1: Schematic diagram of the Thermobox, designed by Schmidt, T., exergia 2019

The maximum dimension of the outside surface of the heating chamber is 520 mm x 520 mm x 470 mm. This dimension includes extended edges and surfaces. As it is considered in this thesis that only one-directional heat conduction occurs through the walls of the Thermobox, these extended surfaces can be neglected while calculating the effective heat transfer area of the outside surface. This effective dimension is found by adding the thickness of the wall to the inside dimensions. This leads to the effective outside dimension of 452 mm x 452 mm x 422 mm. Thus, the effective outside surface area can be calculated as 1.172 m^2.

Figure 3.2 shows a photograph of the complete experimental setup of the Thermobox.

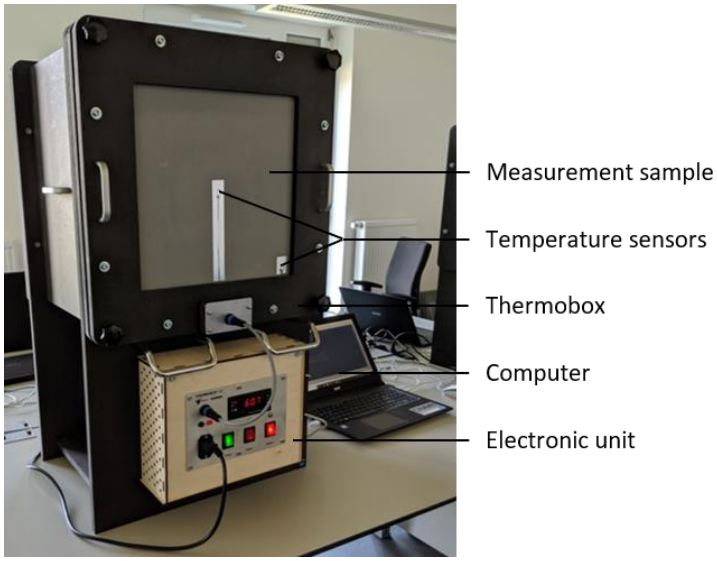

Figure 3.2: Photograph showing the complete setup of the Thermobox. The UHPC element is mounted as the measurement sample in this case.

An MDF frame holds the heating chamber on a table or a floor or any other flat surface. It also holds the electronic unit of the Thermobox. The electronic unit is attached to the frame with screws, which can be removed to make any necessary adjustment to the electronics of the Theermobox. The rear wall of the Thermobox can also be removed, in case any modification or reparation is needed to be performed on the elements inside the heating chamber.

3.1.3 Components of the Heating Chamber

The heating chamber of the Thermobox, along with its different components, is shown in Figure 3.3.

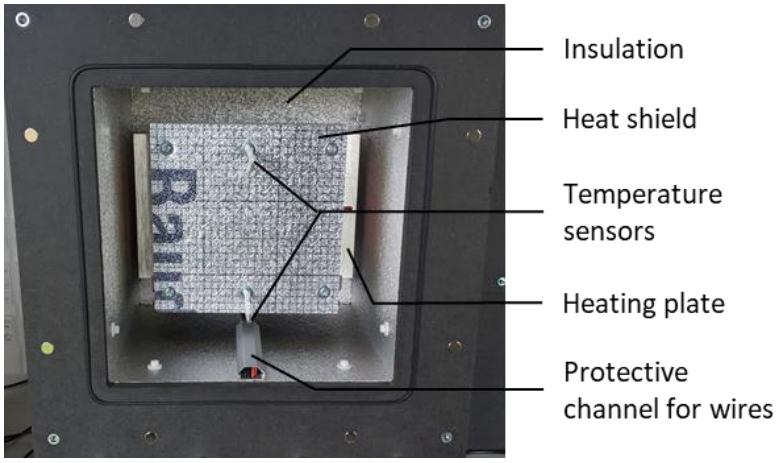

Figure 3.3: Photograph showing the heating chamber of the Thermobox and its components. The temperature sensors measure the temperatures at the top and the bottom of the heating chamber, the average of which gives the box inside temperature, T_{box}.

The heating chamber consists of a heating plate with two heaters, a heat shield and two fans. There are also wires for connecting the different components, sensors for temperature measurement, and protective channel for the wires against heating. Different components of the heating chamber are discussed in this section.

Heating Elements and Heat Shield

The heating chamber of the Thermobox is heated by two silicone heaters. Both heaters are mounted on an aluminium heating plate, each on one side. The heating plate is mounted on the back wall of the Thermobox, along with the heat shield and the fans. One heater is named as the regular heater. This heater is mounted on the front face of the heating plate and is used to maintain a certain temperature inside the heating chamber. The power of the regular heater can be adjusted manually in the software. The regular heater has a maximum power of 125 W.

The other heater is named the power heater and mounted on the rear face of the heating plate. This is a 750 W heater, whose function is to swiftly increase the temperature inside the heating chamber. The power heater can be controlled with a simple on/off switch. When turned on, the heater can only supply constant power into the heating chamber. It automatically turns off when the temperature inside the heating chamber reaches the set safety temperature (normally 40 °C). The switch then needs to be

manually turned off. Further temperature stabilization inside the heating chamber is performed by the regular heater.

The heat shield is placed in front of the heating plate, and it protects the measurement samples from direct exposure to the heaters. The heat shield is a square cuboid made of polyurethane foam. The square faces are covered with aluminium foil and have an area of 250 mm x 250 mm. The thickness of the shield is 40 mm.

Fans

Inside the heating chamber of the Thermobox, there are two DC fans (EBM 4300, model 4314), placed under the heating plate. These fans are used to generate forced circulation of air inside the Thermobox so that the air can carry the heat from the heaters to the measurement samples. Each fan has a dimension of 119 mm x119 mm x 32 mm, and can circulate 47.2 x 10^3 m^3 of air per second (Schmidt, T., exergia 2019). The power consumed by the fans, as measured with an external power measuring device, is about 9.2 W.

Temperature Sensors of the Box

There are two temperature sensors (PT100) inside the heating chamber. These sensors are placed in front of the heat shield, one at the top and the other at the bottom. The temperature inside the Thermobox, T_{box}, is calculated from the average of the two temperatures measured by these two sensors.

A third sensor is placed outside the Thermobox under the heating chamber. This sensor measures the room temperature, T_{room}, which denotes the outside condition of the Thermobox.

Wires and Protective Channel

Power is supplied to the heaters and the fans through wires. These wires are placed under a protective channel inside the heating chamber for protection against high temperatures. This channel also guides the wires from the sensors to the control unit for the acquisition of data.

The back wall holding the heating plate, heaters, fans, heat shield and wires are shown in Figure 3.4.

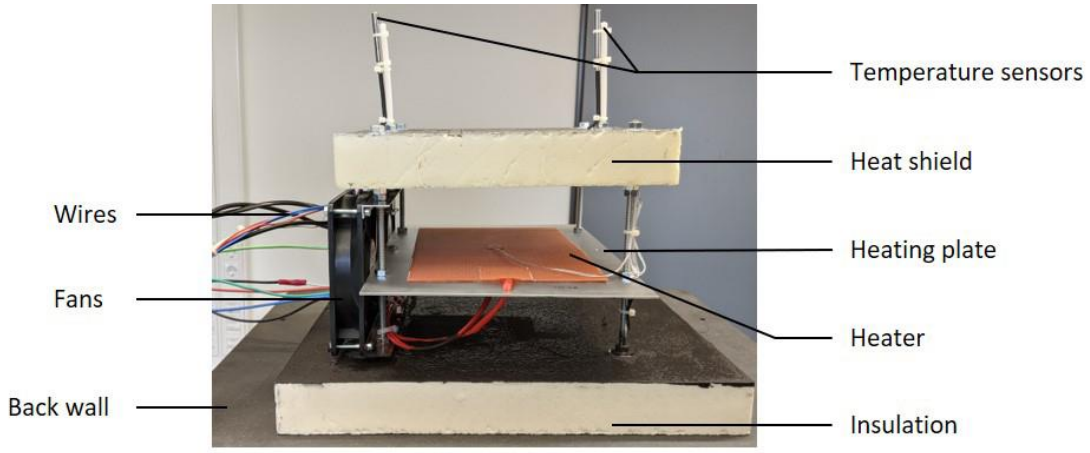

Figure 3.4: Image showing the back wall of the Thermobox. The heater shown here is the regular heater. The power heater is attached similarly on the other side of the heating plate.

3.1.4 Measurement Samples

Seven different elements were mounted in MDF frames as measurement samples for performing measurements using the Thermobox. The samples are i) MDF sample without insulation, ii) MDF sample with inside PUR insulation (MDF+PUR), iii) UHPC sample without insulation, iv) UHPC sample with outside PUR insulation (UHPC+PUR), v) glass sample with single glazing, vi) glass sample with double glazing and air between the glazing layers, and vii) glass sample with double glazing and argon between the glazing layers. The samples can be mounted on the open face of the Thermobox with screws. All the samples have several sensors for measuring the temperatures at different points.

A brief description of the materials of the measurement samples is presented in Table 2. A photograph of the measurement sample, MDF, along with its different components, is presented in Figure 3.5.

Table 2: Description of the materials constructing the measurement samples

Material of the measurement samples	Abbreviation	Type of materials	Short description
Medium-density Fibreboard	MDF	Wood	Engineered wood made from wood fibre, wax and resin, used in construction
Ultra High Performance Concrete	UHPC	Concrete	Strong and durable concrete used in heavy construction
Polyurethane	PUR	Polymer	Insulating material, used in rigid foam insulation panels
Planibel Clearlite	-	Glass	Soda-lime silicate glass with high transmittance (AGC 2011)

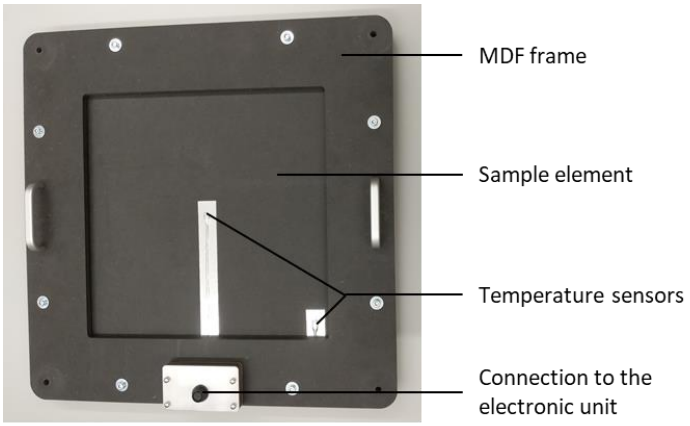

Figure 3.5: Photograph showing the front side of the measurement sample MDF. The sample material, MDF, is held by two MDF frames, each having a thickness of 16 mm, at the front and the back. The connection to the electronic unit connects the temperature sensors on the sample to the electronic unit. Temperature sensors are also placed on the back of the sample at the same positions as the front side.

Figure 3.6 presents the rest of the opaque measurement samples, i.e., UHPC sample without insulation, MDF sample with inside insulation and UHPC sample with outside insulation. The transparent measurement samples, i.e., glass sample with single glazing, glass sample with double glazing and air between the glazing layers, and glass sample with double glazing and argon between the glazing layers are shown in Figure 3.7.

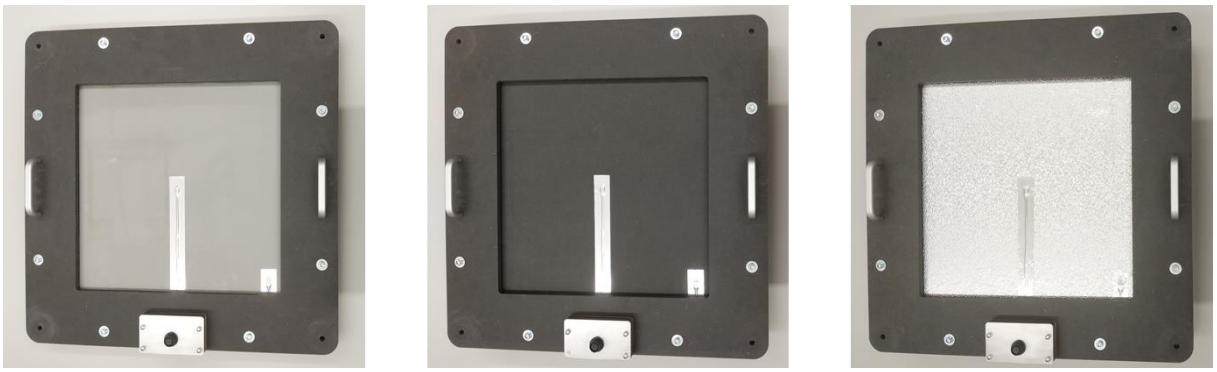

Figure 3.6: Photographs showing from the left the UHPC sample without insulation, the MDF sample with inside insulation and the UHPC sample with outside insulation

Figure 3.7: Photographs showing from the left the glass sample with single glazing, the glass sample with double glazing and air between the glazing layers and the glass sample with double glazing and argon between the glazing layers

Dimension of the Samples

Each measurement sample has a total front surface area of 520 mm x 520 mm including the frame. But only a front surface area of 340 mm x 340 mm is considered for calculations, as that is the actual heat transfer area of a measurement sample. This is because the area of the open face of the Thermobox is also 340 mm x 340 mm, which means that heat is transferred directly through this area from inside the Thermobox, through the samples, and finally to the room.

Each of the samples has a different thickness, but the MDF frames holding them have a thickness of 16 mm, both at the front and the back. The thickness of the elements held between the MDF frames changes from one sample to another. This thickness is considered to be the actual thickness of the samples, as heat flow from inside the Thermobox mainly occurs through this thickness. The actual thickness of each sample is presented in Table 3.

Table 3: Thickness of the measurement samples

Measurement sample	Thickness in mm
MDF	16
MDF with inside insulation (MDF+PUR)	56 (16 mm MDF + 40 mm PUR)
UHPC	16
UHPC with outside insulation (UHPC+PUR)	56 (16 mm UHPC + 40 mm PUR)
Glass	4
Double glazing with air	24
Double glazing with argon	24

Temperature Sensors of the Samples

Each sample has two temperature sensors on the inside surface, one at the centre and the other at the bottom right. These sensors measure the inside surface temperature of the samples. Two sensors are also placed on the outside surface at the same locations as the inside surface. The outside surface temperature of the samples is measured by these sensors. The insulated elements have an additional sensor, placed between the layer of insulation and the layer of MDF or UHPC. This sensor measures the temperature between the layers.

3.1.5 Electronic Unit

The electronic unit of the Thermobox is mounted under the front face of the Thermobox. The cover of the electronic unit, as shown in Figure 3.8, has a display for showing the temperature inside the heating chamber, a main power switch (green) for the Thermobox and the fans, two red switches for the heaters (“Heater” for the regular heater and “Heater+” for the power heater), a plug for supplying power into the Thermobox, and a port to connect the control unit to the sensors on the measurement samples with a wire.

A safety temperature can be set at the display of the electronic unit. If the temperature inside the heating chamber exceeds this safety temperature, the electronic unit, along with the heaters, will shut down to avoid over-heating of the Thermobox and prevent any safety hazard.

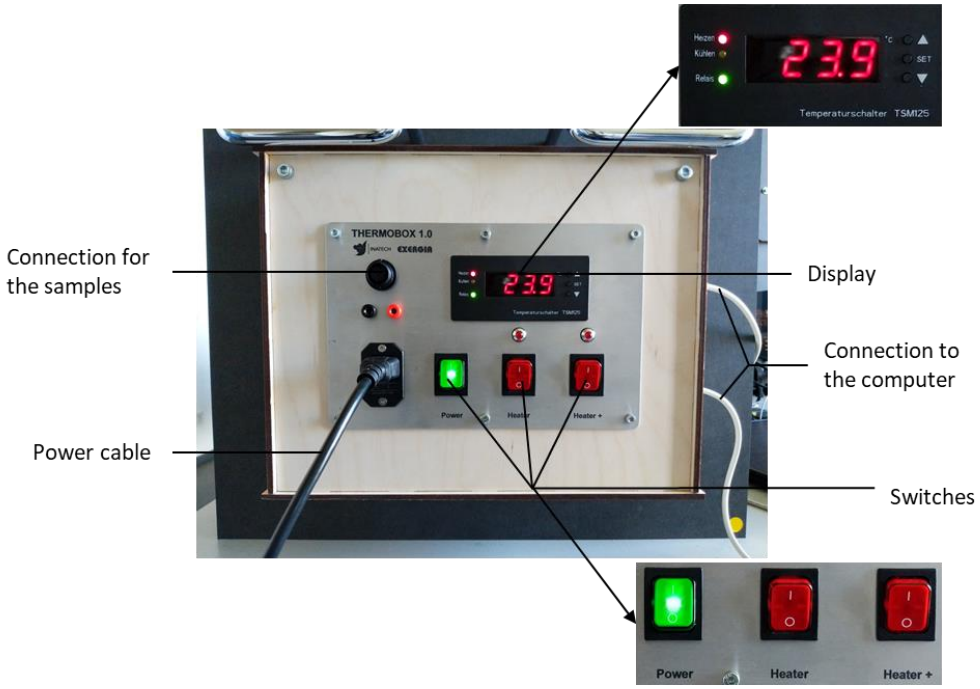

Figure 3.8: Photograph showing the cover of the electronic unit. The display shows the temperature inside the box. The three switches are for the fans, the regular heater and the power heater, from left to right.

The inside of the electronic is shown in Figure 3.9. The unit consists of a power supply for the power heater and also comprises a shunt resistor for measuring the current flowing through the regular heater. The voltages of the regular heater and the shunt resistor are collected by a data logger. These measurements lead to the calculation of the power of the regular heater.

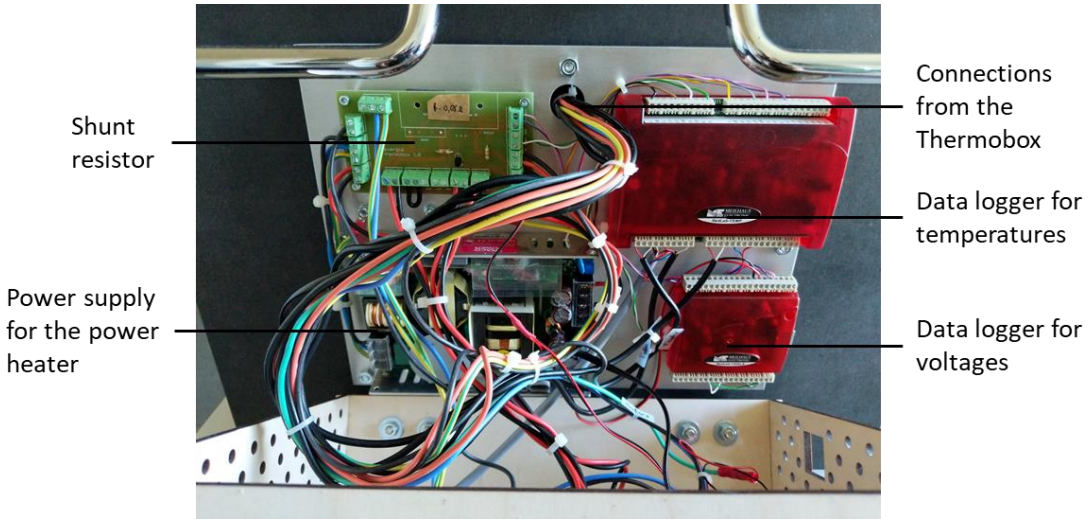

Figure 3.9: Photograph showing the inside of the electronic unit. The data loggers can be connected to the software interface through cables (not shown in the photo).

Another data logger collects the measurements of different temperature sensors. The data loggers are connected to the computer through cables. The computer uses the software, LabView, for performing the measurements.

3.1.6 Software Interface

The experiments are controlled by a program, which was developed with the software LabView by Schmidt, T., exergia 2019. The program allows the user to set the target value of T_{box} by defining an upper limit and a lower limit, and manually adjust the percentage of power that is required to maintain that target value.

To understand the manual control of power, a closer look can be taken into the software interface in Figure 3.10a. Inside the Heating Control section of the software interface, three input areas can be seen, labelled as T-Stop [°C], T-Start [°C] and Power 0-100%. The upper limit of T_{box} can be set in T-Stop [°C] and the lower limit can be set in T-Start [°C]. These two limits mean that the power of the regular heater will be at 100 % if T_{box} is less than the set value of T-Start, and the heater will turn off (0 %) if T_{box} is higher than the set value of T-Stop. A number between 0 and 100 can be set in the box Power 0-100%. This defines the percentage of power supplied by the regular heater into the heating chamber if T_{box} is between T-Start and T-Stop. This percentage of power needs to be manually adjusted so that T_{box} stays in between the set values of T-Start and T-Stop.

The box T-Box [°C] displays the temperature inside the heating chamber, which is T_{box}, and the box Average Heating Power [Watt] displays the heating power supplied into the heating chamber by the regular heater. An indicator at the bottom of the Heating Control section indicates whether the regular heater is supplying power into the heating chamber or not.

Above the Heating Control section, there is a box labelled as Loop Time [ms]. Here the time can be set in milliseconds after which a data will be recorded by the software. A loop time of 1000 ms, for example, means that the software will wait for 1000 ms between measuring two data points.

The graph, shown in Figure 3.10a, displays the average heating power in Watt over time in seconds. Additionally, the graph in Figure 3.10b displays the progression of temperatures at different sensors in °C over time in seconds.

The switch Write to File, which is next to the box Loop Time [ms], is used for the data to be written into a text file in the computer, named as ThermoboxMeasurementData.txt. This file stores the time, the heating power at that time and the temperatures at different sensors at each time step.

When the switch Write to file is on, the text file ThermoboxMeasurementData.txt will either be created or if the text file already exists in the saving directory, then the pre-existing data on the file will be overwritten by the new data. So it is important to rename the file after the completion of each measurement so that no data is accidentally lost. It should also be noted that Write to File needs to be switched off for the text file to be saved. Therefore, before closing the software, it is imperative to ensure that Write to file is switched off, otherwise, the measurement data will be lost.

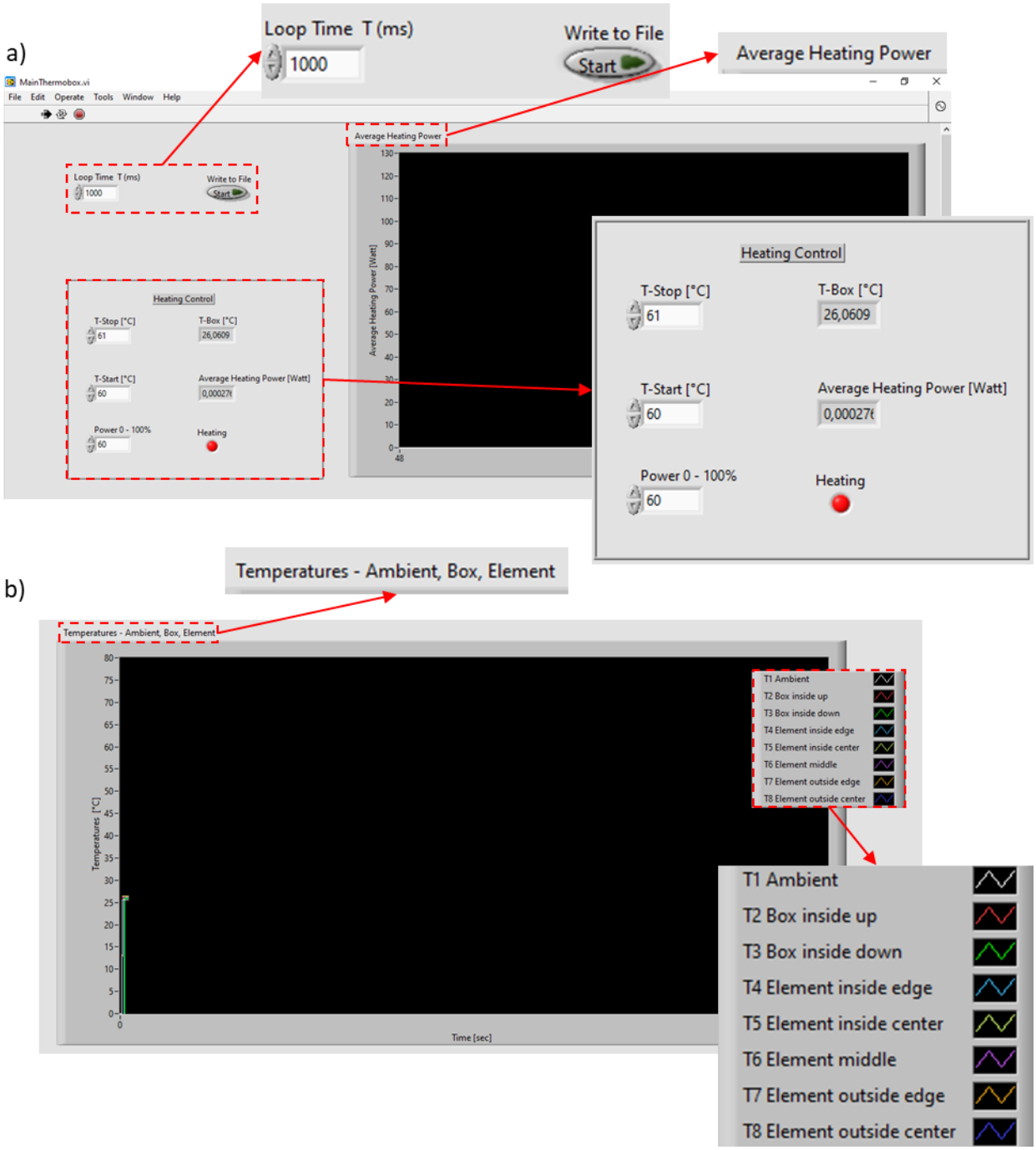

Figure 3.10: Images showing the software interface of the LabView program. Figure 3.10a shows the heating control and the average heating power supplied to the heating chamber. Figure 3.10b shows the graphical presentation of the temperatures at different sensors.

3.2 Thermal Imaging Camera

In order to check the Thermobox for possible thermal bridges and heat losses, a thermal imaging camera (testo 865) is used, which is shown in Figure 3.11. The camera has an accuracy of ±2 °C (Testo Ltd 2020). Thermal images of the Thermobox with different measurement samples are observed and recorded with the thermal imaging camera.

Figure 3.11: Image showing the testo 865 thermal imaging camera (Testo Ltd 2020).

From the recorded thermal images, different thermal bridges and heat loss areas and the temperature distribution of the samples are observed, and further modifications are planned accordingly.

3.3 Emissiometer

Figure 3.12 shows the emissiometer used for measuring the emissivity of different materials in this thesis.

Figure 3.12: Photograph of the emissiometer

The emissiometer is a device used for measuring the emittance of a material. This device is an integral part of the Alpha-Epsilon Meter, which is a device manufactured by Optosol GmbH for measuring the

absorptance, reflectance and emittance of a material. The emissiometer has an integrated sphere, which holds a glow bar as the source of thermal radiation. The sphere homogeneously distributes the radiation from the glow bar and acts as a diffuse radiation source. A detector is used to detect the reflected radiation from the sample materials within a wavelength range of 8-14 µm, which in turn calculates the emittance by $emittance = 1 - reflectance$. After the device heats up properly, a reference with a high emittance (glass, with a measured emittance of 89.4 %) and a reference with a low emittance (aluminium, with a measured emittance of 3.3 %) is used for calibrating the emissiometer. Once the calibration is done, the emissiometer can be placed on a sample and the emittance of the sample can then be measured.

3.4 Heat Flux Sensor

The heat flux method is another procedure for determining thermal conductance and thermal transmittance using the Thermobox besides the temperature method. This method requires the installation of a heat flux sensor.

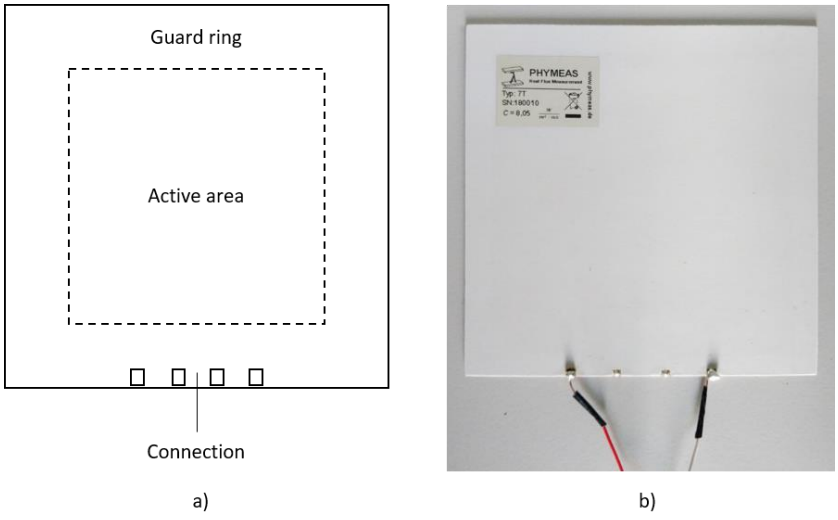

Figure 3.13: a) Schematic diagram of a heat flux sensor (Phymeas 2020a). The active area holds the thermopile. b) Photograph of the heat flux sensor with connecting wires.

The heat flux sensor used in this thesis is an epoxy resin sensor, branded as type 7T by the manufacturer Phymeas, schematically presented in Figure 3.13a. The working principle of the heat flux sensor has been discussed in Section 2.4, and the installation procedure of the sensor is presented later in Section 4.4.2. Figure 3.13b presents an image of the heat flux sensor with connections to the data logger.

4 Experimental Procedure

In this chapter, the experimental procedures of this thesis are presented. Different modifications done to the Thermobox are described, namely the implementation of insulation stripes on the side of the samples, painting the heating chamber of the Thermobox and changing the direction of airflow inside the Thermobox. A further discussion is presented on the steady-state measurement procedure by the temperature method and the heat flux method, followed by a discussion on the dynamic measurement procedure. The installation of the heat flux sensor and the implementation of the PID controller are also discussed in this chapter.

4.1 Adaption of Theories for Measurement with the Thermobox

The theories of heat transmission discussed in the previous section is needed to be reformed to satisfy the need of the Thermobox. Such adaptation of theories is discussed in this chapter.

4.1.1 Steady-state measurement

For the Thermobox, the wall is replaced by the measurement sample. The hotter side is the inside of the box, and the colder side is in room condition. The steady-state heat transmission through a measurement sample is adapted from Figure 2.4 and is presented in Figure 4.1.

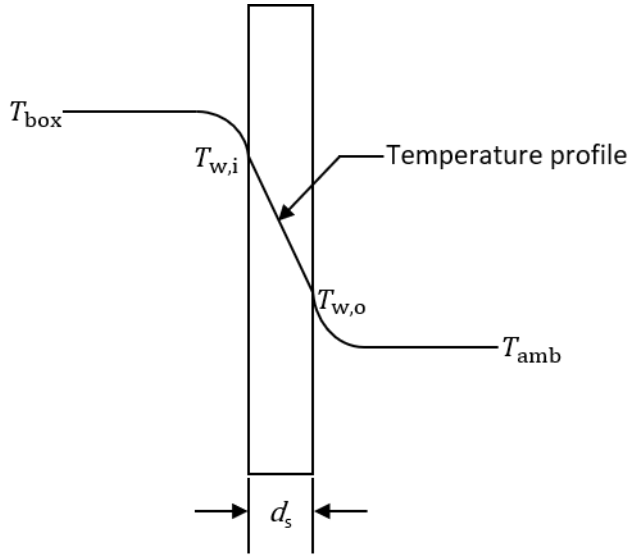

Figure 4.1: Steady-state heat transmission through a measurement sample. Here d_s is the thickness of the sample, T_{box} is the temperature inside the Thermobox, T_{room} is the ambient temperature, $T_{w,i}$ is the inside surface temperature of the sample, and $T_{w,o}$ is the outside surface temperature of the sample.

In addition to the convective effects between the air and the surfaces of the sample, the radiation effects from the heaters to the sample and from the sample to the room are needed to be considered. To achieve that, the convective heat transfer coefficients in Equations 2.10 and 2.11 are replaced with the combined convective and radiative heat transfer coefficients. The heat flux equations for the Thermobox, adapted from Equations 2.9, 2.10 and 2.11, thus can be written as Equations 4.1, 4.2 and 4.3.

$$\dot{q}_{\mathrm{s}} = \frac{k_{\mathrm{s}}}{d_{\mathrm{s}}}(T_{\mathrm{w,i}} - T_{\mathrm{w,o}}) \tag{4.1}$$

$$\dot{q}_{\mathrm{i}} = h_{\mathrm{i}}(T_{\mathrm{box}} - T_{\mathrm{w,i}}) \tag{4.2}$$

$$\dot{q}_{\mathrm{o}} = h_{\mathrm{o}}(T_{\mathrm{w,o}} - T_{\mathrm{room}}) \tag{4.3}$$

Where $\dot{q}_{\mathrm{s}}$ is the heat flux through the sample due to conduction, k_{s} is the thermal conductance of the sample material, $\dot{q}_{\mathrm{i}}$ is the heat flux between the air inside the box and the inner surface of the sample due to convection and radiation, $\dot{q}_{\mathrm{o}}$ is the heat flux between the outer surface of the sample and the air in the room due to convection and radiation, and h_{i} and h_{o} are the heat transfer coefficients considering convection and radiation between the inner surface of the sample and the air inside the Thermobox and between the outer surface of the sample and the air inside the room, respectively.

The inside surface temperature, $T_{\mathrm{w,i}}$, denotes the temperature given by the sensor at the centre of the inside surface of the sample and the outside surface temperature, $T_{\mathrm{w,o}}$, denotes the temperature given by the sensor at the centre of the outside surface of the sample. For calculation, only the centre temperatures are considered because the sensors at the bottom right corner of the samples are close to the sample frames, so their readings may be influenced by the thermal bridges at the edge of the frames.

Steady-state is achieved when the Thermobox temperatures in Figure 4.1, i.e. T_{box}, $T_{\mathrm{w,i}}$ and $T_{\mathrm{w,o}}$, become constant for 20 minutes. At steady-state condition, Equation 2.12 can be written as Equation 4.4.

$$\dot{q}_{\mathrm{tot}} = \dot{q}_{\mathrm{s}} = \dot{q}_{\mathrm{i}} = \dot{q}_{\mathrm{o}} \tag{4.4}$$

If $\dot{q}_{\mathrm{tot}}$ is known, then the thermal conductance of the sample, k_{s}, and the thermal transmittance of the sample, U_{s}, can be calculated. Two different methods can be used to determine the value of $\dot{q}_{\mathrm{tot}}$. The methods are named as a) temperature method and b) heat flux method.

a) Temperature Method

The value of one of the heat transfer coefficients (h_{o} or h_{i}) is required for calculating $\dot{q}_{\mathrm{tot}}$ with the temperature method. The heat transfer coefficient of the outer surface, h_{o}, can be taken from literature. h_{o} can also be calculated experimentally. The calculated parameters of the samples can then be compared for both values of h_{o}.The Determination of literature h_{o} and experimental h_{o} is discussed below.

Literature value of h_{o}

As the outer condition of the Thermobox is in practice the inside condition of a room, the heat transfer coefficient due to convection and radiation at the outer surface of the sample, h_{o}, can be taken from literature. The literature value of h_{o} is calculated from Table 7 of the DIN EN ISO 6946 2018 as 7.69 W/m^{2}K [Appendix A].

This literature value of h_o is calculated from the inside heat transfer resistance of a wall. As the Thermobox is not a wall, rather an object releasing heat into the room, using this value in experiments might not be appropriate. As an alternate approach, an experimental determination of h_o can be considered. The description of the experimental determination of h_o is as follows.

Calculation of h_o from Temperature Measurement

The insulated wood sample has the same construction as the walls of the Thermobox. As a result, equipped with the insulated wood sample, all the sides of the Thermobox can be considered to have the same thermal properties.

In this condition, the power supplied by the regular heater, $\dot{Q}_{box}$, can be measured by the Thermobox, along with the temperatures. At steady-state, this power will be lost through all six walls of the Thermobox. The total outside surface area of the Thermobox, $A_{box,o}$, can be taken as 1.172 m^2, as discussed in Section 3.1.2. For calculating h_o, Equation 4.5 can be used, which is derived from Equation 4.3.

$$h_o = \frac{\dot{Q}_{box}}{A_{box,o}(T_{w,o} - T_{room})} \tag{4.5}$$

This value of h_o can then be used as the heat transfer coefficient due to convection and radiation at the outer surface for all the samples, as the outside environmental condition of the samples remains the same, assuming the effect of material on h_o is neglectable.

From h_o, the total heat flux, $\dot{q}_{tot}$, for different samples can be calculated from Equations 4.3 and 4.4. The equation for calculating $\dot{q}_{tot}$ from h_o is shown in Equation 4.6.

$$\dot{q}_{tot} = h_o(T_{w,o} - T_{room}) \tag{4.6}$$

b) Heat Flux Method

The alternate way of measuring $\dot{q}_{tot}$ is the heat flux method. In this method, a heat flux sensor is used with the measurement samples to obtain the value of $\dot{q}_{tot}$ directly.

After obtaining the value of $\dot{q}_{tot}$, the thermal conductance of the sample, k_s, can be calculated from Equations 4.1 and 4.4, as presented in Equation 4.7.

$$k_s = \frac{\dot{q}_{tot}.d_s}{(T_{w,i} - T_{w,o})} \tag{4.7}$$

And the thermal transmittance of the sample, U_s, can be obtained by adapting Equation 2.17 for the Thermobox. U_s can be calculated by Equation 4.8.

$$U_{\mathrm{s}} = \frac{\dot{q}_{\mathrm{tot}}}{(T_{\mathrm{box}} - T_{\mathrm{room}})} \tag{4.8}$$

Equations 4.7 and 4.8 are the necessary equations for the steady-state measurements with the Thermobox.

4.1.2 Dynamic Measurement

For the Thermobox, the heatwave is propagated from inside the box to the outside. Thus, Figure 2.5 is adapted for the Thermobox. The dynamic heat transmission through a measurement sample, mounted on the Thermobox, is presented in Figure 4.2.

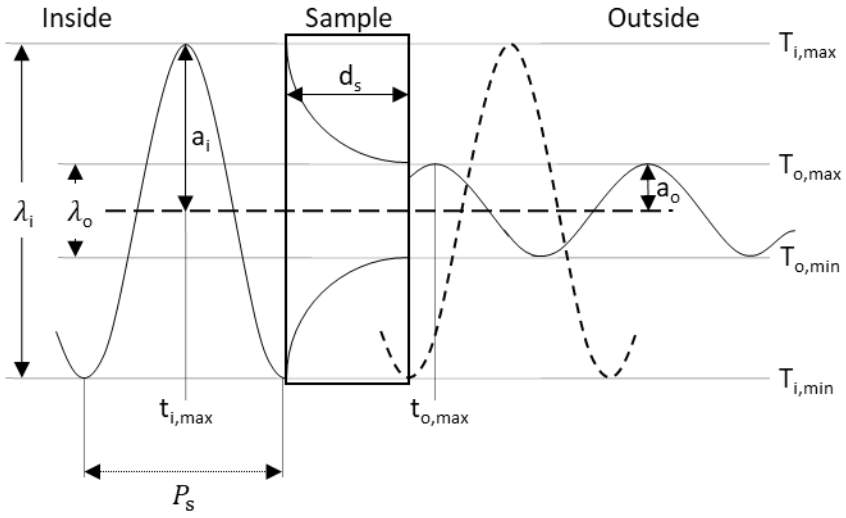

Figure 4.2: Dynamic heat transmission through a measurement sample. The heatwave is propagating from the inside of the box to the outside. Similar to Figure 2.5, a_{i} is the amplitude of the wave at the inner surface of the sample, and a_{o} is the amplitude of the wave leaving the sample. $T_{\mathrm{i,max}}$ and $T_{\mathrm{i,min}}$ are respectively the maximum and the minimum inside surface temperatures, $T_{\mathrm{o,max}}$ and $T_{\mathrm{o,min}}$ are respectively the maximum and the minimum outside surface temperatures. $t_{\mathrm{i,max}}$ is the time when the inside surface temperature is $T_{\mathrm{i,max}}$, $t_{\mathrm{o,max}}$ is the time when the outside surface temperature is $T_{\mathrm{o,max}}$, and P_{s} is the period of wave propagation for a sample. λ_{i} and λ_{o} are the peak-to-peak amplitude of the propagating wave at the inner surface and the outer surface respectively, where $\lambda_{\mathrm{i}} = 2a_{\mathrm{i}}$ and $\lambda_{\mathrm{o}} = 2a_{\mathrm{o}}$.

From Figure 4.2, the time lag, τ_{s}, and the decrement factor, f_{s}, of the sample can be calculated by using Equations 4.9 and 4.10.

$$\tau_s = \begin{cases} t_{o,max} - t_{I,max}; when\ t_{o,max} > t_{I,max} \\ t_{o,max} - t_{I,max} + T; when\ t_{o,max} < t_{I,max} \\ T; when\ t_{o,max} = t_{I,max} \end{cases} \quad (4.9)$$

$$f_s = \frac{\lambda_o}{\lambda_i} = \frac{T_{o,max} - T_{o,min}}{T_{I,max} - T_{I,min}} \quad (4.10)$$

Once the time lag and the decrement factor are obtained from dynamic measurements, thermal diffusivity of a sample, α_s, can be calculated from the obtained values. α_s is calculated from the time lag by using Equations 2.21 and 2.25 and is shown in Equation 4.11.

$$\alpha_s = \frac{P_s}{4\pi} . \left(\frac{d_s}{\tau_s}\right)^2 \quad (4.11)$$

Where P_s is the period of wave propagation for a sample.

Thermal diffusivity can also be calculated from the decrement factor by using Equations 2.21 and 2.26 and is shown in Equation 4.12.

$$\alpha_s = \frac{\pi}{P_s} \left(\frac{d_s}{\ln f_s}\right)^2 \quad (4.12)$$

The specific heat capacity at constant pressure of the sample material, $c_{p,s}$, is calculated by solving Equation 2.24, which leads to Equation 4.13.

$$c_{p,s} = \frac{k_s}{\rho_s \alpha_s} \quad (4.13)$$

Where ρ_s is the density of the sample material. Finally, the thermal mass of a sample, $M_{th,s}$, can be calculated from Equation 2.29 and is shown in Equation 4.14.

$$M_{th,s} = \rho_s c_{p,s} \times 10^{-3} \quad (4.14)$$

Equations 4.11, 4.12, 4.13, and 4.14 are the necessary equations for the dynamic measurements with the Thermobox.

4.2 Reference Thermal Properties of the Sample Materials

In this thesis, different thermal properties are measured experimentally with the Thermobox through steady-state measurements and dynamic measurements. To determine the accuracy of the measurements with the Thermobox, these values are compared to reference or literature values. Thus, it is important to obtain reference values for the sample materials.

As discussed in Section 3.1.4, four of the samples are made of multiple materials, acting as composite walls. The thermal properties of these composite samples are needed to be calculated.

The thermal properties calculated in this thesis are thermal conductance and thermal transmittance from steady-state measurements, and thermal diffusivity, specific heat capacity and thermal mass from dynamic measurements. The reference values of these parameters for different sample elements are discussed in the following sections.

4.2.1 Reference Values for Steady-state Measurements

Equation 4.1 is the equation for heat conduction through a measurement sample of the Thermobox, as discussed in Section 4.1.1.

$$\dot{q}_{\mathrm{s}} = \frac{k_{\mathrm{s}}}{d_{\mathrm{s}}}(T_{\mathrm{w,i}} - T_{\mathrm{w,o}})$$

The term $\frac{d_{\mathrm{s}}}{k_{\mathrm{s}}}$ is the thermal resistance due to conduction through a unit area, r_{cond}, which can be derived from Equation 2.5. As the r_{cond} of the materials of a composite sample are in series connection, they can be simply added to obtain the total thermal resistance due to conduction through a unit area of a composite sample, $r_{\mathrm{cond,tot}}$. This is shown in Equation 4.15.

$$r_{\mathrm{cond,tot}} = \frac{d_{\mathrm{s,tot}}}{k_{\mathrm{s,tot}}} = \frac{d_{\mathrm{s,1}}}{k_{\mathrm{s,1}}} + \frac{d_{\mathrm{s,2}}}{k_{\mathrm{s,2}}}\left(+\frac{d_{\mathrm{s,1}}}{k_{\mathrm{s,1}}}\right) \tag{4.15}$$

Where $d_{\mathrm{s,tot}}$ and $k_{\mathrm{s,tot}}$ are respectively the total thickness and the combined thermal conductance of the composite sample. The subscripts 1 and 2 stand for the two materials of a composite wall. The term in the bracket is used when considering the samples with double glazing, as they have three layers, and the first and the third layers are identical.

From literature values of $k_{\mathrm{s,1}}$ and $k_{\mathrm{s,2}}$, the reference value of the total thermal conductance of a composite wall can be calculated by using Equation 4.15.

Literature thermal conductances of different materials relevant to this thesis are presented in Table 4.

Table 4: Thermal conductance of relevant materials

Material	Reference thermal conductance in W/m.K	Source literature for the reference values
MDF	0.16 (for a density of 1000 kg/m^3)	(Rebolledo et al. 2018)
UHPC	1.8-2.2	(Toman and Černý 2001, p. 9)
PUR	0.022-0.023	(Bauder 2014)
Glass	0.95	(Shackelford and Alexander 2001)
Air	0.0285 (at 330 K and 0.1 MPa)	(Vargaftik 1994, p. 49)
Argon	0.0193 (at 330 K and 0.1 MPa)	(Younglove and Hanley 1986, p. 1333)

Table 5 shows the reference values of the thermal conductances of the Thermobox measurement samples. These values are either directly taken or calculated from Table 4. These are the thermal conductances, which are later used as references for comparing the experimental thermal conductance values determined from the steady-state measurements with the Thermobox.

Table 5: Thermal conductance of the measurement samples, used as references for the steady-state measurements

Measurement sample	**Reference thermal conductance in W/m·K**
MDF without insulation	0.16
MDF with inside insulation	0.025-0.030
UHPC without insulation	1.8-2.2
UHPC with outside insulation	0.031-0.032
Single Glass	0.95
Double glazing with air	0.042
Double glazing with argon	0.029

Another parameter determined in this work with steady-state experiments is thermal transmittance or the U-value. Thermal transmittance depends not only on the material itself but also on the thickness of the material and its surrounding environment, meaning the convective and radiative heat transfer coefficients. These coefficients vary depending on the direction and the speed of the wind, and the roughness of the material surface (Evangelisti et al. 2016). Therefore, it becomes difficult to compare the measured thermal transmittance of the Thermobox measurement samples to standard or literature values, as different measurement principles have different environmental conditions, leading to different values of heat transfer coefficients.

Thus, the thermal transmittance of different measurement samples are calculated experimentally in this thesis, but unlike the thermal conductance values, no comparison was made to standard or literature values.

4.2.2 Reference Values for Dynamic Measurements

Thermal diffusivity, specific heat capacity and thermal mass are calculated experimentally from dynamic experiments with the Thermobox. Dynamic measurements are conducted on selected samples, namely MDF, UHPC and single glass. As discussed in Section 4.1.2, another important parameter for dynamic calculation is the density of the sample elements. The density of the MDF sample, the UHPC sample and the single glass sample are determined experimentally in the lab by measuring the weights and the volumes of the samples. The thermal conductance and the specific heat capacity of the samples are taken from literature. From the aforementioned values, reference values of thermal diffusivity and thermal mass can be calculated by Equations 4.13 and 4.14.

The measured values of density, the literature specific heat capacity, and the calculated reference values of thermal diffusivity and thermal mass for the three selected samples are presented in Table 6.

Table 6: Mass, density, specific heat capacity, thermal diffusivity and thermal mass of MDF, UHPC and single glass, used as the reference for dynamic measurements

Measurement sample	Mass in kg	Density in kg/m³	Specific heat capacity in J/kg.K	Thermal diffusivity in 10^{-7} m²/s	Thermal mass in kJ/m³.K
MDF	2.03	1097.5	1400 (Li 2013, p. 776)	1.04	1536.5
UHPC	6.33	3422.3	850 (Sudholt-Wasemann 2019)	7.56	2909.0
Single glass	1.53	3308.8	720 (AGC 2011)	3.99	2382.4

4.3 Modifications of the Thermobox

An important part of this thesis is modifying the Thermobox, aiming for improving its heat transfer performance. These modifications are discussed in the following sections.

4.3.1 Sample Side Insulation

The thermal imaging of the measurement sample UHPC with the thermal camera reveals that extensive heat is lost from the side of the sample. The main heat loss area is at the gap between the MDF frames holding the sample. An additional heat loss occurs at the gap between the frame and the Thermobox. This thermal image is shown in Figure 4.3.

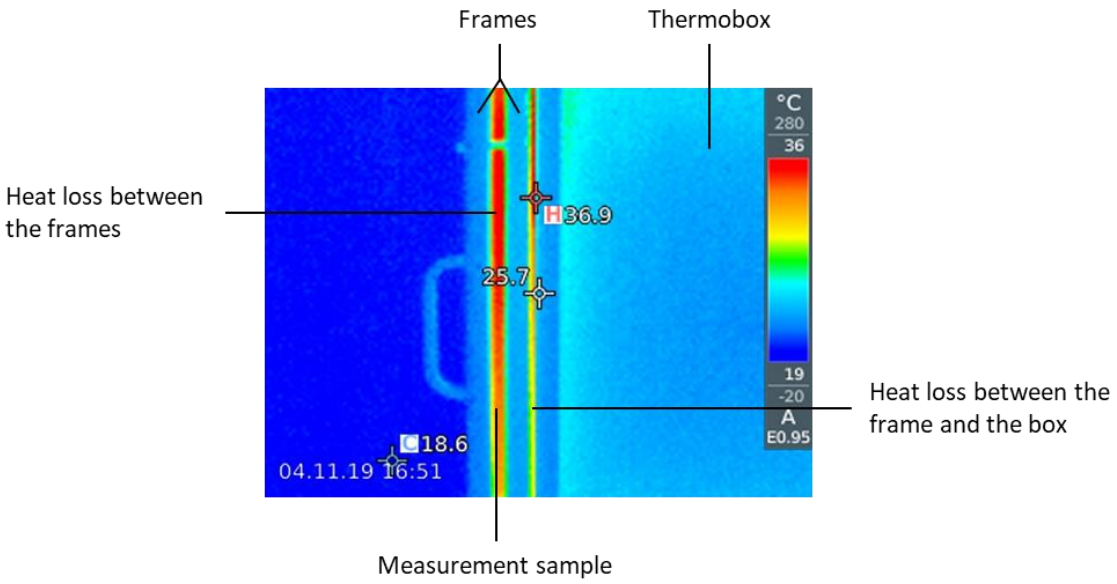

Figure 4.3: Thermal imaging of the UHPC sample from the right side. The red areas are the heat loss areas at the side of the sample.

As a measure to reduce the heat loss through the gap between the frames of the sample, insulation stripes are fixed in the gap of the frame for each sample. The effect of implementing this side insulation on the UHPC sample is discussed in Section 5.1.2.

4.3.2 Painting the Inside of the Heating Chamber Black

The heating chamber of the Thermobox, as discussed in Section 3.1, consists of a 40 mm layer of polyurethane insulation. This layer is covered with a layer of aluminium foil. The thermal performance of the aluminium foil, observed with an emissiometer, reveals that it has an emittance of 31.6 %. As $emittance + reflectance = 1$, the aliminium foil has a reflectance of 68.4 %. This high value of reflectance leads to a high reflection of heat from the aluminium foil, which can have an interfering influence on the sensors inside the chamber of the Thermobox. This can negatively affect the measurements. Additionally, according to Bartl & Baranek (2004), aluminium has a varying emittance withing a range of 0 µm and 10 µm, as shown in Figure 4.4. This irregular emittance can also contribute to the interfering influence on the sensors inside the heating chamber.

As an attempt to improve this radiation effect, the heating chamber of the Thermobox is decided to be painted. As for colours, either black or white is considered. The emittance values are 94.8 % and 97.5 % respectively for white paint and black paint, as measured with the emissiometer.

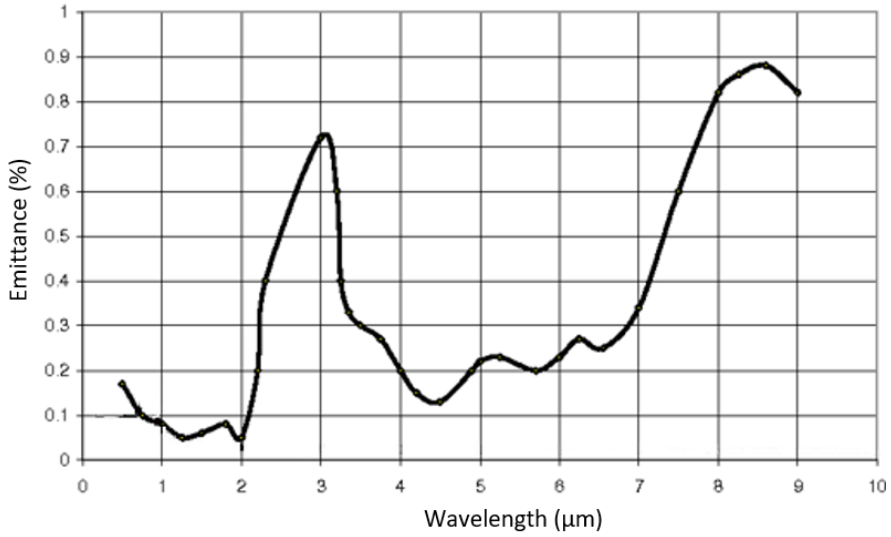

Figure 4.4: Emittance of aluminium within a wavelength range of 0 µm and 10 µm. From about 0.5 µm, the emittance fluctuates irregularly over the wavelength range (Bartl and Baranek 2004)

Taking a further look at the absorptance and the reflectance of the paints, from Howell et al. (2011, pp. 107–108), it is seen that white has high reflectance at shorter wavelengths, and at longer wavelengths, the reflectance decreases. Black paint, on the other hand, has low reflectance over the same wavelength range. This is presented in Figure 4.5.

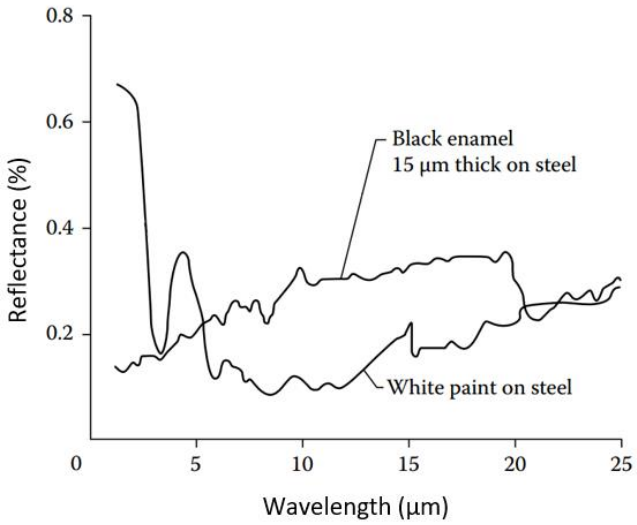

Figure 4.5: Comparison of reflectance of black and white paint on a metallic (steel) surface (Howell et al. 2011, p. 108). For white, the reflectance is high at short and low at long wavelengths, whereas black has an overall low reflectance.

A similar trend is also observed for absorptance by Silverman (1995). According to his report, black has almost a constant absorptance (and emittance) for all wavelengths, whereas white has low absorptance at shorter wavelengths and high emittance at longer wavelengths, as shown in Figure 4.6.

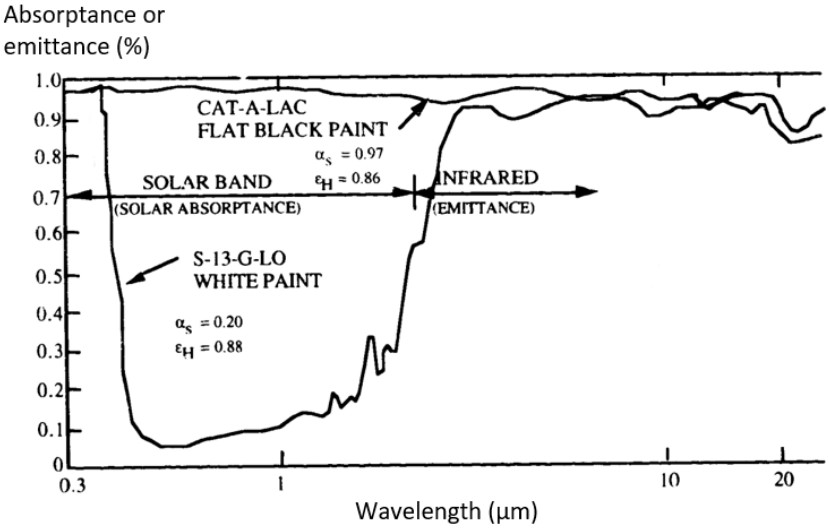

Figure 4.6: Absorptance or emittance of black and white paint, adapted from Silverman (1995). At longer wavelengths, the paint has a similar response, but at shorter wavelengths, white has low absorptance.

To summarize, aluminium has an irregularly fluctuating emittance (Figure 4.4), white paint has low absorptance and high reflectance at shorter wavelengths and high emittance and low reflectance at longer wavelengths, and black paint has high absorptance and high emittance but low reflectance over a similar wavelength range (Figure 4.5 and Figure 4.6). Thus, black paint is selected for painting the inside of the

heating chamber of the Thermobox to achieve a more uniform radiation effect while performing the measurements.

4.3.3 The Direction of Air Circulation

The air circulation by the fans inside the heating chamber is initially directed upwards. Observing the measurement samples with the thermal imaging camera, it is detected that the upper portion of the samples reaches a higher temperature compared to the lower portion, as shown in Figure 4.7.

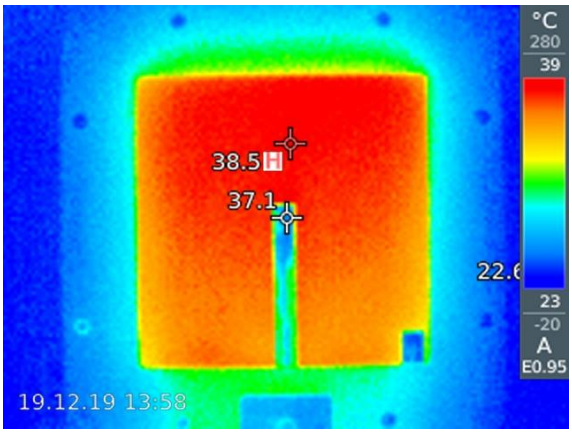

Figure 4.7: Thermal imaging of the MDF sample from the front. The temperature is higher at the top and lower at the bottom.

This inhomogeneous distribution of temperature on the sample may lead to defective measurements. The reason behind the higher temperatures at the top of the box, and consequently, at the top of the samples may be the direction of air circulation. As the air heats up, it becomes less dense and moves upwards. Additionally, the fans are also moving the air upwards, forcing hot air to reach the top of the sample first. As a result, both the natural and the forced circulations cause the hot air to flow upwards, and the temperature at the top becomes higher than the bottom.

As an attempt to improve this situation, the fan directions are inverted, so that the air circulation by the fans.is now downwards It is expected that the hot air will flow downwards to upwards by natural circulation inside the heating chamber, and by forced circulation, hot air will reach the bottom part of the sample first, and consequently, more uniform heating of the samples can be achieved.

To change the direction of airflow, the rear wall of the Thermobox is detached from the heating chamber by removing the screws. The fans, as well as the heating plates, are mounted on the rear wall. The fans are then detached from their mounting, inverted, and reattached. After that, the rear wall is attached back to the heating chamber.

4.4 Advancements of Steady-state Measurements

The modifications of the Thermobox are followed by steps to improve the steady-state measurements with the Thermobox. These advancements are the implementation of the PID controller and the installation of the heat flux sensor.

4.4.1 Implementation of the PID Controller

To achieve better temperature control for the Thermobox, a PID controller is implemented into the Labview software for the Thermobox. The motivation for the controller and its implementation, as well as controller parameterization, are discussed in the following sections.

a) Motivation and Controller Implementation

The Thermobox has manual control for the power of the regular heater for controlling the temperature inside the heating chamber, T_{box}. As discussed in Section 3.1.6, the power of the regular heater needs to be frequently adjusted to keep T_{box} at its target value, which requires constant supervision and can be inconvenient for the user. This also increases the chance of human error. A PID controller is thus implemented in an attempt to replace the manual power control with an automated one.

The software used to perform the experiments for this thesis, LabView, consists of a PID toolkit, labelled as PID.vi. This toolkit is implemented into the block diagram of the Thermobox software. At the setpoint of the PID.vi, the target value of T_{box} can be adjusted. T-box is set as the process variable, which means that the PID toolkit will operate to keep T-box at the set value of T_{box}. The output is set as heating power, which means that the PID toolkit will adjust the power of the regular heater by comparing the value of T-box to the defined set point. A switch is also implemented, which can be used to switch between the manual control and the PID control. The PID gains of the toolkit are the PID control parameters, K_{p}, T_{i} and T_{d}. These parameters can be calculated by performing step tests for each sample. The block diagram for implementing the PID controller into the software is presented in Figure C-1 in Appendix C.

b) Step Test for Controller Parameterization

To perform the step test, the response of T_{box} is observed for a step-change in the power of the regular heater. To do so, a sample is mounted on the Thermobox and the power of the regular heater is kept at 0%. After a short time, the power is directly increased to 60%, and the progression of T_{box} is recorded and observed. This step test is performed until T_{box} becomes constant. Individual tests are conducted with all the samples, as each sample responds differently to the change in power.

Followed by the step tests, the step response curves are plotted (Figure B-1.in Appendix B shows the step response curve of the MDF sample), and as discussed in Section 2.3.4, initial values of the control parameters, K_{p}, T_{i} and T_{d}, are determined. Starting with these initial values, the PID controller is tested by performing steady-state measurements on the measurement samples with the PID controller. The progression of T_{box} is observed during these measurements. With the initial values of the parameters, T_{box} for each sample is observed to have high fluctuations. The parameters are then manually adjusted so that a stable control can be achieved. This further tuning of the controller leads to the final values of K_{p}, T_{i} and T_{d} for each measurement sample. Once the final values of the control parameters are determined, steady-state measurements are performed on each sample to check the usability of the PID controller.

4.4.2 Installation of the Heat Flux Sensor

In order to integrate the heat flux sensor to the Thermobox, wires are soldered to the connection points, and proper connections are made with the data logger. The installed heat flux sensor on a measurement sample is presented in Figure 4.8.

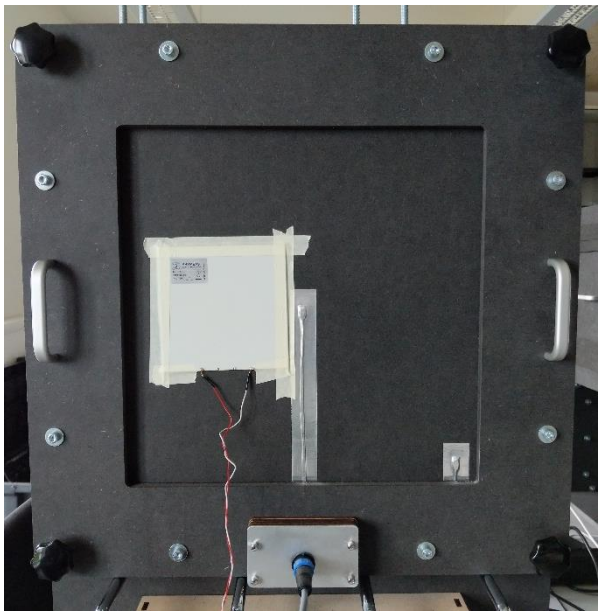

Figure 4.8: Photograph showing a measurement sample (MDF) with the heat flux sensor. The sensor is installed with adhesive tape. The red and the white wires are connected to the data logger in the control unit.

As only one heat flux sensor is used for the measurements, the sensor is connected only to the main Thermobox. As a result, steady-state measurements with the heat flux method can only be performed with the main Thermobox. Necessary adjustments are done to the main LabView programme so that the voltage output of the sensor, V_{th}, is displayed and saved as the heat flux, $\dot{q}_{\mathrm{tot}}$ (shown in Figure C-2 in Appendix C). As the same heat flux sensor is used for all the measurement samples, the sensor is mounted on the samples with a simple adhesive tape for quick installation and removal.

After installing the heat flux sensor, steady-state experiments are performed on all the samples to determine the values of thermal transmittance, U_{s}, and thermal conductance, k_{s}, using the heat flux method. The value of h_{o} is also calculated and compared with the values of h_{o} from literature and the experiment. The heat flux measurements are conducted at three different temperatures inside the Thermobox (50 °C, 60 °C and 70 °C),

4.4.3 Modifications in the Software Interface

After implementing the PID controller into the LabVIEW software, and installing the heat flux sensor and connecting it to the control unit, the software interface, shown in Figure 3.10, is also modified so that the control parameters and the setpoint for the PID controller can be adjusted, and the output of the heat flux sensor is displayed at the software interface. The modified Heating Control section of the software interface is shown in Figure 4.9.

In the modified interface, the Heat Flux [W/m^2] box displays the heat flux through the measurement samples, measured by the heat flux sensor. In the Set Point box, the set point of the PID controller can be defined. The control parameters can be adjusted in the PID gains box. The PID switch, which is at the bottom left corner of the Heating Control section, can be used to switch between manual control and automatic (PID) control.

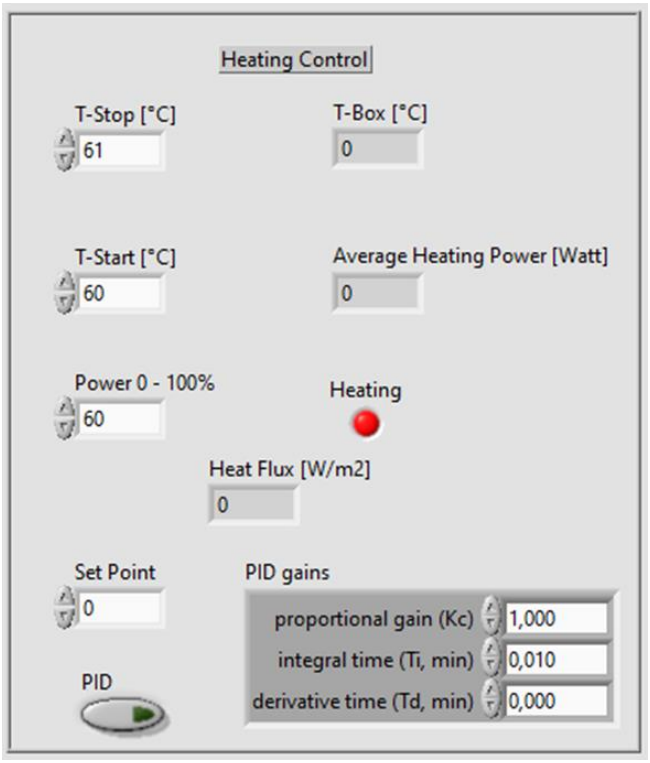

Figure 4.9: Modified Heating Control section of the Thermobox software interface, adjusting to the implementation of the PID controller and the heat flux sensor

4.5 Implementation of Dynamic Measurements

To perform dynamic measurements with the Thermobox, a cyclic temperature profile is needed to be applied to a sample. To that extent, the temperature inside the Thermobox, T_{box}, is needed to be changed periodically. This periodical change in T_{box} will also cause the temperatures at different sensors to shift accordingly, and a sinus heatwave propagation through a sample can be achieved.

The Thermobox, as discussed previously, comprises control only for heating. The cooling, however, cannot be controlled. Once heated up, the Thermobox, along with all its components, needs to cool down naturally. As each measurement samples have distinct thermal properties, the time required for cooling the heating chamber of the Thermobox, t_{cool}, will be different for different samples and different inside temperatures. Because the Thermobox does not consist of a cooling system, this t_{cool} cannot be adjusted. On the other hand, the time required for heating, t_{heat}, can be adjusted with the manual heating control. Since t_{cool} and t_{heat} are required to be equal for achieving a sinus heatwave, t_{heat} needs to be modified according to t_{cool} for each sample. As a first step towards the dynamic measurements with the

Thermobox, t_{cool} and t_{heat} for the MDF sample, the UHPC sample and the single glass sample are investigated.

The time required for cooling, t_{cool}, of the Thermobox with a specific sample needs to be determined first before t_{heat} can be investigated. To do so, the sample is heated with T_{box} at 60 °C until it reaches steady-state. From there, T_{box} is increased to 70 °C, and then the heater is turned off so that T_{box} cools down to 50 °C. The time required for T_{box} to drop from 70 °C to 50 °C, t_{cool}, is subsequently measured for each sample.

Once t_{cool} of a sample is determined, the percentage of heating power required to increase T_{box} from 50 °C to 70 °C, H_{per}, is modified through trial and error so that t_{heat} becomes equal to the measured t_{cool}. For example, if at 80 % power, t_{heat} is less than t_{cool}, this would mean that the heating phase is faster than the cooling phase, and the percentage of heating power needs to be decreased to slow down the heating process.

4.6 Performed Measurements

Steady-state measurements are performed with the Thermobox before and after implementing the modifications. These measurements are conducted with manual control. Further steady-state measurements are performed with the heat flux sensor at different T_{box}. These measurements are conducted with the PID controller. Then H_{per} is determined for MDF, UHPC and single glass, and dynamic measurements are performed on these samples. Finally, five identical steady-state measurements are performed on the MDF sample for conducting a sensitivity analysis of the Thermobox measurements. The performed measurements are discussed below.

4.6.1 Primary Steady-state Measurement

Using the Thermobox at its manufactured condition, a set of primary steady-state measurements is performed on all the measurement samples. The experiments were conducted using the temperature method, as discussed in Section 4.1.1.

A measurement sample is first placed at the open face of the Thermobox and is tightened to secure its installation. Then the element is connected to the data logger through the connection cable (Figure 3.8). The Thermobox is subsequently turned on, and proper adjustments are made at the software, as shown in Figure 3.10. The primary measurement is done at a steady-state temperature of 60 °C, and the temperature is manually controlled. As the manual control is difficult, the control temperatures (T-Start and T-Stop, Figure 3.10a) are set from 60 °C to 65 °C. After that, the regular heater and the power heater are turned on. Once the power heater turns off automatically at about 40 °C, the switch of the power heater is manually turned off to avoid overheating.

The heating power of the regular heater is then manually controlled to keep T-box, which is the temperature inside the heating chamber, T_{box}, within the set range. The manual control is previously discussed in Section 3.1.6.

The same experiment is conducted for all seven measurement samples. The last ten minutes of the steady-state measurement data is recorded. Afterwards, the thermal conductance, k_{s}, and the thermal

transmittance, U_s, of each sample are calculated by the temperature method from the average value of the recorded temperatures with the literature value of h_o (7.69 W/m^{2}K). The calculated values are presented and discussed in Section 5.1.1.

4.6.2 Steady-state Measurements with Black Paint

After implementing side insulations on the samples and painting the inside of the heating chamber of the Thermobox black, a set of steady-state measurements is performed on all the measurement samples. The measurements are conducted with the manual control of power. The target value of T_{box} is 60 °C, similar to the primary steady-state measurements. To that extent, T-Stop and T-Start are set to 62 °C and 60 °C, respectively. Afterwards, k_s and U_s are calculated for each sample by the temperature method. The literature value of h_o, 7.69 W/m^{2}K, is used for the calculation. The effect of the black paint on the measurement results is discussed in Section 5.1.2.

4.6.3 Steady-state Measurements with Inverted Fan Direction

Once the heating chamber is painted black and steady-state measurements are performed with the black paint, the fan direction is inverted and another set of steady-state measurements is performed on all the measurement samples. Similar to the previous two measurements, the steady-state measurements with inverted fan direction are also performed with manual control, with a target T_{box} of 60 °C and with set values of T-Stop and T-Start at 62 °C and 60 °C, respectively. After performing the measurements, k_s and U_s are calculated for each sample by the temperature method. For the calculation, the literature value of h_o, 7.69 W/m^{2}K, is used. Further calculations are then done to obtain k_s and U_s for each sample with the experimental value of h_o. The calculated k_s and U_s of the samples are then compared for both values of h_o.

The effect of changing the direction of the fans on the measurement results is discussed in Section 5.1.2. The comparison of the calculations performed with the literature and the experimental values of h_o is also discussed in Section 5.1.2.

4.6.4 Steady-state Measurements with Heat Flux Method via PID Control

For steady-state measurements with the heat flux method, the PID controller is used to control the power of the regular heater for maintaining the target value of T_{box}. The measurement procedure is thus marginally different from the previous steady-state measurements.

The measurement sample is first attached to the open face of the Thermobox and is connected to the electronic unit. Then the heat flux sensor is fixed to the outside surface of the sample with an adhesive tape. The sensor is placed next to the temperature sensor on the centre of the outside surface. It is ensured that there is no gap between the sensor and the surface of the sample. Afterwards, the PID switch is turned on in the software interface. The set point is defined, and the control parameters of the measurement sample obtained from Section 4.4.1 are inputted as PID gains. The heaters are then turned on as before, and the measurement is performed until the sample reaches steady-state. Similar to previous measurements, ten minutes of steady-state data is recorded, and k_s and U_s of all the samples are calculated with both the heat flux method and the temperature method, so that a comparison between

the two methods can be made. For the temperature method, the literature value of h_o, 7.69 W/m^{2}K, is used.

Steady-state measurements with the heat flux method are performed with three different set values of T_{box}, which are 50 °C, 60 °C and 70 °C. k_s and U_s of the samples are calculated for each value of T_{box}, and a comparative analysis is performed. The value of h_o is also calculated from the heat flux method, and is compared to the literature value.

The measurement results of the heat flux method are discussed in Section 5.1.4.

4.6.5 Sensitivity Analysis

To analyze the reliability of each measurement performed with the Thermobox, a sensitivity analysis is conducted. The analysis is done by performing five identical steady-state measurements on the MDF sample with the heat flux method. These five measurements are then compared to obtain the standard deviation of the Thermobox measurements.

The target value of T_{box} is set as 60 °C, and the PID controller is used for controlling the heating power. The last ten minutes of the steady-state is recorded, and k_s and U_s are subsequently calculated with both the heat flux method and the temperature method. The literature value of h_o (7.69 W/m^{2}K) is used for calculating with the temperature method. Such measurements are performed on the MDF sample five times, and from the calculated values of k_s and U_s, the standard deviation of the measurements can be determined by adapting 2.33 for the Thermobox. The standard deviation of k_s is calculated by Equation 4.16 and the standard deviation of U_s is calculated by Equation 4.17.

$$SD_{k_s} = \sqrt{\frac{\sum(k_s - \bar{k}_s)^2}{5}} \tag{4.16}$$

$$SD_{U_s} = \sqrt{\frac{\sum(U_s - \bar{U}_s)^2}{5}} \tag{4.17}$$

Where SD_{k_s} is the standard deviation of the calculated k_s values, SD_{U_s} is the standard deviation of the calculated U_s values, $\bar{k}_s$ is the mean value of the calculated k_s values, and $\bar{U}_s$ is the mean value of the calculated U_s values.

The standard deviation can be used to assess the reliability of the Thermobox measurements. The sensitivity analysis is discussed in Section 5.1.5.

4.6.6 Dynamic Measurements

Once H_{per} has been determined for MDF, UHPC and single glass, the dynamic behaviour of the samples can be investigated with the Thermobox.

At first, steady-state experiment is performed on a measurement sample with T_{box} at 60 °C. The heating power is controlled with the PID controller to reach steady-state. Once steady-state is reached, the PID controller is switched off, shifting the heating power to manual control. Afterwards, T_{box} is further

increased to 70 °C. The power of the heater during this heating process is set at H_{per}. This is the initiation of the heatwave.

After T_{box} reaches 70 °C, the heater is manually turned off. T_{box} still slightly increases for a short while. The Thermobox then starts to cool down and temperatures start to gradually decrease. T_{box} eventually reaches 50 °C after t_{cool}, and the heater is again manually turned on at H_{per} so that T_{box} is once more increased to 70 °C. T_{box} slightly decreases for a short while before the box starts to heat up again. A cooling phase from 70 °C to 50 °C and a consequent heating phase from 50 °C to 70 °C together form a cycle. Three of these cycles are repeated, and the data is stored.

For investigating the dynamic behaviour of the samples, it is necessary to observe the temperature profiles at the inside surface and the outside surface of the samples. Therefore, from the experimental data, the inside centre temperature and the outside centre temperature of the sample are plotted over time to generate a heatwave propagation graph. This is done for each sample on which dynamic experiments are performed. From the graph, the time lag and the decrement factor, as well as the period of the wave, are determined. The thermal diffusivity, α_{s} the specific heat capacity, $c_{\mathrm{p,s}}$ and the thermal mass of the samples, $M_{\mathrm{th,s}}$, are then calculated using Equations 4.11, 4.13 and 4.14, described in Section 4.1.2. The calculated values are subsequently compared to literature. The results of the dynamic measurements are discussed in Section 5.2.

5 Results and Discussion

This chapter presents discussions on the results obtained from the experimental procedures described in Chapter 4. Steady-state measurement results from the temperature method and the heat flux method are analyzed. The influence of the Thermobox modifications on the steady-state measurements is also investigated. An additional discussion is presented on the effect of changing the temperature inside the Thermobox on the steady-state measurement results. The impact of the PID controller on the steady-state measurements is also observed. Additionally, the results of the sensitivity analysis of the steady-state measurements on the MDF sample are discussed. Finally, the results of the dynamic measurements are analysed.

5.1 Steady-state Measurements

Steady-state measurements are performed on all the measurement samples for calculating k_s and U_s of the samples from the measurement data. The calculated values are then compared to the reference values from Section 4.2.

5.1.1 Primary Steady-state Measurements

A graph showing the temperature progression of different sensors and the steady-state region is presented in Figure 5.1.

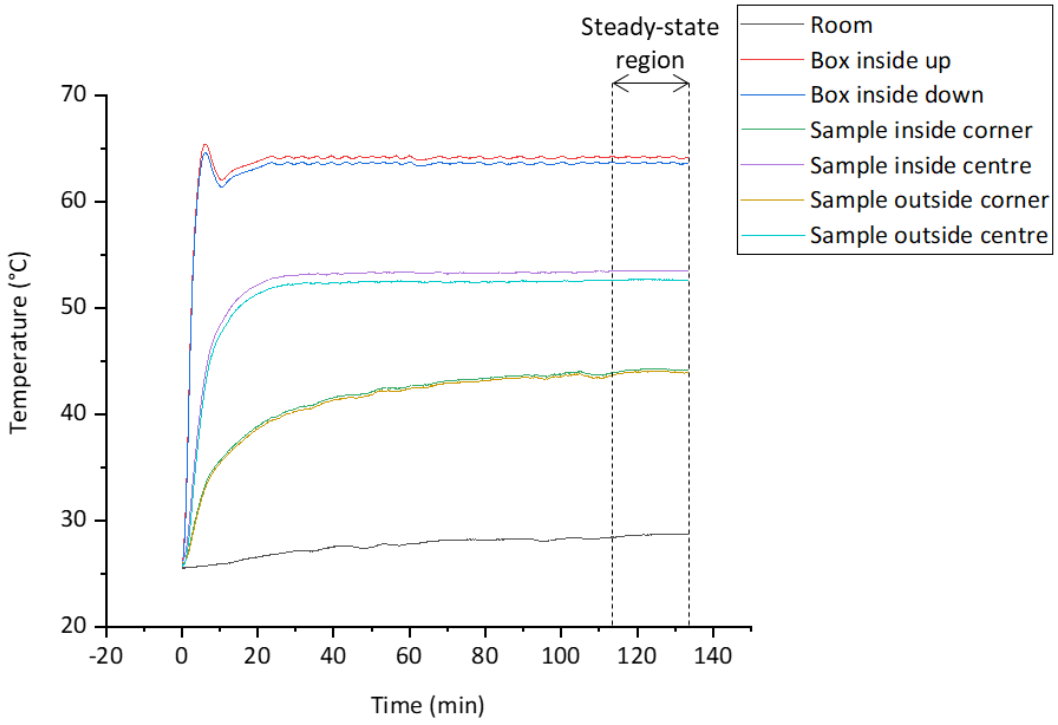

Figure 5.1: Temperature progression of different sensors of the single glass sample during the primary steady-state measurement

The single glass sample is taken as an example here. From the graph, it can be seen that the box inside temperatures and the temperatures at the centre of the inside surface and the outside surface of the

sample become stabilized after a short time. The temperatures at the corners, on the contrary, take longer to reach steady-state condition. Once all the temperatures reach steady-state, thermal conductance and thermal transmittance can be calculated from the temperature differences, as discussed in Section 4.1.1.

Similar temperature progression graphs can be plotted for all the other measurement samples for determining the steady-state region. The results of the primary steady-state measurements are discussed below.

a) Temperature Profile of the Samples

A closer look at the steady-state temperature profiles of the measurement samples can provide a better understanding of the thermal behaviour of the samples. Figure 5.2 presents the steady-state temperature profiles of the UHPC sample without insulation and the UHPC sample with insulation.

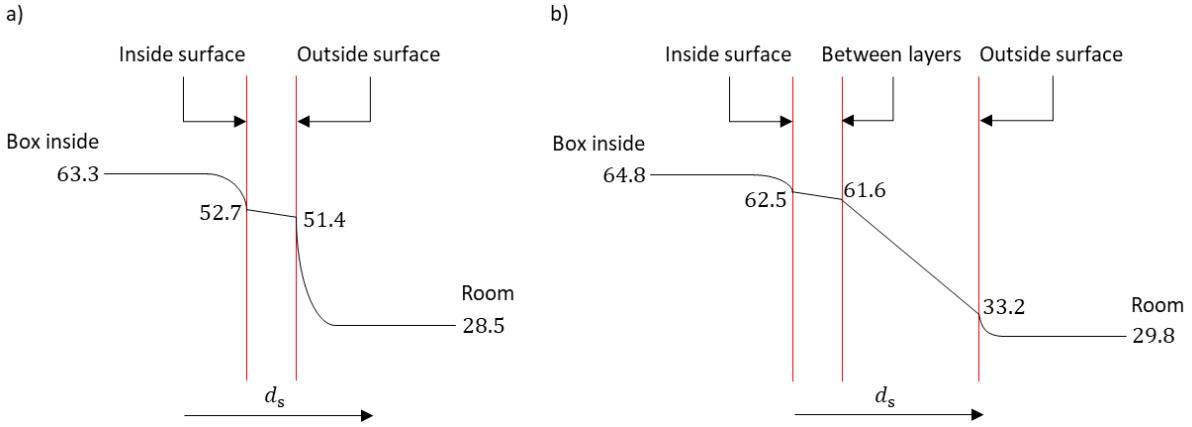

Figure 5.2: Temperature profile of a) UHPC without insulation and b) UHPC with outside insulation

It can be seen that UHPC, having a high thermal conductivity, has relatively close temperatures at the inside and the outside surfaces. On the other hand, UHPC with outside insulation has a much lower outside surface temperature. Thus, the heat loss is much lower for insulated UHPC as the outside surface temperature is much closer to the ambient temperature. The temperature profiles of the other samples can be found in Appendix D.

The measured temperatures from the primary steady-state measurements of different measurement points are presented in Table 7.

The behaviour of the measured temperatures of the samples can be explained by their thermal conductances. Comparing the data from the table, it can be seen that the temperature drop from the inside surface to the outside surface is much higher for MDF without insulation than UHPC without insulation. This is due to UHPC having a higher thermal conductance than MDF. The temperature drop from the inside surface to the outside surface is really small for the single glass sample, whereas the glass samples with double glazing have larger temperature drops. The reduction of temperature is higher for double glazing with argon than for double glazing with air, as the former has a smaller thermal conductance value than the latter.

Table 7: Steady-state temperatures at different measurement points of the Thermobox and the samples

Measurement sample	Temperature inside the Thermobox (°C)		Temperature at the inside surface (°C)	Temperature in between layers (°C)	Temperature at the outside surface (°C)	Room temperature (°C)
	Up	Down				
MDF without insulation	62.9	62.7	56.4	N/A	43.5	27.6
MDF with inside insulation	67.1	66.8	65.9	33.7	31.1	29.4
UHPC without insulation	63.4	63.1	52.7	N/A	51.4	28.5
UHPC with outside insulation	64.9	64.7	62.6	61.8	33.3	29.8
Single glass	64.2	63.6	53.5	N/A	52.6	28.7
Double glazing with air	65.2	64.7	57.6	N/A	41.7	28.5
Double glazing with argon	65.2	64.7	60.9	N/A	35.4	29.2

It can also be observed that the temperature in between the layers is much lower for MDF with insulation than UHPC with insulation. This can be explained by the position of the insulating layer. For the insulated UHPC sample, the insulation is on the outer side. As a result, the temperature remains high in the middle of the UHPC and the insulation (PUR) layers. On the other hand, the insulated MDF sample has inside insulation, and thus the temperature in the middle of the MDF and the PUR layers experiences a sharp drop from the inside surface temperature.

b) Thermal Conductance, k_s, and Thermal Transmittance, U_s

The calculated thermal conductance of different samples from primary steady-state measurements and their comparison with the reference values, as well as the experimental thermal transmittances are shown graphically in Figure 5.3. The values are also presented in Table E-1 in Appendix E.

From the bar chart, it can be seen that the UHPC sample without insulation has the highest thermal conductance among all the samples, and MDF with insulation has the lowest. Also in the case of thermal transmittance, the lowest value belongs to MDF with insulation. It can be seen that the single glass sample has the highest value of thermal transmittance among all the measurement samples. This is due to glass

having a high thermal conductance of 0.88 W/mK compared to other samples, and due to the single glass sample having a small thickness.

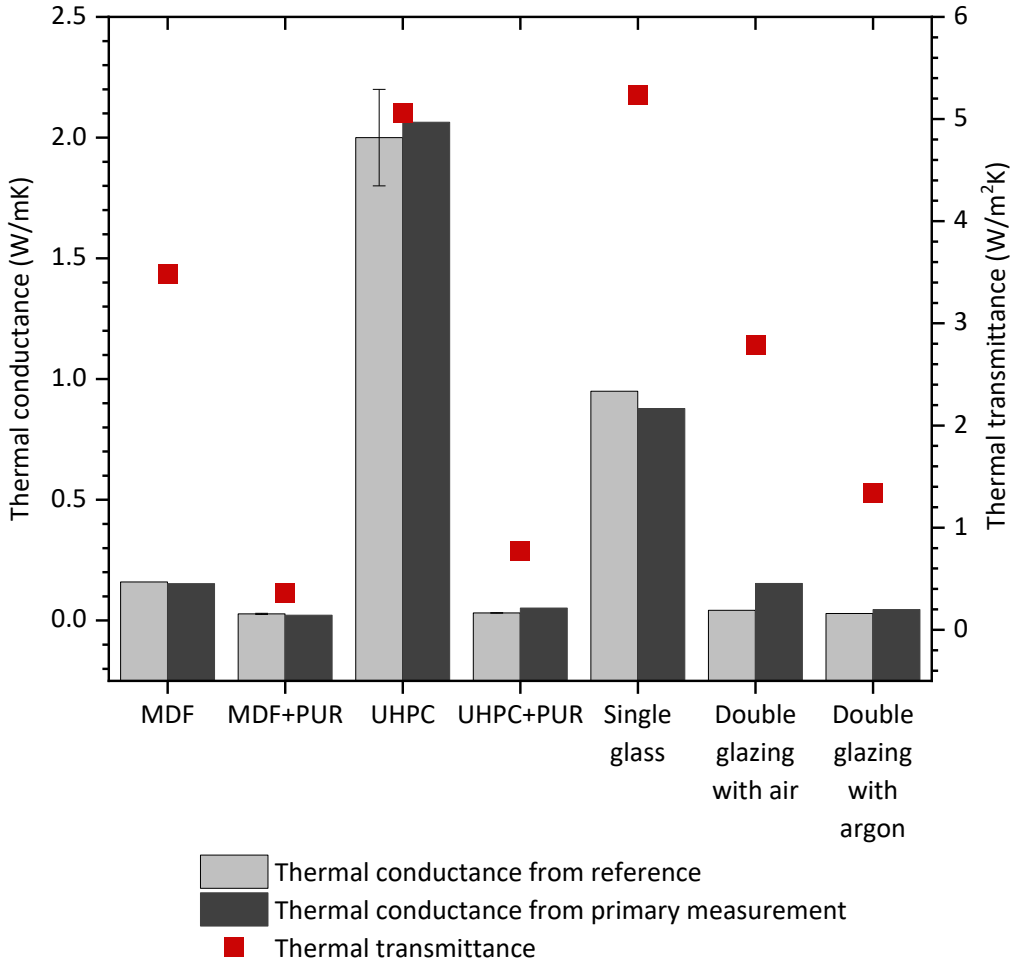

Figure 5.3: Graphical comparison of the reference (with range) and the experimental thermal conductance of measurement samples, along with the experimental thermal transmittance from the primary steady-state measurements

Calculating thermal conductance with $h_o = 7.69$ W/m²K, the experimental values for MDF and UHPC are within the range of the reference values. The calculated k_s for MDF with insulation is 12.4 % lower than the lower range of the reference value, and the calculated k_s for UHPC with insulation is 62.5 % higher than the reference value.

The glass samples have widely varying values. The single glass sample has a calculated thermal conductance, which is 7.6 % lower than the reference value. The calculated conductance value for double glazing with air is 0.15 W/mK and for double glazing with argon is 0.045 W/mK. The deviation from the reference is much higher for the samples with double glazing compared to the single glass sample. The experimental k_s of double glazing with air is about 266 % higher than the reference value and for double glazing with argon the experimental k_s is about 55 % higher than the reference value.

Thermal transmittance, U_S, of the measurement samples is also calculated by taking the value of h_o as 7.69 W/m^{2}K. It can be noticed that the addition of a PUR insulating layer with UHPC and MDF shows a significant reduction in the thermal transmittance. The value of thermal transmittance is also much lower for the double glazing samples compared to that of the single glass sample. This is due to the gaseous layers between the glass panes, which behave like insulating layers due to their low thermal conductance (Table 4). The double glazing with air sample has a higher thermal transmittance, consequently, a higher heat loss than the double glazing with argon sample, as the thermal conductance is higher for the former than the latter.

5.1.2 Influence of the Thermobox Modifications

The influence of the Thermobox modifications on the measurement samples and measurement results is discussed in this section.

a) Influence on the Measurement Samples

Examining the measurement samples with the thermal camera after each modification leads to the following observations.

Effect of Side Insulation and Black Paint

As discussed in Section 4.3.1, thermal imaging of the UHPC sample reveals heat loss through the sides. As an attempt to counter that, insulating stripes are implemented on the side of the samples. Figure 5.4 shows the effect of this side insulation on the UHPC sample.

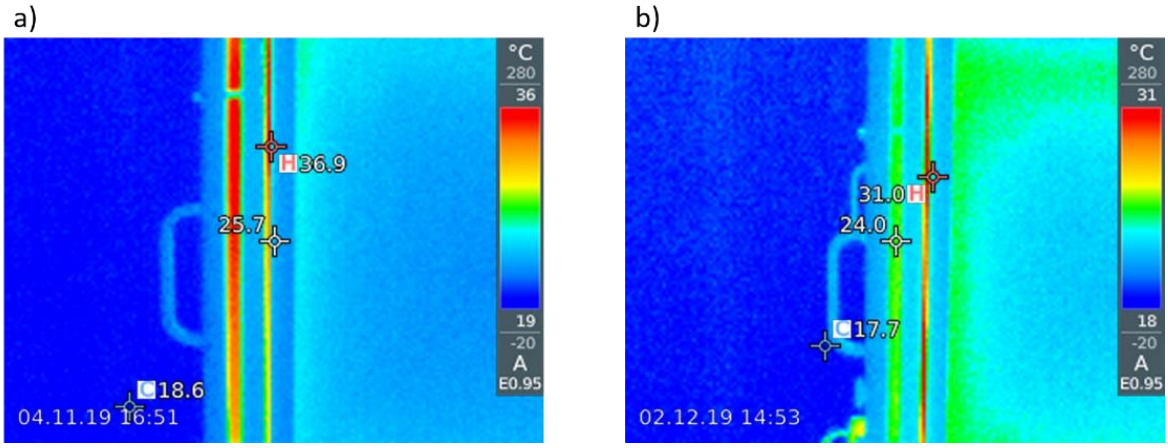

Figure 5.4: Thermal imaging from the side of the UHPC sample with a) no side insulation and b) with side insulation

As shown, the temperature at the gap between the frames drops from about 37 °C (from the colour profile) without side insulation to 24 °C with side insulation, thus reducing the heat loss through the sides of the sample. Depending on this observation, insulating stripes are also implemented on the sides of all the other samples.

After insulating the sides of the samples, the heating chamber of the Thermobox is painted black, and the influence of this modification is observed. Thermal images of the UHPC sample before and after implementing the black paint is shown in Figure 5.5.

The thermal images show that painting the heating chamber black has a small effect on the temperature profile of the samples. Implementing the black paint reduces the maximum temperature on the UHPC sample by 1.5 °C. It is also noticeable that the room temperature is higher in Figure 5.5b than in Figure 5.5a.

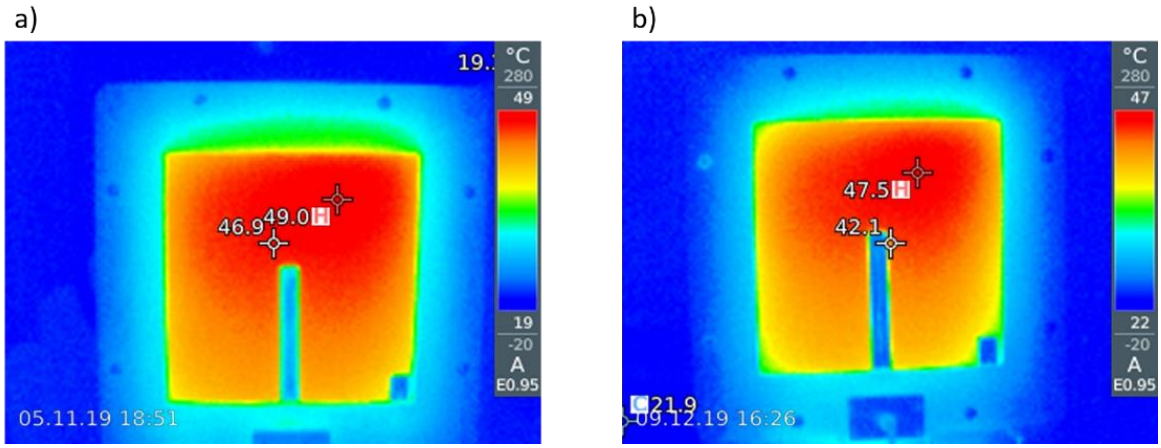

Figure 5.5: Thermal imaging of the front side of the UHPC sample with a) before painting the heating chamber ($T_{\mathrm{box}} = 61.5$ °C) and b) after painting the heating chamber ($T_{\mathrm{box}} = 61.7$ °C)

Effect of Changing the Direction of Air Circulation

After implementing the side insulation and the black paint, the direction of the fans is inverted. The thermal imaging of the MDF sample before and after changing the fan direction is presented in.Figure 5.6.

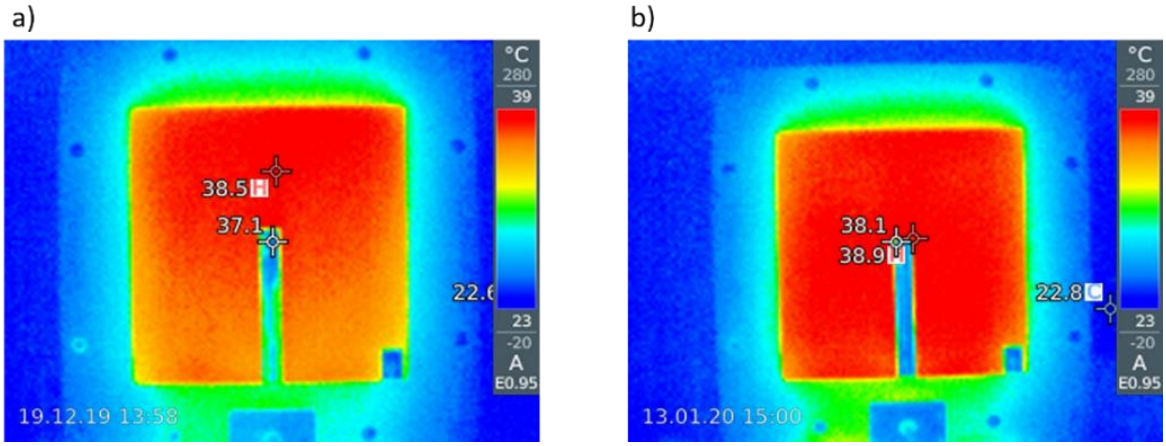

Figure 5.6: Effect of changing the direction of air circulation inside the Thermobox on the MDF sample, with a) original direction of air circulation and b) inverted direction of air circulation. The temperature profile is more distributed after the direction of the fans was changed.

It can be seen that changing the direction of air circulation has a positive effect on the MDF sample. The sample is now heated more uniformly, and as a result, a more uniform temperature distribution can be observed on the outer surface.

Thermal images showing the effect of changing the direction of air circulation on the UHPC sample is presented in Figure 5.7.

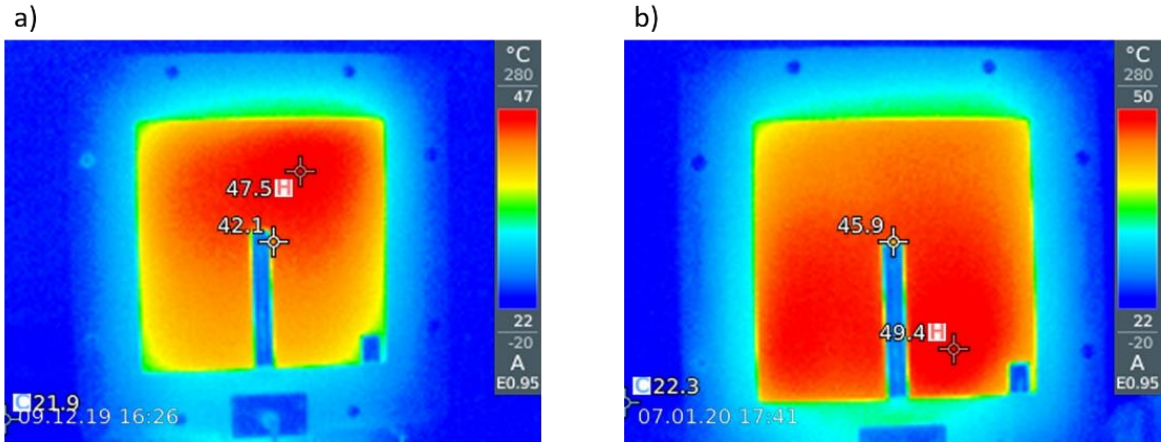

Figure 5.7: Effect of changing the direction of air circulation inside the Thermobox on the UHPC sample, with a) original direction of air circulation and b) inverted direction of air circulation. The temperature profile is more distributed after the direction of the fans was changed, with the hottest region shifting from the top of the sample to the centre and bottom, where the sensors are positioned.

Figure 5.8 and Figure 5.9 show the effect of changing the direction of air circulation on the MDF sample with inside insulation and the UHPC sample with outside insulation, respectively. It can be seen that changing the direction of the fans does not have a noticeable effect on the insulated samples.

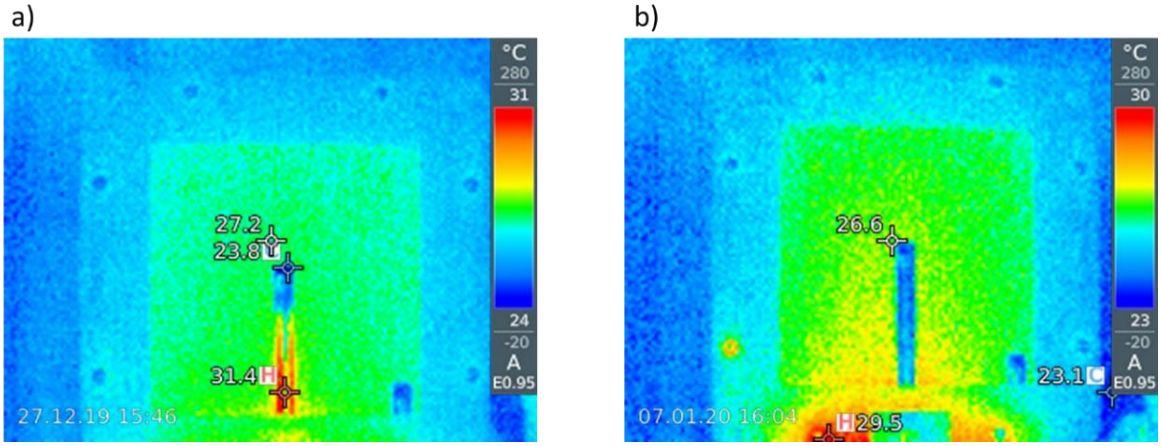

Figure 5.8: Effect of changing the direction of air circulation on the MDF sample with insulation, with a) original direction of air circulation and b) inverted direction of air circulation

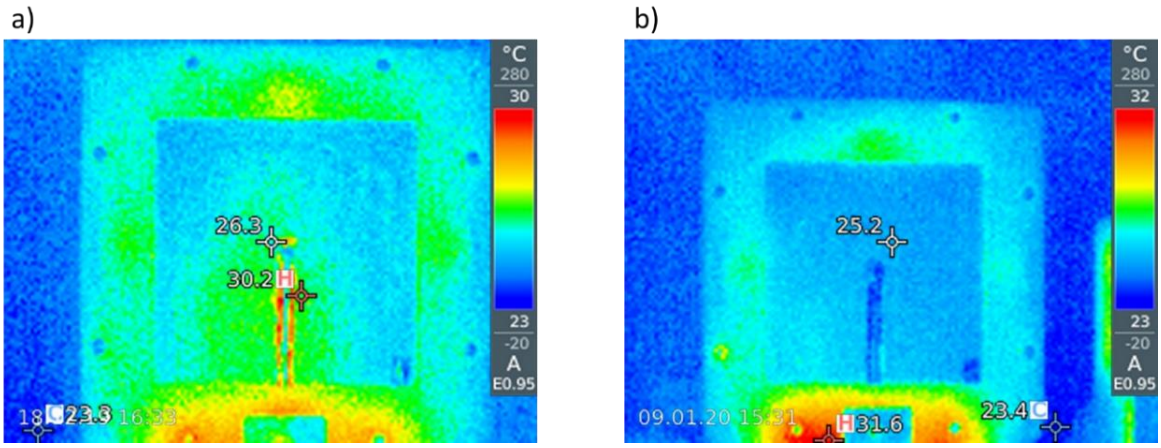

Figure 5.9: Effect of changing the direction of air circulation on the UHPC sample with insulation, with a) original direction of air circulation and b) inverted direction of air circulation

Figure 5.10 shows the effect of changing the direction of air circulation on the single glass sample. Figure 5.11 and Figure 5.12 respectively show the influence of inverting the direction of the fans on double glazing with air and double glazing with argon.

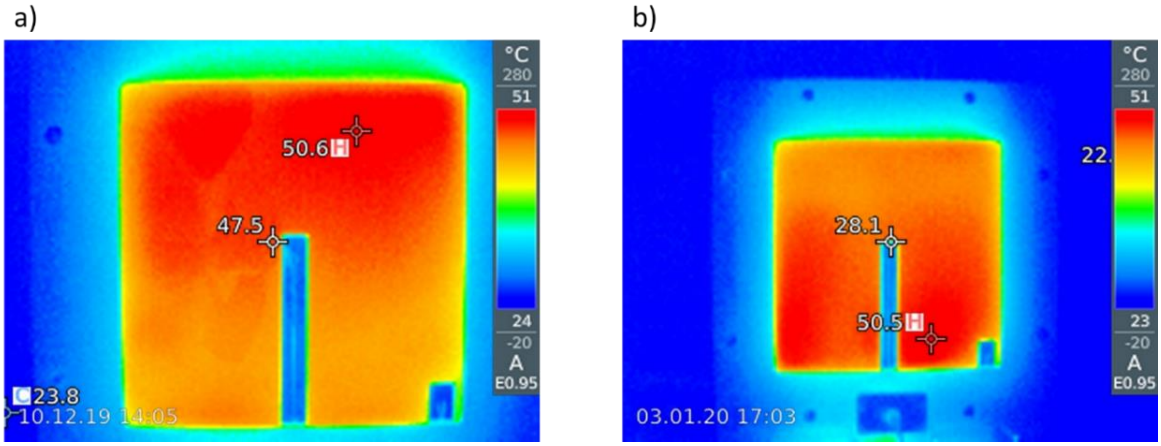

Figure 5.10: Effect of changing the direction of air circulation on the single glass sample, with a) original direction of air circulation and b) inverted direction of air circulation. The hottest region shifts to the bottom of the sample after inverting the fan direction.

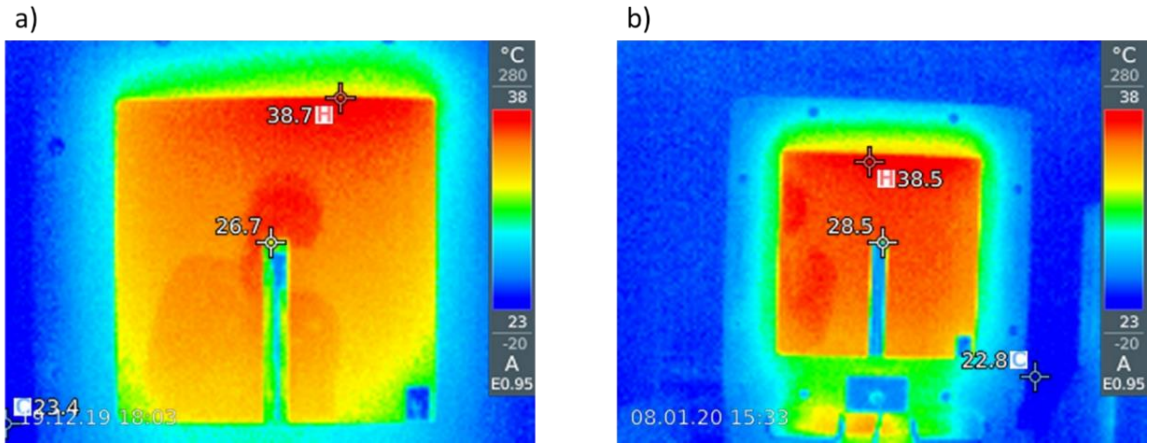

Figure 5.11: Effect of changing the direction of air circulation on the double glazing with air sample, with a) original direction of air circulation and b) inverted direction of air circulation

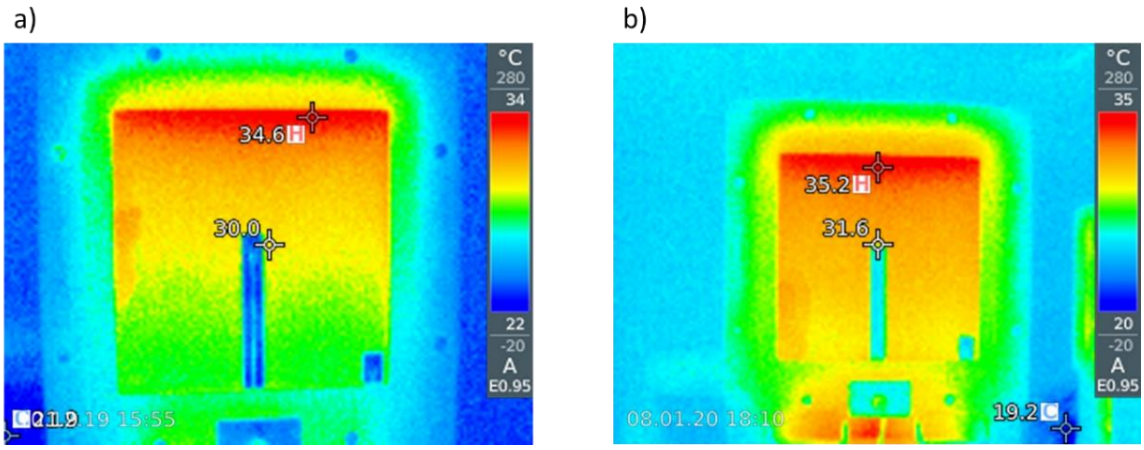

Figure 5.12: Effect of changing the direction of air circulation on the double glazing with argon sample, with a) original direction of air circulation and b) inverted direction of air circulation

It can be seen from Figure 5.11 that for double glazing with air, the temperature distribution on the outer side of the sample becomes more uniform after changing the direction of the fans, even though the hottest region remains on the top side of the sample. This observation can be more clearly seen for double glazing with argon in Figure 5.12, where a distinct hot layer at the very top of the sample can be noticed. The presence of this hot layer at the top of the sample can be explained by the presence of fluids in between the glass panes of the samples with double glazing. Air and argon both are gaseous substances. As the samples with double glazing heat up, the density of the gas between the panes decreases. As a result, hot gas accumulates at the top in the gap between the glass panes, resulting in the hot layer seen in Figure 5.11 and Figure 5.12.

In addition to observing the samples with the thermal camera, the effect of the Thermobox modifications on the measurement results is further assessed from the thermal conductance and thermal transmittance values, which are calculated from the steady-state experiments performed after each modification.

b) Influence on the Measurement Results

Steady-state measurements are performed on the measurement samples after applying the modifications on the Thermobox. One set of measurements is performed after implementing the side insulation and black paint, and another set of measurements is performed after inverting the fan direction. Effect of the Thermobox modifications on these steady-state measurement results is discussed in this section.

First, the behaviour of different measurement temperatures is observed. The steady-state temperatures measured at different points during the steady-state measurements are presented below.

Table 8 shows the steady-state temperatures during measurements with side insulation and black paint.

Table 8: Steady-state temperatures at different measurement points of the Thermobox and the samples during steady-state measurements after the implementation of side insulation and black paint

Measurement sample	Temperature inside the Thermobox (°C)		Temperature at the inside surface (°C)	Temperature in between layers (°C)	Temperature at the outside surface (°C)	Room temperature (°C)
	Up	Down				
MDF without insulation	60.9	60.5	54.0	N/A	41.8	26.0
MDF with inside insulation	61.2	60.9	60.0	31.4	29.1	26.2
UHPC without insulation	62.0	61.5	50.5	N/A	49.1	26.0
UHPC with outside insulation	61.1	60.7	59.5	58.7	30.7	26.3
Single glass	61.9	61.4	51.5	N/A	50.6	26.4
Double glazing with air	60.3	59.8	53.4	N/A	39.0	25.6
Double glazing with argon	60.3	59.9	56.4	N/A	33.0	25.6

Table 9 shows the steady-state temperatures during measurements with the inverted fan direction.

Table 9: Steady-state temperatures at different measurement points of the Thermobox and the samples during steady-state measurements after inverting the fan direction

Measurement sample	Temperature inside the Thermobox (°C)		Temperature at the inside surface (°C)	Temperature in between layers (°C)	Temperature at the outside surface (°C)	Room temperature (°C)
	Up	Down				
MDF without insulation	61.5	61.2	55.6	N/A	43.0	26.2
MDF with inside insulation	60.9	60.5	60.0	30.4	27.9	25.8
UHPC without insulation	61.4	61.2	52.0	N/A	50.7	26.6
UHPC with outside insulation	60.7	60.4	59.6	58.8	31.1	26.5
Single glass	61.8	61.6	53.1	N/A	52.4	26.0
Double glazing with air	62.0	61.7	56.1	N/A	40.9	26.4
Double glazing with argon	61.8	61.5	58.7	N/A	34.3	26.4

Comparing the values from Table 8 and Table 9 with the earlier presented values in Table 7, it can be seen that the behaviour of the temperatures measured at different points is not affected by the modifications.

Next, it is investigated how the Thermobox modifications influence the steady-state measurement results. The calculations are performed with the literature value of h_o, which is 7.69 W/m2K. The calculated thermal conductance of different samples and their comparison with the reference values, as well as the experimental thermal transmittance from the primary measurements and after the Thermobox modifications are shown graphically in Figure 5.13. It is also shown in the figure how the values change with the modifications from the primary steady-state measurements. Detailed values can be found in Table E-2 in Appendix E.

Comparing the values from primary steady-state measurements to the values after the modifications, as presented in Figure 5.13, the general observation can be made that the experimental k_s values increase from the primary measurement values with each modification. The only exception is the MDF sample with insulation, the experimental k_s value for which first increases from primary measurements to side insulation and black paint, and then slightly decreases after inverting the fan direction. This pattern is also followed by the U_s value of MDF with insulation. For the other samples, except for UHPC without

insulation, U_s increases with the increase of k_s. For UHPC without insulation, even though k_s increases after implementing side insulation and black paint, U_s decreases. This was due to the temperature difference between the inside of the Thermobox and the room, which increased after the first modification.

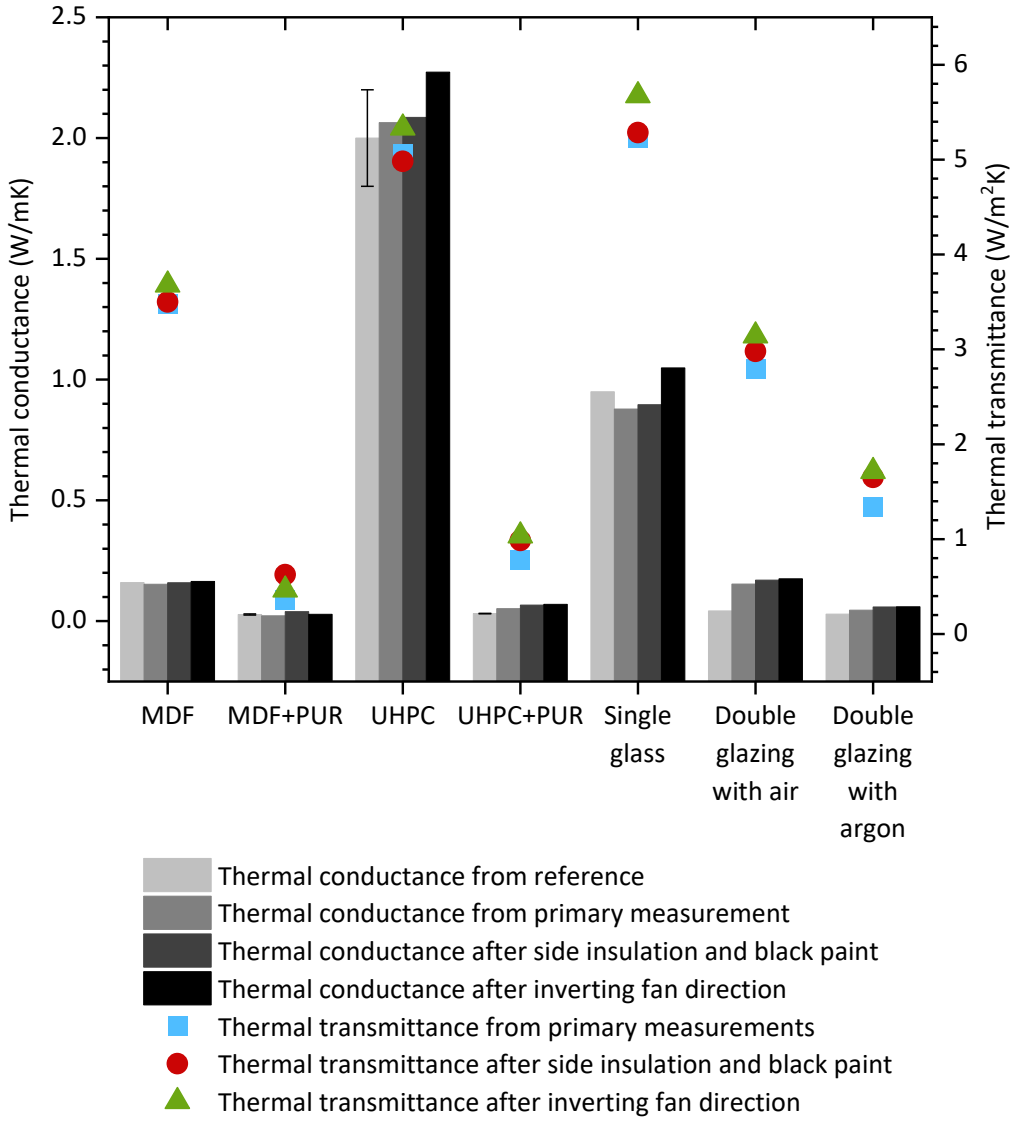

Figure 5.13: Graphical comparison of the reference (with range) and the experimental thermal conductance of measurement samples, along with the experimental thermal transmittance from the primary steady-state measurements and measurements after the modifications

Assessing the results, it can be seen that the experimental k_s for MDF without insulation is still within the reference range for both modifications. The experimental k_s of MDF with insulation is higher than the reference k_s with side insulation and black paint, but stays within the range with inverted fan direction. The experimental k_s of UHPC without insulation crosses the reference range with inverted fan direction. For UHPC with insulation with both modifications, the experimental k_s is over 100 % more than the reference value. The experimental k_s for single glass remains lower than the reference after the first

modification, and with inverted fan direction, the experimental k_s becomes higher. The double glazing samples have much bigger deviations from the reference values, similar to the primary steady-state measurements. The experimental k_s is more than 300 % higher for double glazing with air and about 103 % higher for double glazing with argon.

Assessing U_s of each sample after the modifications, it can be seen that the insulated samples have smaller U_s values than the samples without insulation. Similar to primary measurements, MDF with insulation has the lowest value of U_s after both modifications and single glass has the highest value of U_s with both modifications.

c) Calculation with Experimental h_o

Using the measurement data from the steady-state measurements after inverting the fan direction, k_s and U_s can also be calculated with the experimental value of h_o (7.28 W/m²K, discussed in Section 4.1.1). The results with the literature h_o and the experimental h_o are then presented and compared in Table 10.

Table 10: Experimental k_s and U_s values of the measurement samples after changing the direction of air circulation inside the heating chamber, with $h_o = 7.69$ W/m²K and $h_o = 7.28$ W/m²K

Measurement sample	Reference k_s (W/mK)	With $h_o = 7.69$ W/m²K			With $h_o = 7.28$ W/m²K		
		Experimental k_s (W/mK)	Experimental U_s (W/m²K)	Deviation of k_s from reference (%)	Experimental k_s (W/mK)	Experimental U_s (W/m²K)	Deviation of k_s from reference (%)
MDF without insulation	0.16	0.16	3.68	0	0.16	3.48	0
MDF with inside insulation	0.025-0.030	0.028	0.47	0	0.027	0.44	0
UHPC without insulation	1.8-2.2	2.27	5.34	3.3	2.15	5.05	0
UHPC with outside insulation	0.031-0.032	0.069	1.04	116.3	0.066	0.98	104.8
Single glass	0.95	1.05	5.68	10.4	0.99	5.37	4.5
Double glazing with air	0.042	0.18	3.14	317.6	0.17	2.98	295.3
Double glazing with argon	0.029	0.059	1.72	104.6	0.056	1.62	93.7

From the values presented in Table 10, it can be seen that the values calculated with $h_o = 7.69$ W/m²K are mostly smaller than the values calculated with $h_o = 7.28$ W/m²K. This is understandable that the calculated values will decrease with decreasing value of h_o, as the calculation of k_s and U_s is influenced directly by the value of h_o. It can also be observed that the calculated k_s of the measurement samples with the experimental value of h_o are much closer to the reference values than the calculated values with the literature value of h_o.

5.1.3 Parameterization and Effect of the PID Controller on Steady-state Measurements

The goal of implementing the PID controller is to achieve automatic control for performing steady-state measurements. After the PID controller is implemented into the software, step tests of all the samples and further tuning lead to the determination of the controller parameters. The final values of the control parameters, K_p, T_i and T_d, are presented in Table 11. These values of K_p, T_i and T_d can then be used to perform steady-state measurements with the Thermobox.

Table 11: Final control parameters for the measurement samples

Measurement samples	Proportional gain, K_p	Integral time, T_i, in min	Derivative time, T_d, in min
UHPC	1200	35.6	0.52
MDF	1000	32	0.53
Glass	2000	31	0.67
Double glazing with air	1000	33	0.67
Double glazing with argon	1000	47.6	0.52
UHPC with outside insulation	1000	14	0.67
MDF with inside insulation	1000	47.8	0.45

After the determination of the control parameters, the effect of the controller on the steady-state measurements can be observed by comparing the temperature progression curves of the samples for both manual control and PID control. The temperature progression curves during the steady-state measurements of the UHPC sample and the MDF sample with $T_{box} = 60$ °C are presented in Figure 5.14 and Figure 5.15. The first shows the temperature progression of the samples when the power of the regular heater is controlled manually. The latter shows the temperature progression of the samples when the power is controlled with the PID controller.

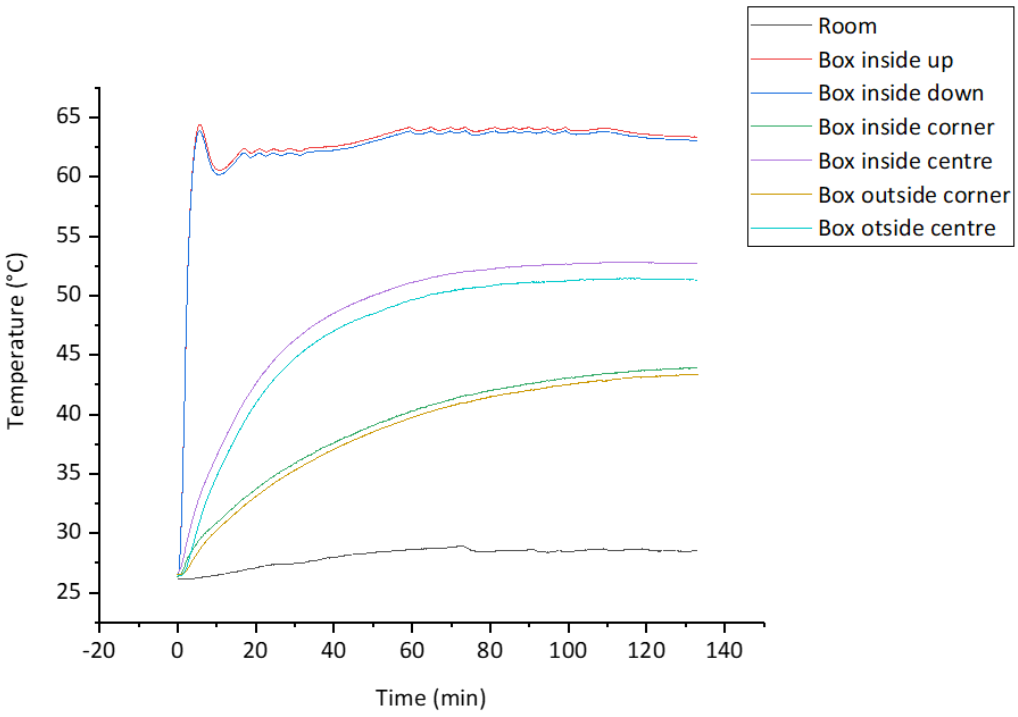

a)

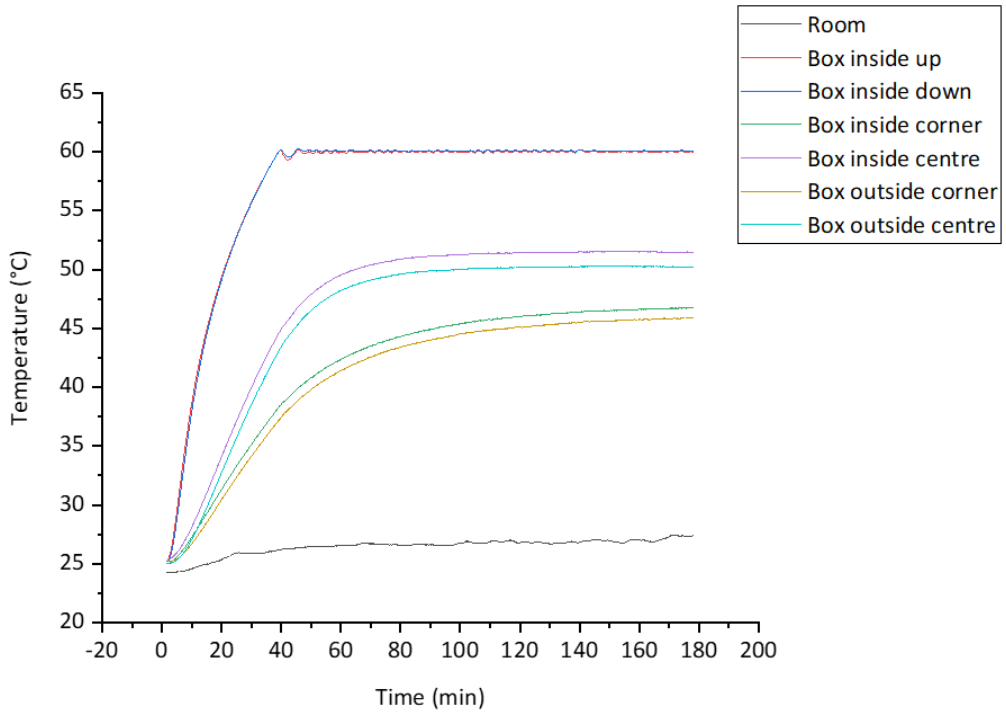

b)

Figure 5.14: Temperature progression curve of a) UHPC sample with manual control and b) UHPC sample with PID control

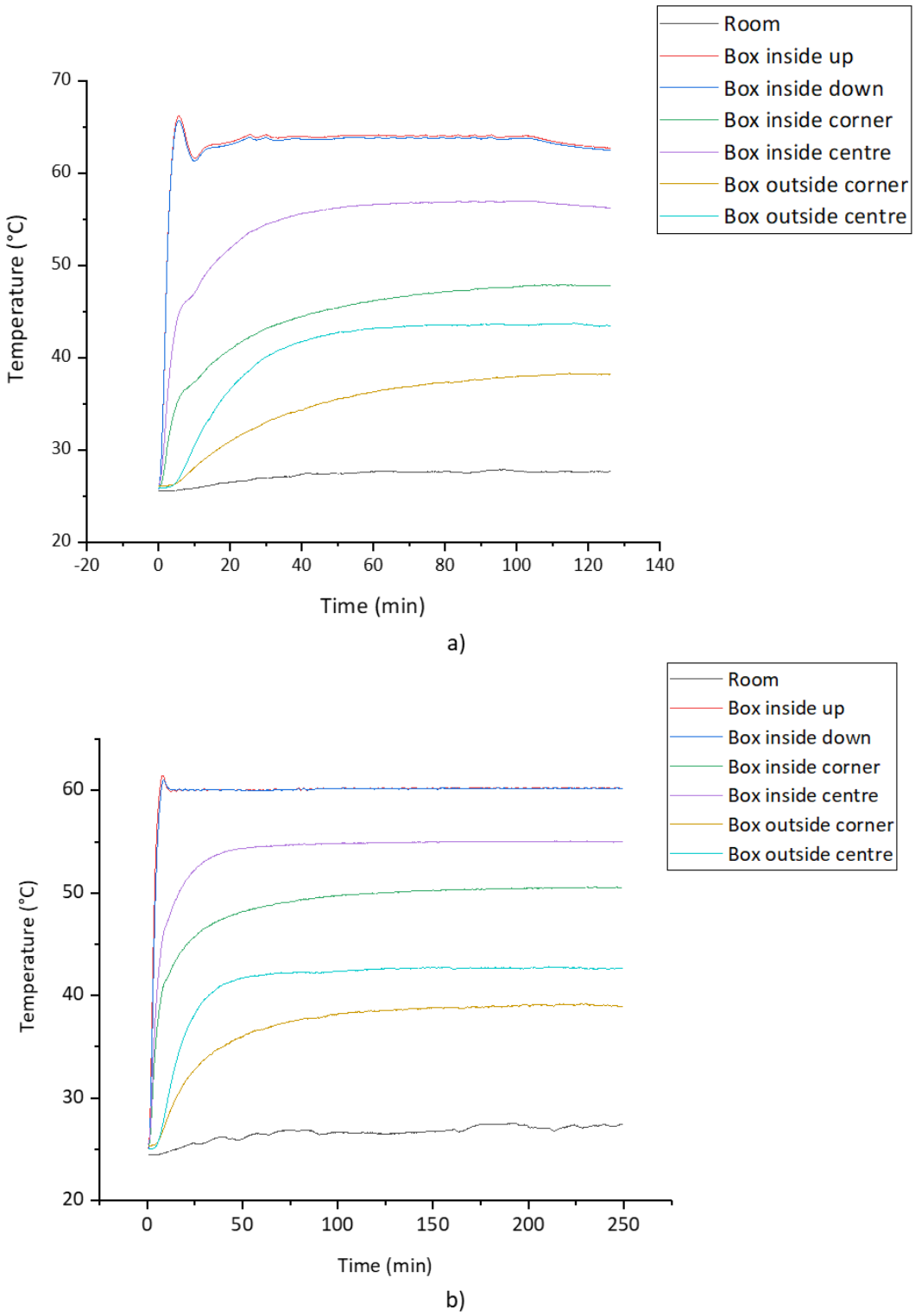

Figure 5.15: Temperature progression curve of a) MDF sample with manual control and b) MDF sample with PID control

It can be seen from the graphs in Figure 5.14a and Figure 5.15a that it is difficult to achieve a steady temperature inside the heating chamber of the Thermobox with manual control. For both UHPC and MDF, even after 120 minutes, the temperature inside the box is not stable. This instability can cause disturbance for the other temperatures, eventually leading to faulty measurements.

The temperature progression of the samples with the PID controller, on the other hand, is much more stable. Figure 5.14b and Figure 5.15b show the temperature progression curves of UHPC and MDF with the PID controller. The temperature inside the Thermobox becomes stable at the set point of 60 °C much faster than the manual control, which is around 50 minutes with for UHPC and around 25 minutes for MDF. It is to be noted that the time to reach steady-state condition with either control does not vary significantly. This constant heating temperature inside Thermobox leads to uniform heating of the samples. The temperatures become stabilized over time without any adjustments, so there is no need for supervision. Thus performing experiments with the PID controller leads to a more precise steady-state, and consequently increases the reliability of the steady-state measurements with the Thermobox.

5.1.4 Measurements with the Heat Flux Method

Steady-state measurements with the heat flux sensor are performed with the temperature inside the Thermobox, T_{box}, at 50 °C, 60 °C and 70 °C. The measurements are carried out by controlling the heating power with the PID controller. Subsequently, thermal conductance and thermal transmittance of the measurement samples are calculated from these measurements. As the temperature progression data is also recorded during the heat flux measurements, the heat flux method and the temperature method (with $h_{\mathrm{o}} = 7.69$ W/m^{2}K) from the same experiment can be compared. The calculated values from both the heat flux method and the temperature method are thus compared. Furthermore, the effect of changing the temperature inside the box, T_{box}, on the results with the heat flux method and the temperature method is investigated.

a) Manual Control vs PID control with T_{box} = 60 °C

As mentioned above, the heat flux measurements are conducted with the PID controller. From the recorded temperature values during the steady-state measurements with the heat flux sensor at $T_{\mathrm{box}} = 60$ °C, thermal conductance and thermal transmittance can be calculated with the temperature method. These calculated values can then be compared to the values obtained from the steady-state measurements after inverting the fan direction. Thus, a comparison between the manual control and the PID control on the measurement result can be made.

Figure 5.16 shows a graphical comparison between the effect of the manual control and the PID control on the measurement results. The difference in the k_{s} values from the reference can also be observed from the graph. It is to be noted that for the calculations, the literature value of h_{o} (7.69 W/m^{2}K) is used.

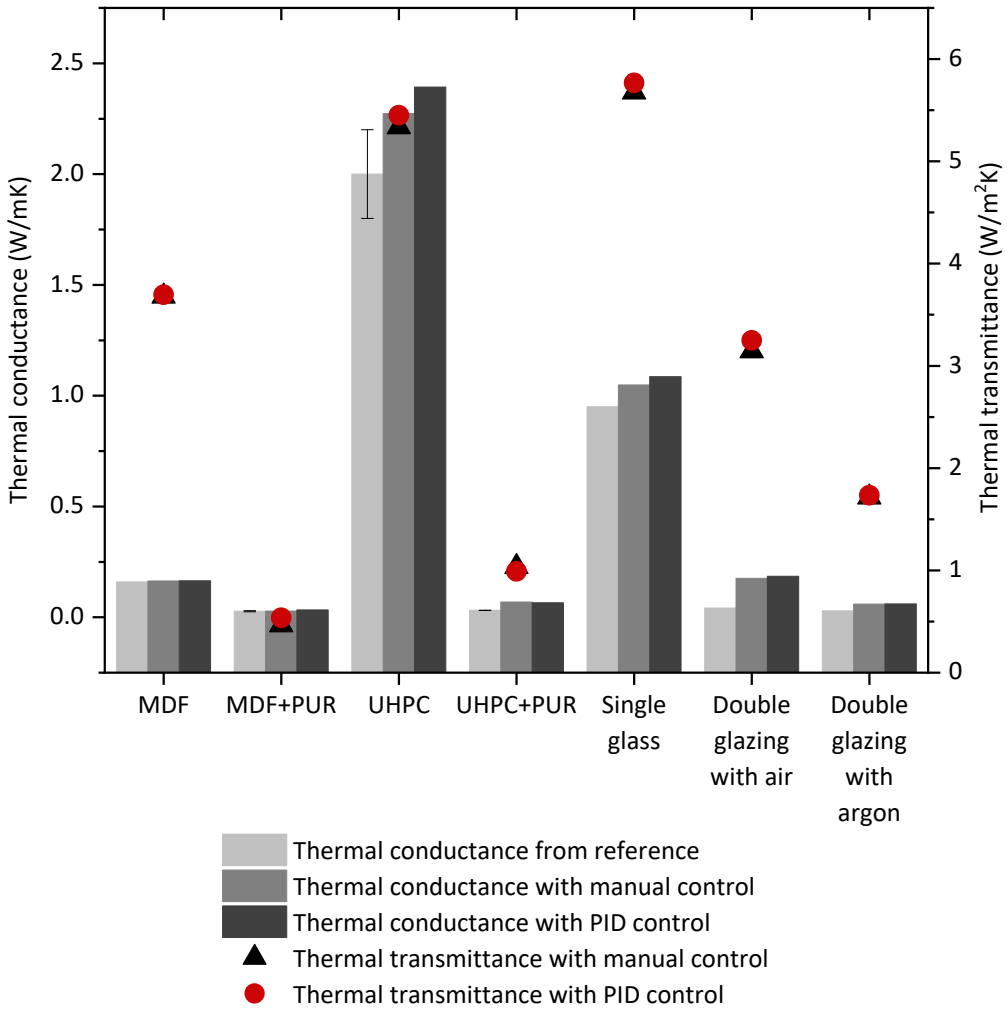

Figure 5.16: Comparison of the calculated thermal conductance and thermal transmittance with manual control and PID control

It can be seen that the calculated values of k_s remain almost the same (MDF, MDF with insulation, UHPC with insulation and samples with double glazing) or slightly increase (UHPC and single glass) from manual control to PID control. The change is more prominent on the samples with higher thermal conductance. The calculated values with both controls show the same behaviour with respect to the reference values.

The calculated U_s values for MDF with insulation, UHPC, single glass and double glazing with air with PID control are slightly higher than the values calculated with manual control. UHPC with insulation, on the other hand, has a marginally lower value with PID control to manual control. The U_s for MDF without insulation and double glazing with argon remains the same with both control methods.

b) Measured Steady-state Temperature and Average Heat Flux

The steady-state temperatures at different measurement points of the Thermobox and the samples, along with the average steady-state heat flux during the heat flux measurements at $T_{\mathrm{box}} = 50\ °\mathrm{C}$ are presented in Table 12.

Table 12: Steady-state temperatures at different measurement points of the Thermobox and the samples and average steady-state heat flux during steady-state measurements at $T_{\mathrm{box}} = 50\ °\mathrm{C}$

Measurement sample	Temperature inside the Thermobox (°C)		Temperature at the inside surface (°C)	Temperature in between layers (°C)	Temperature at the outside surface (°C)	Room temperature (°C)	Average heat flux (W/m²)
	Up	Down					
MDF without insulation	51.1	50.8	47.2	N/A	38.0	25.9	95.4
MDF with inside insulation	52.2	51.8	51.5	29.7	27.8	26.0	15.7
UHPC without insulation	50.3	50.1	44.6	N/A	43.6	26.7	152.0
UHPC with outside insulation	51.2	50.8	50.4	49.6	28.9	26.0	18.7
Single glass	51.1	50.9	45.6	N/A	44.9	26.1	166.5
Double glazing with air	51.1	50.8	47.4	N/A	36.6	26.2	84.8
Double glazing with argon	51.2	50.8	49.0	N/A	30.7	25.3	45.0

Comparing the data from Table 12 with previous steady-state measurements, it can be seen that the behaviour of the steady-state temperatures at different points remains the same. Observing the average heat flux values for the samples, it is seen that the insulated samples (MDF with insulation, UHPC with insulation and glass samples with double glazing) require much less heat flux for maintaining the same T_{box} than the samples without insulation. The steady-state temperature and heat flux measurements at $T_{\mathrm{box}} = 60\ °\mathrm{C}$ and $T_{\mathrm{box}} = 70\ °\mathrm{C}$, as presented in Table 13 and Table 14, also show similar behaviour.

Table 13: Steady-state temperatures at different measurement points of the Thermobox and the samples and average steady-state heat flux during steady-state measurements at $T_{\mathrm{box}} = 60\ °\mathrm{C}$

Measurement sample	**Temperature inside the Thermobox (°C)**		**Temperature at the inside surface (°C)**	**Temperature in between layers (°C)**	**Temperature at the outside surface (°C)**	**Room temperature (°C)**	**Average heat flux (W/m²)**
	Up	**Down**					
MDF without insulation	61.0	60.7	55.4	N/A	43.0	26.4	133.1
MDF with inside insulation	61.4	61.0	60.5	30.7	28.2	25.8	20.3
UHPC without insulation	60.5	60.4	51.7	N/A	50.5	26.3	233.0
UHPC with outside insulation	61.0	60.7	59.8	58.9	30.2	25.6	25.3
Single glass	60.5	60.3	52.5	N/A	51.8	25.8	243.1
Double glazing with air	60.9	60.6	55.3	N/A	40.6	25.9	122.6
Double glazing with argon	60.2	59.9	57.2	N/A	33.8	26.1	66.7

From the data presented in Table 12, Table 13 and Table 14, it can be seen that with the increasing temperature inside the Thermobox, all the associated temperatures are also increasing. At the same time, the average heat flux also increases.

Table 14: Steady-state temperatures at different measurement points of the Thermobox and the samples and average steady-state heat flux during steady-state measurements at $T_{\mathrm{box}} = 70\ °\mathrm{C}$

Measurement sample	**Temperature inside the Thermobox (°C)**		**Temperature at the inside surface (°C)**	**Temperature in between layers (°C)**	**Temperature at the outside surface (°C)**	**Room temperature (°C)**	**Average heat flux (W/m²)**
	Up	**Down**					
MDF without insulation	70.2	70.0	63.2	N/A	47.2	26.6	171.1
MDF with inside insulation	70.2	69.8	69.0	33.1	29.8	26.3	25.2
UHPC without insulation	69.2	69.1	57.8	N/A	56.3	26.6	292.5
UHPC with outside insulation	70.2	69.8	68.5	67.4	31.2	26.1	30.1
Single glass	69.9	69.8	59.3	N/A	58.4	26.5	311.5
Double glazing with air	70.2	69.9	63.0	N/A	45.1	26.6	155.7
Double glazing with argon	70.2	69.8	66.1	N/A	37.0	27.3	85.2

A comparison between the measured average heat flux and the target temperature inside the Thermobox (50 °C, 60 °C and 70 °C) is presented graphically in Figure 5.17.

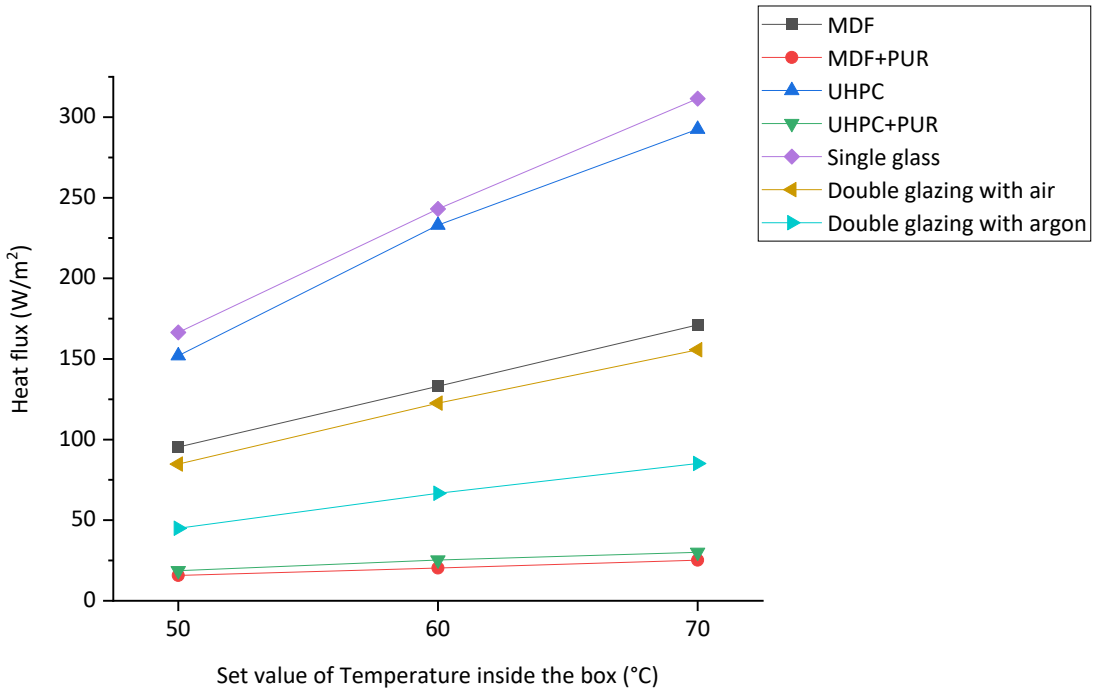

Figure 5.17: Average heat flux at different set values of T_{box}

It is observed from Figure 5.17 that the average heat flux increases linearly with the increasing set value of T_{box}. Single glass requires the highest average heat flux for maintaining the target value of T_{box}, whereas the required heat flux is the lowest for MDF with insulation.

c) Heat Flux Method vs Temperature Method

From the heat flux measurement data, k_s and U_s can be calculated by both the heat flux method and the temperature method. Considering the measurement data from the heat flux measurements at $T_{box} = 60\,°C$, a comparison can be made between the experimental values of k_s and U_s obtained by the temperature method and the heat flux method. This comparison is presented in Figure 5.18. The literature value of h_o (7.69 W/m²K) is used for the calculation with the temperature method.

The general observation can be made from the figure that the calculated values of k_s with the heat flux method are much higher than the values calculated with the temperature method. Consequently, the experimental k_s obtained from the heat flux method deviates more from the reference values. The only exception is seen for UHPC with insulation, the experimental k_s for which significantly decreases with the heat flux method than the temperature method.

The experimental values of U_s follow the same pattern as the k_s values. U_s for UHPC with insulation decreases with the heat flux method than the temperature method, whereas the rest of the sample have higher values of U_s with the heat flux method than the temperature method.

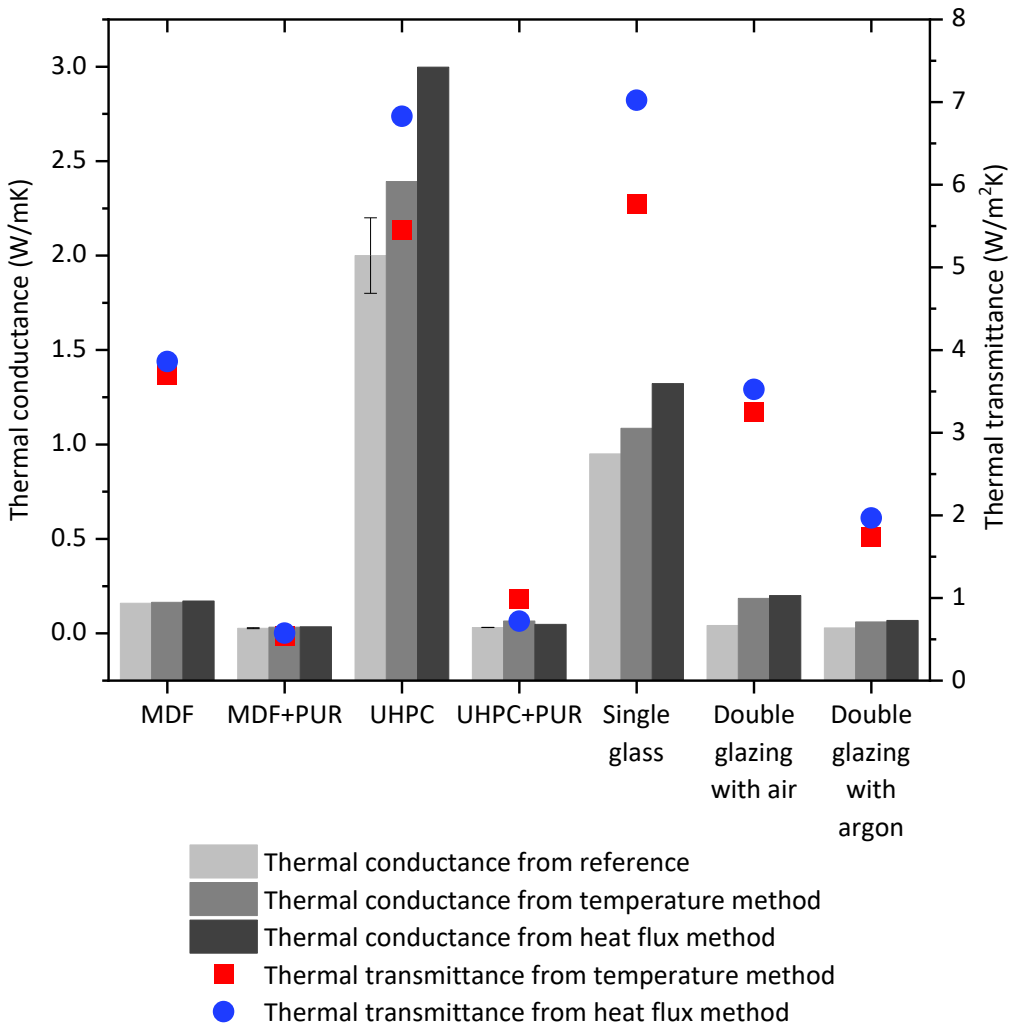

Figure 5.18: Comparison of the calculated thermal conductance and thermal transmittance by the temperature method and the heat flux method with T_{box} at 60 °C

To understand the behaviour of the measurement results from the temperature method and the heat flux method, h_{o} can be calculated from the heat flux measurements for each measurement samples. The value of h_{o} obtained from literature, from the experiment described in Section 4.1.1 and from the heat flux method is presented in Table 15.

It can be seen from the table that the values obtained from the heat flux method are higher than the literature value of h_{o}, with UHPC with insulation being the only exception. The h_{o} from the heat flux method for UHPC with insulation is much smaller than the literature value, which is used for the calculation by the temperature method. This can explain the above-mentioned behaviour of the calculated k_{s} and U_{s} from the temperature method and the heat flux method for UHPC with insulation.

Table 15: h_o values from literature, experiment and heat flux method

Measurement sample	h_o from literature (W/m²K)	h_o from experiment (W/m²K)	h_o from heat flux method (W/m²K)
MDF without insulation	7.69	7.28	8.04
MDF with inside insulation			8.23
UHPC without insulation			9.63
UHPC with outside insulation			5.59
Single glass			9.37
Double glazing with air			8.34
Double glazing with argon			8.72

The low value of h_o for UHPC with insulation can be explained by the aluminium foil on the outside surface. Aluminium, a metal, has a low emittance value (31.6 %), which leads to smaller heat transfer by radiation at the outside surface of the UHPC with insulation sample. As a result, the combined convection and radiation heat transfer coefficient, h_o, can be smaller than the other samples, which have a non-metallic outside surface.

It can also be seen from Table 15 that single glass has a higher value of h_o than the other transparent samples, even though the outside surface of the transparent samples are constructed from the same material. The changing values of h_o for the transparent samples may be explained by the changing outside surface temperatures (Table 13). Higher temperatures can lead to a higher heat loss due to radiation (Equation 2.8).

It can also be observed that the value of h_o obtained from the heat flux method is different for each sample. This h_o is calculated directly from the measured heat flux through the samples and the temperature difference between the outside surface and the room, thus providing the actual heat transfer scenario for each sample. While performing steady-state calculations with the temperature method, the literature value of h_o is considered, and it is assumed that this value remains the same for all the samples. But from the calculated values of h_o, it can be seen that this assumption may not be correct.

d) Steady-state Measurements at Different T_{box}

Heat flux measurements are performed at three different temperatures inside the Thermobox (50 °C, 60 °C and 70 °C). k_s and U_s can be calculated from the steady-state measurement data by both the heat flux method and the temperature method. Then an analysis can be made on how the measurement results change with the change in T_{box}.

Calculation with the Heat Flux Method at Different T_{box}

The thermal conductances of the measurement samples (k_s) and the thermal transmittances of the measurement samples (U_s), which are calculated by the heat flux method from the steady-state measurements with the heat flux sensor at different set values of T_{box}, are presented graphically Figure 5.19. The values are presented in Table E-3 in Appendix E.

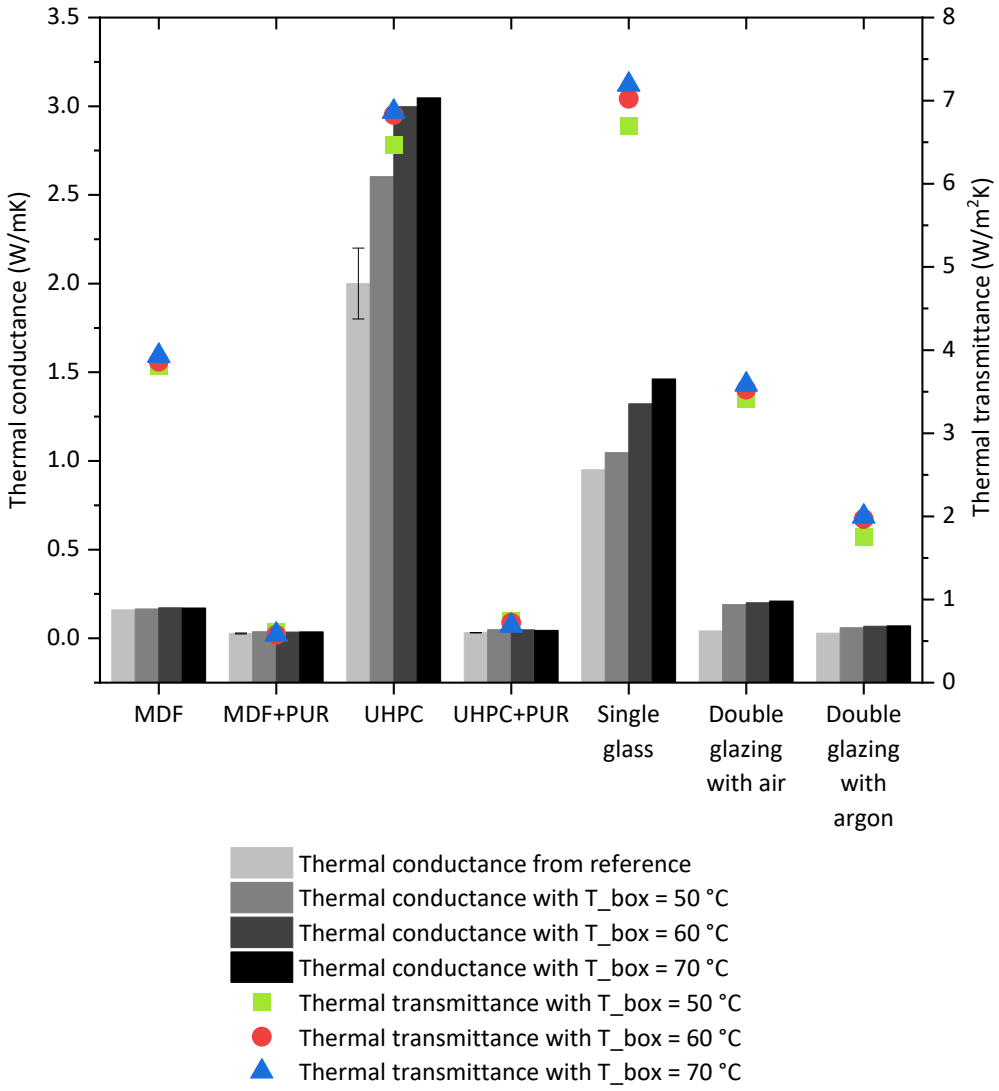

Figure 5.19: Comparison of the calculated thermal conductance and thermal transmittance of the samples at different set values of the temperature inside the Thermobox with the heat flux method

It can be seen from the figure that the behaviour of experimental k_s with temperature is not the same for all the samples. The calculated k_s for the glass samples, as well as for the UHPC sample without insulation, increase with increasing temperature. The increasing thermal conductance of the glass samples is supported by the findings of van der Tempel et al. (2000), where it was found that with increasing

temperature, the thermal conductivity of soda-lime glasses increases slightly. On the other hand, for UHPC, as well as for MDF and PUR, no literature was found for comparison.

Even though k_s increases with temperature for UHPC without insulation, it decreases with temperature for UHPC with insulation, as seen in Figure 5.19. The experimental k_s of the MDF samples remains fairly the same with temperature, with only small fluctuations for MDF with insulation.

Comparing the k_s values from the heat flux method to the heat flux values presented in Figure 5.17, it can be seen that even though the heat flux increases with temperature, the value of k_s, depending on the sample, can increase, decrease or remain constant with increasing temperature.

It is also seen from Figure 5.19 that for most of the samples, U_s increases with temperature, i.e. with increasing temperature, the heat loss through these samples increases. MDF with insulation and UHPC with insulation behave differently from the other samples. U_s of MDF with insulation decreases from 50 °C to 60 °C, but then increases at 70 °C. U_s of UHPC with insulation, on the other hand, decreases with temperature. Comparing these values to the heat flux values presented in Figure 5.17, it can be seen that except for MDF with insulation and UHPC with insulation, U_s increases with increasing heat flux.

In addition to k_s and U_s, the effect of the increasing temperature on the value of h_o, calculated by the heat flux method, is investigated and presented in Figure 5.20.

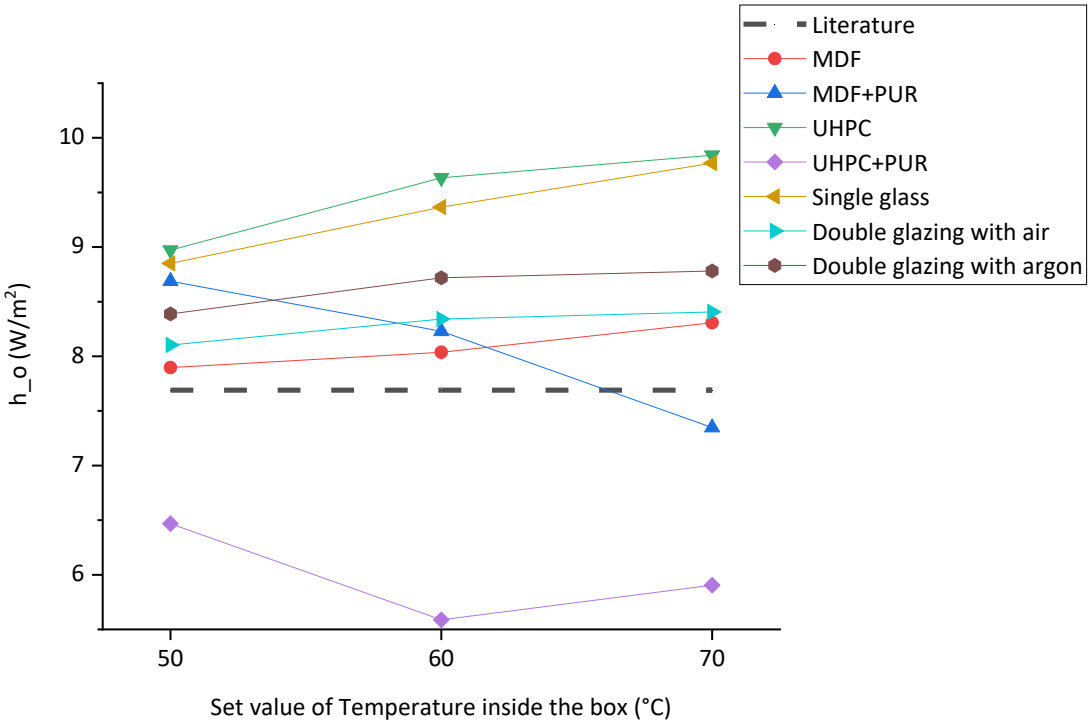

Figure 5.20: Experimental h_o values of the measurement samples at different set values of T_{box} calculated by the heat flux method, along with the literature value

It can be seen from the figure that with increasing temperature, the calculated values of h_o change. The change is not the same for each sample. From general observation, MDF without insulation, UHPC without insulation and the transparent samples have increasing values of h_o with increasing temperature. MDF

with insulation, on the contrary, has decreasing values of h_o with increasing temperature. In contrast, the calculated h_o for UHPC with insulation decreases from 50 °C to 60 °C, but then increases at 70 °C.

It can also be observed in the figure that except for UHPC with insulation, all the calculated values of h_o are higher than the literature value. Another exception is MDF with insulation, for whom the calculated h_o at 70 °C is lower than the literature value.

Investigating the calculated values of the convective and radiative heat transfer coefficient at the inner surface of the samples, h_i, as presented in Figure 5.21, it is seen that for MDF with insulation and UHPC with insulation, h_i decreases sharply with temperature. For the rest of the samples, h_i does not change much with temperature, only small fluctuations can be seen.

The experimental values of h_o and h_i from the heat flux method at different T_{box} can be found in Table E-4 in Appendix E.

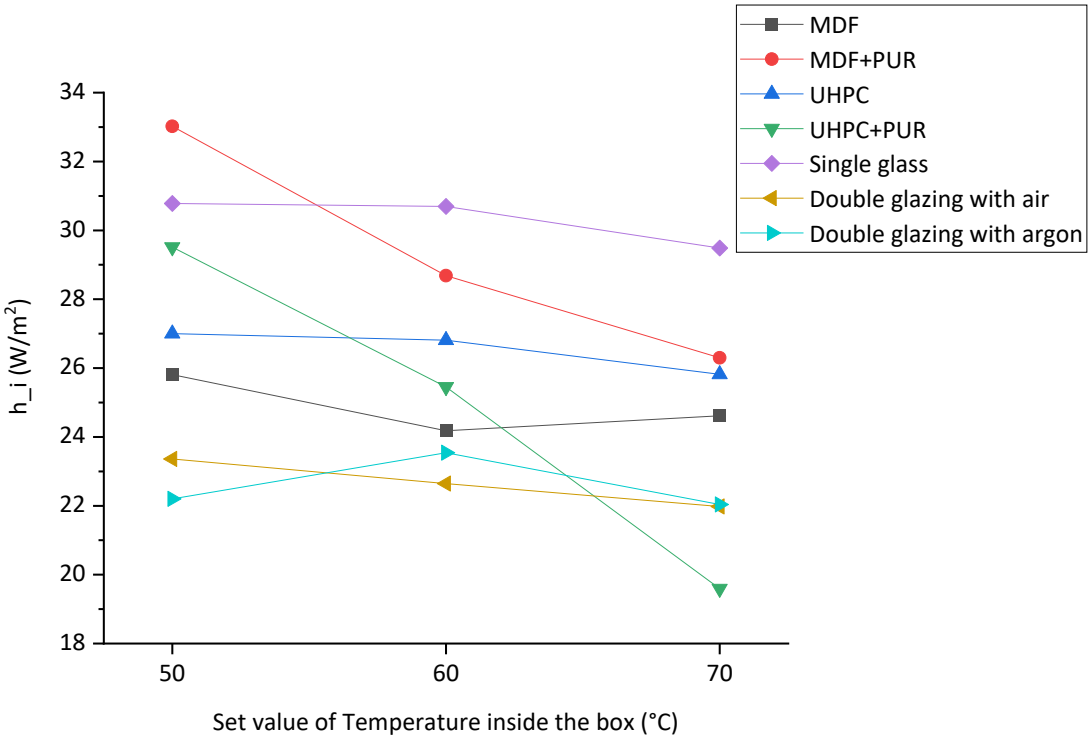

Figure 5.21: Experimental h_i values of the measurement samples at different set values of T_{box} calculated by the heat flux method

Analyzing the results of the heat flux method, it is found that for the transparent samples, as well as the UHPC sample without insulation, k_s and h_o increase with temperature, whereas h_i remains fairly unchanged. Thus it is understandable that the values of U_s of these samples, which is a function of k_s, h_o and h_i (Equation 2.16), increase with the increase in temperature. For MDF without insulation, the increasing values of U_s can be said to be dictated by the increasing values of h_o, as k_s of MDF remains the same and h_i only has small fluctuation. For MDF with insulation, k_s, h_o and h_i decrease with temperature from 50 °C to 60 °C, consequently U_s also decreases. From 60 °C to 70 °C, on the other hand, U_s increases. This increment is influenced by the value of k_s, which increases within the mentioned temperature range,

whereas h_o and h_i decrease. UHPC follows the same pattern as MDF with insulation from 50 °C to 60 °C, where k_s, h_o and h_i, and consequently U_s, decrease. U_s continues to decrease from 60 °C to 70 °C, even though h_o increases within this temperature range. Thus, the decrement of U_s from 60 °C to 70 °C is influenced by k_s and h_i, which decrease within the same temperature range.

Calculation with the Temperature Method at Different T_{box}

The reference k_s of the samples and the experimental k_s and U_s, calculated by the temperature method from the steady-state measurement data with the heat flux sensor, are presented graphically in Figure 5.22. The values can be found in Table E-5 in Appendix E.

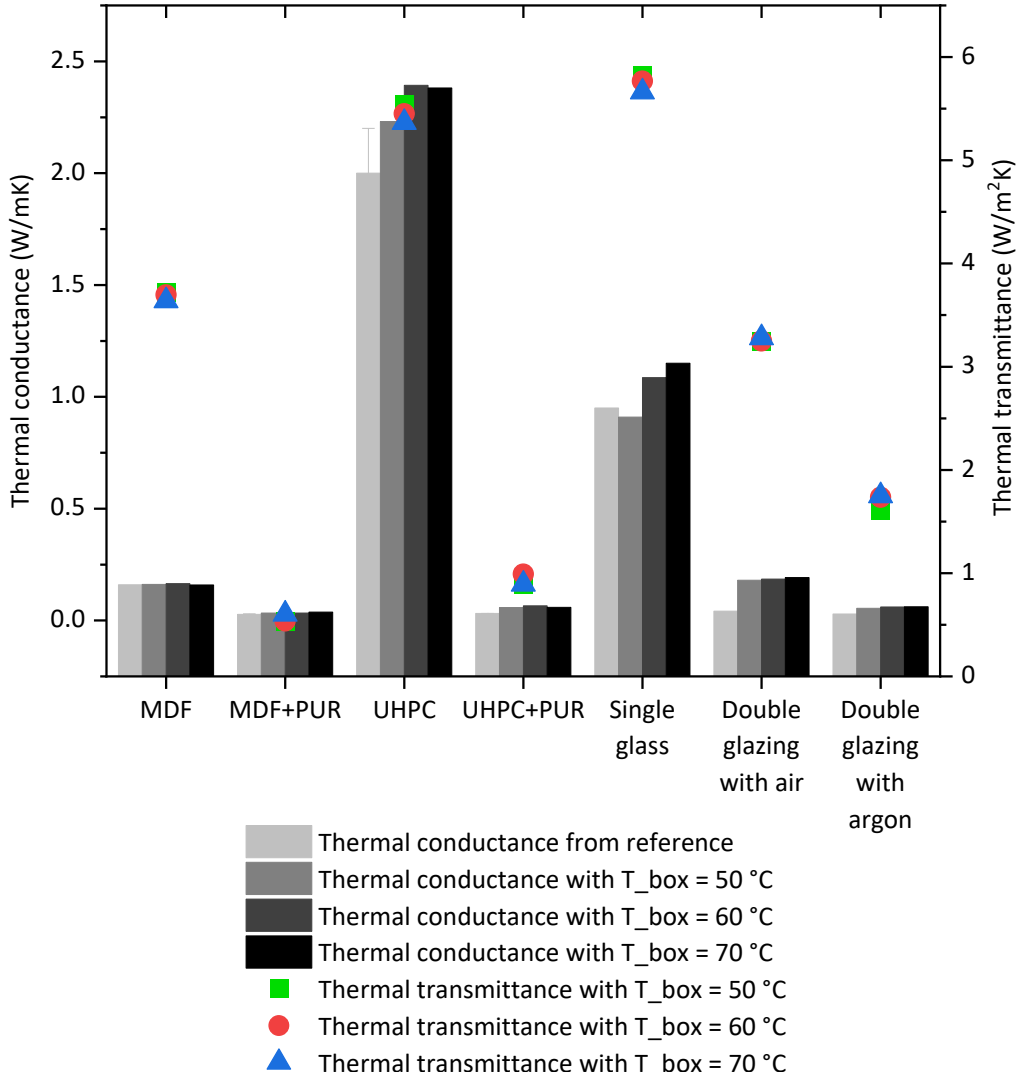

Figure 5.22: Comparison of the calculated thermal conductance and thermal transmittance of the samples at different set values of the temperature inside the Thermobox with the temperature method

From the figure, it can be seen that the calculated thermal conductance of the glass samples with the temperature method follows the same pattern as the heat flux method, where k_s increases with increasing temperature. The calculated k_s of the MDF sample without insulation remains the same with temperature,

which is the same as observed for the heat flux method calculations. k_s of MDF with insulation remains the same from 50 °C to 60 °C, but increases slightly at 70 °C. k_s of the UHPC samples increase slightly from 50 °C to 60 °C, and then decrease.

The figure also shows the calculated values of U_s change differently for different samples. For MDF without insulation, UHPC without insulation and single glass, U_s decreases with temperature increase. On the other hand, U_s of the double glazing samples increases with temperature. For MDF with insulation, U_s remains the same from 50 °C to 60 °C, but increases slightly at 70 °C. For UHPC with insulation, in contrast, U_s increases from 50 °C to 60 °C, but decreases to the initial value at 70 °C.

5.1.5 Results of the Sensitivity Analysis

From the five steady-state measurements performed on the MDF sample for the sensitivity analysis of the Thermobox, k_s and U_s values can be calculated both with the temperature method and the heat flux method. From these experimental values of k_s and U_s, the mean values of k_s and U_s can be calculated. Consequently, the standard deviation of these values can be calculated using Equations 4.16 and 4.17.

The experimental thermal conductance, k_s, and thermal transmittance, U_s, of the MDF sample calculated with the temperature method and the heat flux method from the five steady-state measurements, along with their mean values and standard deviations, are presented in Table 16.

Table 16: Experimental k_s and U_s of the MDF sample from the five steady-state measurements with both methods, and their respective means and standard deviations

Measurements	**Temperature method (with $h_o = 7.69$ W/m²K)**		**Heat flux method**	
	k_s (W/mK)	**U_s (W/m²K)**	**k_s (W/mK)**	**U_s (W/m²K)**
Measurement 1	0.170	3.76	0.174	3.85
Measurement 2	0.175	3.82	0.168	3.66
Measurement 3	0.168	3.74	0.174	3.87
Measurement 4	0.171	3.77	0.173	3.82
Measurement 5	0.174	3.80	0.173	3.78
Mean	**0.171**	**3.78**	**0.172**	**3.80**
Standard deviation	**0.003**	**0.03**	**0.002**	**0.07**

It can be seen from the table that the k_s values calculated with the temperature method has a standard deviation of 0.003 W/mK. This means that most measurement values vary with a deviation of 0.003 from the mean (0.171 W/mK), i.e. within a range of 0.168-0.174 W/mK. Among the calculated k_s values with the temperature method, only the k_s from the second measurement is not within this range and is slightly higher. The same pattern is observed with the calculated U_s values, where the standard deviation is

0.03 W/m^{2}K, and thus the range of U_s values within one standard deviation from the mean (3.78 W/m^{2}K) is 3.75-3.81 W/m^{2}K.

In the case of the heat flux method, the standard deviation for k_s is 0.002, which is slightly lower than the standard deviation of k_s with the temperature method. The standard deviation of U_s, on the other hand, is much higher with the heat flux method (0.007 W/m^{2}K) than the temperature method. From the mean values of k_s and U_s from the heat flux method and their respective standard deviations, the range of the values within one deviation from the mean can be specified as 0.170-0.174 W/mK for k_s and 3.73-3.87 W/m^{2}K for U_s. The results from the second measurement with the heat flux method, as are also seen with the temperature method, do not stay within the specified ranges.

Taking a look at the measured heat fluxes and temperature differences (Appendix 0 Table F-1), it can be seen that measured heat flux from the second measurement is much lower than the other measurements, which explains the results from the second measurement with the heat flux method being lower than the specified range. But this measured heat flux does not influence the temperature method calculations, where only the temperature differences are used. Table F-1 shows that some temperature differences for the second measurement vary from the other measurements with very small margins, namely the temperature difference between the inside surface and the outside surface, and the temperature difference between the inside of the Thermobox and the room.

Thus, it can be concluded from the sensitivity analysis for the MDF sample without insulation that most measurement results (80 % of the results from the five measurements) stay within one standard deviation of the mean values. It can also be inferred that small fluctuations in the temperature differences can result in high deviations of the measurement results. It is to be noted that the conclusion was drawn by comparing only five measurements, which may not lead to reliable observations. Performing sensitivity analysis with more measurements may result in more decisive conclusions.

5.1.6 Summary of the Steady-state Measurements

From the discussed results of the steady-state measurements performed with the Thermobox, it is seen the Thermobox can determine the thermal conductance of the MDF sample without insulation, the MDF sample with inside insulation, the UHPC sample without insulation and the single glass sample quite accurately. The results are either within the reference range or deviate slightly from the reference values. The fluctuation is generally higher for the single glass sample, with a maximum deviation of 10.4 % higher than the reference with the temperature method and 53.9 % higher than the reference with the heat flux method ($T_{box} = 70\ °C$).

On the other hand, the Thermobox is not able to accurately determine the thermal conductance of the UHPC sample with outside insulation with the temperature method (with more than 100 % deviation from the reference), but with the heat flux method, the results are much closer to the reference value. The maximum deviation is 52.4 % higher than the reference with the heat flux method ($T_{box} = 50\ °C$). The accuracy of calculating the thermal conductance of the UHPC sample with insulation is improved due to the change in the $h_o$value with the heat flux method, as discussed in Section c). It is also seen that the experimental values of h_o for the samples calculated with the heat flux method are different from the

literature value of h_o (7.69 W/m^{2}K) or the experimental value of h_o determined from temperature measurements (7.28 W/m^{2}K).

In the case of the samples with double glazing, the Thermobox is not able to determine the thermal conductance values accurately. Both the temperature method and the heat flux method measurements show high deviations from the reference values. This inaccuracy might be explained by the movement of the gas between the glass panes of the double glazing samples. As the gas (air or argon) between the panes heats up, it becomes lighter and starts to move upward. This causes a change in the density of the gas and consequently a circulation of air within the panes. Thus, the simple calculation procedure of the reference thermal conductance values for the double glazing samples described in Section 4.2.1 might not be correct for measurements with the Thermobox.

It is also noticeable from the results that with the modifications, the experimental thermal conductance and thermal transmittance values of the samples generally increase. Due to the side insulation on the side of the samples, less heat is lost through the sides, whereas more heat passes through the sample. Implementing black paint inside the heating chamber improves the radiation effect and inverting the fan direction leads to more uniform heating of the samples. These modifications may result in more heat passing through the samples, leading to the increment in the experimental values.

The heat flux method calculates k_s and U_s of the samples from the actual heat flux through the samples, which is measured with the heat flux sensor. The results of the heat flux method can thus be considered to be more accurate than the temperature method. With the heat flux method, the individual heat transmission scenarios for the samples are considered, whereas with the temperature method a more general heat transmission is considered, by taking the same value of h_o for all the samples.

One issue with the heat flux method is the position of the sensor on the samples. As seen in Figure 4.8, the heat flux sensor is positioned next to the centre temperature sensor at the outside surface of the sample (MDF in this case). From the thermal imaging of the samples, presented in Section 5.1.2, it can be seen that for most of the samples, the temperature on the outside surface is not uniformly distributed. Which means that the temperature at the centre and the temperature at any other point on the surface of a sample may not be the same. From the thermal images, it is also apparent that this distribution of temperature does not follow the same pattern for all the samples. On the contrary, for calculation with the heat flux method, the temperature difference between the inside centre and the outside centre is considered. For some samples, this temperature difference may represent the actual temperature difference at the area where the heat flux is measured (e.g. MDF, presented in

Figure 5.6, where the temperature distribution can be considered uniform). But for some samples, this temperature difference may be different than the actual temperature difference at the heat flux measurement area (e.g. single glass, presented in Figure 5.9, where the temperature is higher in the areas left and right of the centre temperature sensor than the centre of the sample surface). This positioning problem of the heat flux sensor may have some implication on the experimental results obtained with the heat flux method.

Taking a closer look at the density of the samples, it is seen in Table 6 that the density of the MDF sample can be taken as 1000 kg/m^3. The density of the UHPC sample, according to Toman & Černý (2001, p. 9), is

2200-2290 kg/m^3. The density of the MDF and the UHPC samples measured in the lab, as shown in Table 6, is 1097 kg/m^3 and 3422 kg/m^3 respectively. The measured density of MDF is slightly higher than the reference, whereas the measured density of UHPC is much higher than the reference. According to MacLean (1941), the thermal conductivity of wood increases with density, and according to Fontana et al. (2016, p. 4), the thermal conductivity of UHPC also increases with density. As a result, the actual reference values of thermal conductance of MDF and UHPC should be higher than the reference values considered in Table 4. Similarly, the Thermobox measurement samples, depending on their densities, may have slightly different reference values of thermal conductance than the reference values considered for this thesis.

The sensitivity analysis is performed on the MDF sample without insulation, and the observation from the measurements is that four out of five measurements lead to results that are within one standard deviation of the mean values. One measurement result is not within this range. This deviation is influenced by the fluctuation in the temperature differences between different measurement points of the Thermobox and the measured heat flux.

5.2 Dynamic Measurements

Performing dynamic measurements on the MDF, the UHPC and the single glass samples with the Thermobox lead to their wave propagation graphs. Figure 5.23, Figure 5.24 and Figure 5.25 show the wave propagation graphs of the MDF sample, the UHPC sample and the single glass sample respectively. As mentioned in 4.6.6, the samples are first brought to steady-state at $T_{\mathrm{box}} = 60$ °C, and then T_{box} is changed between 70 °C and 50 °C to achieve periodic heating of the samples.

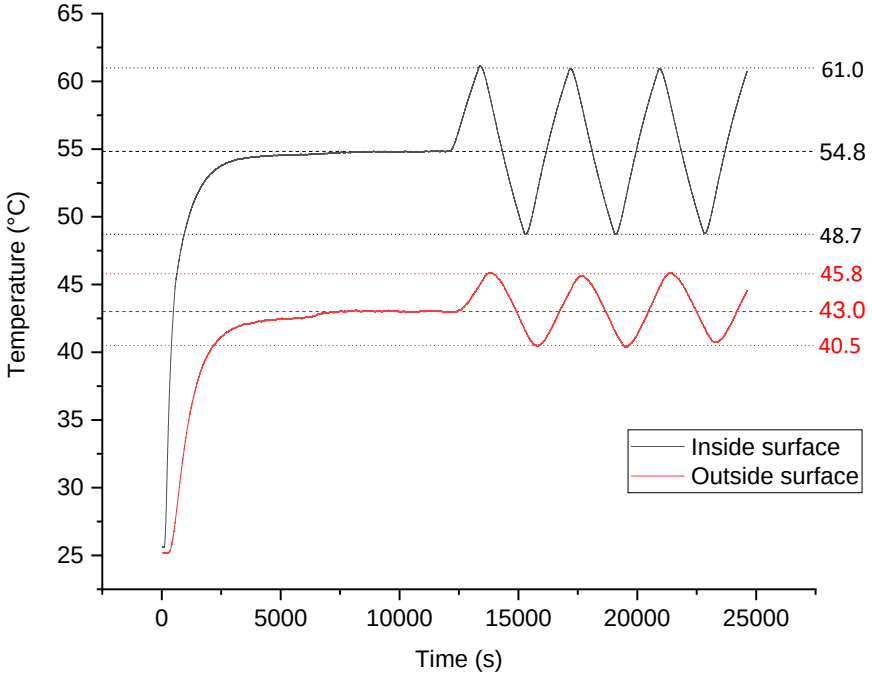

Figure 5.23: Wave propagation curve of the MDF sample. The base temperatures at the inside and the outside surfaces are 54.8 °C and 43 °C respectively (dashed lines). The average maximum and minimum temperatures are 61 °C and 48.7 °C at the inside surface and 45.8 °C and 40.5 °C at the outside surface, respectively.

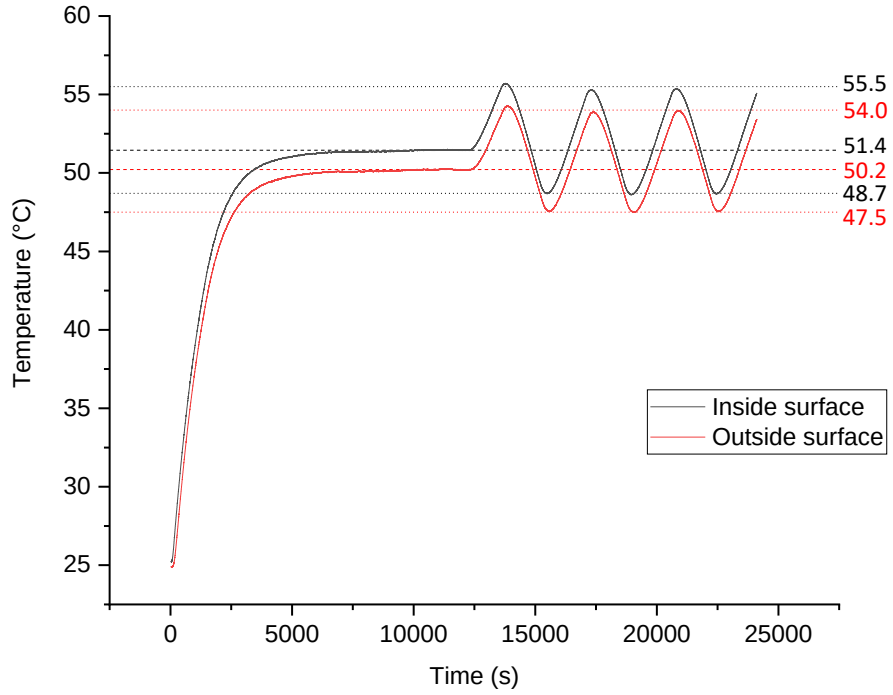

Figure 5.24: Wave propagation curve of the UHPC sample. The base temperatures at the inside and the outside surfaces are 54.82 °C and 43 °C respectively (dashed lines). The maximum and the minimum temperatures are 61 °C and 48.7 °C at the inside surface and 45.8 °C and 40.5 °C at the outside surface, respectively.

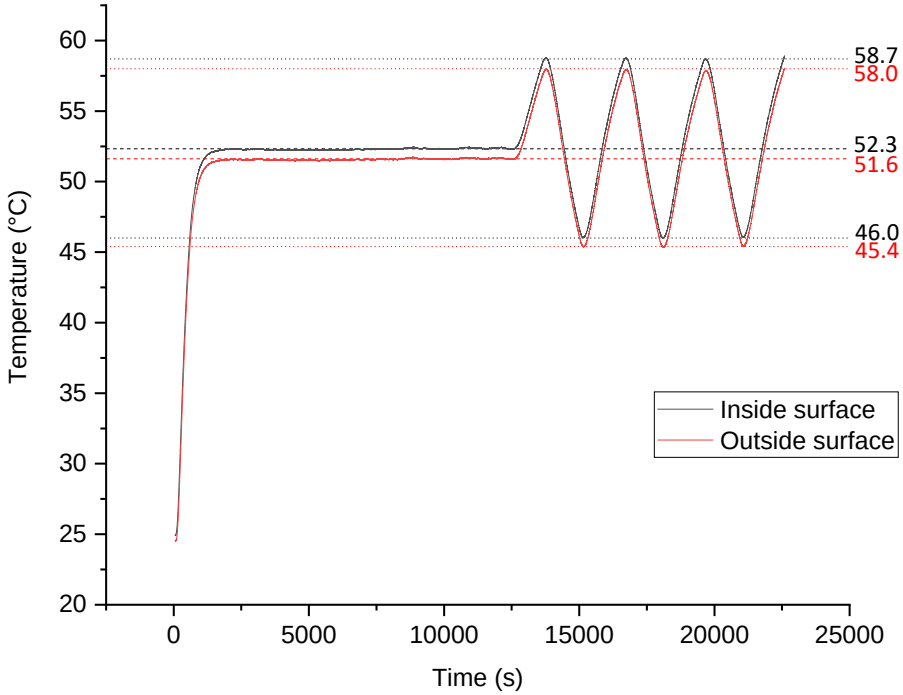

Figure 5.25: Wave propagation curve of the single glass sample. The base temperatures at the inside and the outside surfaces are 52.3 °C and 51.6 °C respectively (dashed lines). The maximum and the minimum temperatures are 58.7 °C and 46 °C at the inside surface and 58 °C and 45.4 °C at the outside surface, respectively.

As it can be seen from Figure 5.23, Figure 5.24 and Figure 5.25, each wave propagation graph has three cycles. The time lag and the decrement factor, as well as the period of the propagated wave, can be determined from the graphs by averaging the respective values for each cycle. The values of time lag and decrement factor for UHPC, MDF and glass are presented in Table 17. The respective thermal conductances, which are also required for dynamic calculations, can additionally be calculated from the steady-state region before the wave propagation using the heat flux method. They are also presented in Table 17.

Table 17: The determined time lag, decrement factor and period of the propagated waves from the wave propagation graphs, and the thermal conductance of the samples from the heat flux method

Measurement sample	**Time lag (s)**	**Decrement factor**	**Thermal conductance (W/mK)**	**Period of the wave (s)**	**Maximum and minimum temperatures at the inside surface (°C)**	**Maximum and minimum temperatures at the outside surface (°C)**
MDF	474	0.43	0.17	3758	61.0/48.7	45.8/40.5
UHPC	87.67	0.96	2.76	3488	55.5/48.7	54.0/47.5
Single glass	16.33	0.99	1.26	2962	58.7/46.0	58.0/45.4

Analyzing the values Table 17, a time lag of 87.67 s for UHPC means that the heatwave takes 87.67 s to reach the outside surface from the inside surface. The time lag for MDF is much higher, 474 s, and for glass, it is much lower, 16.33 s. Taking a look at the decrement factor values, a decrement factor of 0.43 for MDF means that the peak-to-peak amplitude of the wave at the outside surface of MDF is 43 % of the peak-to-amplitude of the wave at the inside surface of MDF. The decrement factor for UHPC is 0.96 and for glass, it is 0.99. It is apparent from the graphs that a lower value of decrement factor means that more amplitude reduction happens from the inside surface to the outside surface of the samples.

It can also be observed from the table and the graphs that for MDF, the time lag is much higher and the decrement factor is much lower than the other two samples. This can be explained by the thickness and the thermal conductance of the samples. MDF is four times thicker than the glass sample (Table 3) and has a much lower thermal conductance compared to UHPC and glass, as shown in Table 17. Thus the heat flow through MDF is lower than the other samples, resulting in a higher time lag and a lower decrement factor.

The thermal diffusivity of a sample, α_{s}, as discussed in Section 4.1.2, can be calculated either from the time lag, as shown in Equation 4.11, or the decrement factor, as shown in Equation 4.12. From the values of thermal diffusivity obtained from these two equations, the specific heat capacity, c_{p}, and the thermal mass, M_{th}, can be further calculated using Equations 4.13 and 4.14, respectively.

The values of α_{s} of the samples obtained from their respective time lags, and the consequently calculated values of c_{p} and M_{th} of the samples are presented in Table 18. The values of α_{s} of the samples obtained from their respective decrement factors, and the consequently calculated values of c_{p} and M_{th} of the samples are presented in Table 19.

Table 18: Thermal diffusivity, specific heat capacity and thermal mass of the samples calculated from their respective **time lags**, along with their reference values

Measurement sample	Thermal diffusivity (10^{-7} m²/s)		Specific heat capacity (kJ/kg.K)		Thermal mass (kJ/m³.K)	
	Reference	Experimental	Reference	Experimental	Reference	Experimental
MDF	1.04	3.41	1.4	0.45	1539.07	498.7
UHPC	7.56	92.5	0.85	0.087	3013.26	298.4
Single glass	3.99	141	0.72	0.027	2487.02	89.0

Table 19: Thermal diffusivity, specific heat capacity and thermal mass of the samples calculated from their respective **decrement factors**, along with their reference values

Measurement sample	Thermal diffusivity (10^{-7} m²/s)		Specific heat capacity (kJ/kg.K)		Thermal mass (kJ/m³.K)	
	Reference	Experimental	Reference	Experimental	Reference	Experimental
MDF	1.04	3.0	1.4	0.52	1539.07	566.1
UHPC	7.56	1380	0.85	0.006	3013.26	20.0
Single glass	3.99	1680	0.72	0.002	2487.02	7.5

It can be seen from Table 18 and Table 19 that the experimentally obtained α_s, c_p and M_{th} values of the samples deviate with huge margins from the reference values. These deviations, as can also be seen from the tables, are not the same for all the samples and the calculation methods. For example, the experimental α_s, c_p and M_{th} calculated from the time lag of the MDF sample are similar to the respective values calculated from the decrement factor. For UHPC and single glass, on the contrary, such similarities can not be observed.

In general, it can be concluded that the dynamic measurements performed with the Thermobox are not able to determine the thermal diffusivity, and consequently the specific heat capacity and the thermal mass of the measurement samples. One reason behind this inability might be the small thickness of the measurement samples, especially for UHPC and single glass, which also have high thermal conductances. From the values presented in Table 17, it can be noticed that the time lag of the propagated wave for UHPC and single glass is really small, only about 87 s and 16 s respectively. The time lag for MDF, which is 474 s or about 8 minutes, is also not significantly high. This means that the heatwave takes very little time to propagate from the inside surface to the outside surface. On the other hand, the decrement factors for UHPC and single glass are close to 100 %, which means that the amplitude dampening is extremely small for these samples. Such low values of time lag and high values of decrement factor, resulting from the small thicknesses of the samples, may not be able to properly represent the actual dynamic heat transfer scenario for the materials of the measurement samples.

6 Conclusion

In this thesis, steady-state and dynamic measurements are performed on seven measurement samples to experimentally obtain different thermal parameters with the experimental setup Thermobox. Several modifications are performed in an attempt to improve the heat transfer behaviour of the Thermobox and consequently the measurement results. The implication of the modifications on the steady-state measurement results, calculated with the temperature method, was observed and discussed. Furthermore, a PID controller was developed and implemented to replace the manual control of power with automated control for reducing human error and improving the stability of measurements. The performance of this PID controller was assessed and compared to the manual control. To develop an alternate method for calculating the steady-state parameters, a heat flux sensor was installed in one of the Thermobox. The measurement results form the heat flux method were compared to the temperature method results. The influence of changing the temperature inside the Thermobox on the measurement results was also investigated. Additionally, five identical steady-state measurements were conducted on the MDF sample without insulation to find and discuss the standard deviation of the measurement results. Finally, dynamic measurements were performed on the MDF sample without insulation, the UHPC sample without insulation and the single glass sample to investigate their dynamic behaviour. The dynamic measurement results were then analyzed by comparing the results to the reference values.

From the steady-state measurement results, with both the temperature method and the heat flux method, it can be concluded that with the Thermobox, the thermal conductances of the MDF sample without insulation, the MDF sample with insulation, the UHPC sample without insulation and the single glass sample can be determined accurately or within small deviations from the considered references. On the other hand, the thermal conductance of the samples with double glazing could not be accurately determined with the Therrmobox. In the case of the UHPC sample with outside insulation, the experimental thermal conductance from the temperature method had higher deviations from the reference value, whereas with the heat flux method, the experimental values became much closer to the reference. This lead to the investigation of the convective and radiative hear transfer coefficient at the outer surface of the samples, h_{o}. It was concluded that considering the same value of h_{o} for all the measurement samples may not be accurate, as h_{o} is different for each sample and it also varies with temperature. Further investigation for determining the actual h_{o} values for the samples may lead to more accurate measurement results.

From the density measurement, it was discovered that the measured densities of MDF and UHPC were higher than the density of these samples considered as reference. The change in density suggests that the reference thermal conductances of MDF and UHPC may be different than what was considered. Additionally, from the thermal imaging of the samples with double glazing, it was seen that the gas between the glass panes move upward with temperature and creates a layer of hot gas at the top edge of the gap between the glass panes. This changes the density of the gas between the panes. This observation implies that the reference thermal conductances for the samples with double glazing may not be calculated as simply as it was considered in this thesis. Thus, it would be interesting to take a closer look at the reference thermal conductance values of the measurement samples.

The PID controller was implemented to achieve more stable heating inside the Thermobox by automatically controlling the heating power of the regular heater. The controller was developed with the temperature inside the Thermobox, T_{box} as the process variable, and to that extent, step tests for T_{box} were performed on the measurement samples to determine the relevant control parameters. As a next step, further step tests can be performed for other measurement temperatures to obtain the relevant control parameters. This would lead to the parameterization of the PID controller for temperatures other than T_{box} and the implication of having different temperatures as the process variable of the PID controller can be investigated.

While observing the heat transfer behaviour of the Thermobox, only the front side was observed with the thermal imaging camera. But the Thermobox may have additional heat losses through the other sides of the heating chamber. For example, further heat losses may occur at the intersection of the top wall and the sidewalls due to the thermal bridge effect. Moreover, the heating elements, the heat shield and the fans are mounted on the back wall of the Thermobox with four metal screws. This screws may lead to conductive heat losses through the back wall. Further investigation with the thermal imaging camera will lead to the identification and mitigation of these other heat losses through the Thermobox. These mitigation strategies may include the implementation of insulation at the thermal bridges and replacing the metal screws used for mounting with screws with lower thermal conductance.

From the dynamic measurement results, it was seen that the Thermobox was not able to accurately determine the thermal diffusivity, the specific heat capacity and the thermal mass of the samples. It was also observed that for samples with higher thermal conductance, the time lag is smaller and the decrement factor is bigger. These values may be attributed to the small thicknesses of the measurement samples. Thus, it would be interesting to perform dynamic measurements on samples with different thickness to investigate the implication of thickness on the measurement results and to assess whether higher thicknesses can lead to more accurate measurement results.

Literature Cited

AGC, 2011. *Technical Data Sheet- Planibel* [online], AGC Glass Europe. Available from: https://www.agc-yourglass.com/de/en/brands/planibel-clear [Accessed 15 Mar 2020].

Ahmad, A., Maslehuddin, M., and Al-Hadhrami, L.M., 2014. In situ measurement of thermal transmittance and thermal resistance of hollow reinforced precast concrete walls. *Energy and Buildings*, 84, 132–141.

Asan, H., 2000. Investigation of wall's optimum insulation position from maximum time lag and minimum decrement factor point of view. *Energy and Buildings*, 32 (2), 197–203.

Asan, H., 2006. Numerical computation of time lags and decrement factors for different building materials. *Building and Environment*, 41 (5), 615–620.

Aste, N., Angelotti, A., and Buzzetti, M., 2009. The influence of the external walls thermal inertia on the energy performance of well insulated buildings. *Energy and Buildings*, 41 (11), 1181–1187.

Azar, K., 2009. *Thermal Fundamentals: Heat Flux Gauges: What They Are and What They Do* [online], Advanced Thermal Solutions, Inc. Available from: https://www.qats.com/Qpedia-Thermal-eMagazine [Accessed 13 Jan 2020].

Baggs, D. and Mortensen, N., 2006. Thermal Mass in Building Design. *Environment Design Guide* [online], 4, 1–9. Available from: www.jstor.org/stable/26148285 [Accessed 3 May 2020].

Balaji, N.C., Mani, M., and Venkatarama Reddy, B.V., 2019. Dynamic thermal performance of conventional and alternative building wall envelopes. *Journal of Building Engineering*, 21, 373–395.

Barlow, R.J., 2013. *Statistics: A Guide to the Use of Statistical Methods in the Physical Sciences*. New York: John Wiley & Sons.

Bartl, J. and Baranek, M., 2004. Emissivity of aluminium and its importance for radiometric measurement. *Measurement Science Review*, 4, 31–36.

Bauder, 2014. *BauderPIR FA TE: Technische Daten* [online], Paul Bauder GmbH & Co. KG. Available from: https://www.bauder.de/ [Accessed 16 Apr 2020].

Bodas, A., Gandia, V., and Lopez-Baeza, E., 1998. An undergraduate experiment on the propagation of thermal waves. *American Journal of Physics*, 66 (6), 528–533.

Breithaupt, J., 2001. *Key science: Physics.* 3rd ed. Cheltenham: Nelson Thornes.

Christmann, E.P., 2012. *Beyond the numbers: Making sense of statistics*. Arlington: NSTA Press.

Dante, R.C., 2016. *Handbook of friction materials and their applications*. Amsterdam: Elsevier.

DIN EN ISO 6946, 2018. *Building components and building elements- Thermal resistance and thermal transmittance- Calculation methods (ISO 6946:2017*.

Evangelisti, L*., et al.*, 2016. Experimental investigation of the influence of convective and radiative heat transfers on thermal transmittance measurements. *International Communications in Heat and Mass Transfer*, 78, 214–223.

Fontana, P*., et al.*, 2016. Composite UHPC façade elements with functional surfaces. *In:* E. Fehling, B. Middendorf, and J. Thiemicke, eds. *Ultra-High Performance Concrete and High Performance Construction Materials*. Kassel: Kassel University Press GmbH.

Gregory, K*., et al.*, 2008. Effect of thermal mass on the thermal performance of various Australian residential constructions systems. *Energy and Buildings*, 40 (4), 459–465.

Haugen, F., 2004. *PID control*. Trondheim: Tapir Academic Press.

Haynes, W.M.(E.), ed., 2017. *CRC handbook of chemistry and physics: A ready-reference book of chemical and physical data.* 97th ed. Boca Raton: CRC Press.

Hens, H.S.L., 2012. *Building Physics -- Heat, Air and Moisture: Fundamentals and Engineering Methods with Examples and Exercises*. Berlin: Wiley.

Holzner, S., 2009. *Physics for dummies*. Hoboken: Wiley.

Howell, J.R., Siegel, R., and Mengüç, M.P., 2011. *Thermal radiation heat transfer.* 5th ed. Boca Raton: CRC Press.

Jin, X*., et al.*, 2012. Thermal performance evaluation of the wall using heat flux time lag and decrement factor. *Energy and Buildings*, 47, 369–374.

Kaviany, M., 2002. *Principles of Heat Transfer*. New York: Wiley.

Kreith, F. and Chhabra, R.P.(E.), 2017. *CRC handbook of thermal engineering*. Boca Raton: CRC Press.

Li, K., 2013. On Determining Density and Specific Heat of New Zealand Medium Density Fibreboard. *Procedia Engineering*, 62, 769–777.

MacLean, J.D., 1941. Thermal Conductivity of wood. *Heating, piping & air conditioning*, 13 (6), 380–391.

Mark, J.E., ed., 2007. *Physical Properties of Polymers Handbook*. Berlin: Springer.

Mohammad, S. and Shea, A., 2013. Performance Evaluation of Modern Building Thermal Envelope Designs in the Semi-Arid Continental Climate of Tehran. *Buildings*, 3 (4), 674–688.

Oral, G.K., Yener, A.K., and Bayazit, N.T., 2004. Building envelope design with the objective to ensure thermal, visual and acoustic comfort conditions. *Building and Environment*, 39 (3), 281–287.

Phymeas, 2020a. *Heat Flux Measurement* [online]. Available from: http://www.phymeas.de/?page_id=2&lang=en [Accessed 6 Feb 2020].

Phymeas, 2020b. *Heat Flux Measurement: Functional Principle* [online]. Available from: http://www.phymeas.de/?page_id=27&lang=en [Accessed 6 Feb 2020].

Rebolledo, P., Cloutier, A., and Yemele, M.-C., 2018. Effect of Density and Fiber Size on Porosity and Thermal Conductivity of Fiberboard Mats. *Fibers*, 6 (81).

Reilly, A. and Kinnane, O., 2017. The impact of thermal mass on building energy consumption. *Applied Energy*, 198, 108–121.

Rohsenow, W.M., Cho, Y.I., and Hartnett, J.P., 1998. *Handbook of heat transfer.* 3rd ed. New York: McGraw-Hill Education.

Salazar, A.n., 2003. On thermal diffusivity. *European Journal of Physics*, 24 (4), 351–358.

Schmidt, T., exergia, 2019. *Thermobox Documentation*. Freiburg, Germany.

Shackelford, J.F. and Alexander, W., 2001. *CRC materials science and engineering handbook.* 3rd ed. Boca Raton: CRC Press.

Shahrokhi, M. and Zomorrodi, A., 2003. Comparison of PID Controller Tuning Methods. *8th National Iranian Chemical Engineering Congress* [online]. Available from: https://www.civilica.com/Paper-NICEC08-NICEC08_348.html [Accessed 27 Feb 2020].

Silverman, E.M., 1995. *Space environmental effects on spacecraft: LEO materials selection guide, part 2* [online], National Aeronautics and Space Administration. Available from: https://ntrs.nasa.gov/search.jsp?R=19960000861 [Accessed 11 Feb 2020].

Snow, D.A., ed., 2002. *Plant engineer's reference book.* 2nd ed. Oxford: Butterworth-Heinemann.

Spence, W.P., 2006. *The home carpenter & woodworker's repair manual*. New York: Sterling.

Sudholt-Wasemann, 2019. *Technical data UHPC: Material data* [online], Sudholt-Waswmann GmbH. Available from: https://www.sudholt-wasemann.de/de/technologie [Accessed 16 Apr 2020].

Testo Ltd, 2020. *testo 865 - thermal imager* [online]. Available from: https://www.testo.com/en-UK/testo-865/p/0560-8650 [Accessed 10 Feb 2020].

Thomas, J.M.*, et al.*, 2006. Materials selection for thermal comfort in passive solar buildings. *Journal of Materials Science*, 41 (21), 6897–6907.

Toman, J. and Černý, R., 2001. Thermal Conductivity of High Performance Concrete in Wide Temperature and Moisture Ranges. *Acta Polytechnica*, 41 (1), 8–10.

van der Tempel, L., Melis, G.P., and Brandsma, T.C., 2000. Thermal Conductivity of a Glass: I. Measurement by the Glass–Metal Contact. *Glass Physics and Chemistry*, 26 (6), 606–611.

Vargaftik, N.B., 1994. *Handbook of thermal conductivity of liquids and gases*. Boca Raton: CRC Press.

VDI-Gesellschaft Verfahrenstechnik und Chemieingenieurwesen, ed., 2010. *VDI Heat Atlas*. Berlin: Springer.

Vollmer, M. and Möllmann, K.-P., 2010. *Infrared thermal imaging: Fundamentals, research and applications*. Weinheim: Wiley-VCH.

Welke, M. and Beck, M., 2019. *Climate Action in Figures: Facts, Trends and Incentives for German Climate Policy* [online]. Berlin, Federal Ministry for the Environment, Nature Conservation and Nuclear Safety (BMU). Available from: www.bmu.de/english [Accessed 9 Dec 2019].

Xue, D., Chen, Y., and Atherton, D.P., 2007. *Linear feedback control: Analysis and design with MATLAB*. Philadelphia: Society for Industrial and Applied Mathematics.

Younglove, B.A. and Hanley, H.J.M., 1986. The Viscosity and Thermal Conductivity Coefficients of Gaseous and Liquid Argon. *Journal of Physical and Chemical Reference Data*, 15 (4), 1323–1337.

Zhang, Y.*, et al.*, 2006. Ideal thermophysical properties for free-cooling (or heating) buildings with constant thermal physical property material. *Energy and Buildings*, 38 (10), 1164–1170.

Appendix

A Calculation of the Literature Value of h_o

Table A-1 shows the conventional heat transfer resistances from the DIN EN ISO 6946 standard. Here R_{si} and R_{se} represent the heat transfer resistances respectively for the inner surface and the outer surface.

Table A-1: Conventional heat transfer resistances from DIN EN ISO 6946 (2018, 24, Tabelle 7)

Heat transfer resistance m²·K/W	Direction of heat flow		
	Upward	Horizontal	Downward
R_{si}	0.10	0.13	0.17
R_{se}	0.04	0.04	0.04

The outside condition of the Thermobox is in practice the room inside condition, and the direction of heat flow through the Thermobox is considered horizontal. Thus, from Table A-1, the value of R_{si} can be taken as 0.13 m²K/W. Then reciprocating the value of R_{si}, h_o is calculated as 7.69 W/m²K. This value of h_o is used in the steady-state calculations with the temperature method.

B Step Response Curves of the Samples for Controller Parameterization

Figure B-1 presents the step response curve of the MDF sample for obtaining the parameters K_m, τ_m and d_m. These parameters are required for determining the control parameters for the PID controller using the CHR method, as shown in Table 1.

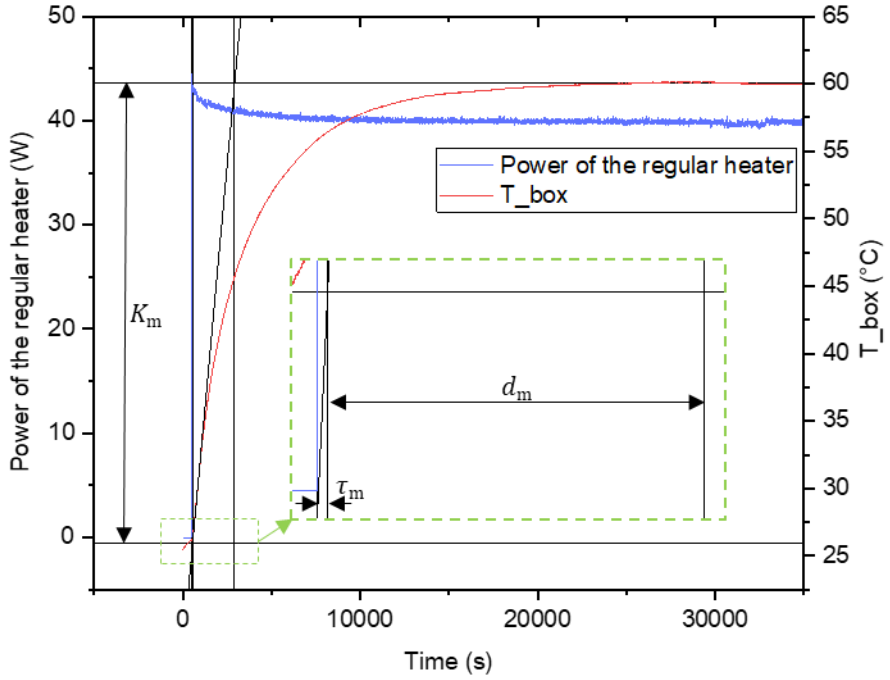

Figure B-1: Step response curve of the MDF sample for obtaining K_m, τ_m and d_m

C LabVIEW Block Diagrams for the PID Controller and the Heat Flux Sensor

For implementing the PID controller and the heat flux sensor into the Thermobox, necessary adjustments are made to the LabVIEW software. The block diagrams for these adjustments are shown below.

LabVIEW Block Diagram for Implementing the PID Controller

Figure C-1 shows the block diagram for the implementation of the PID controller into the LabVIEW software for the Thermobox.

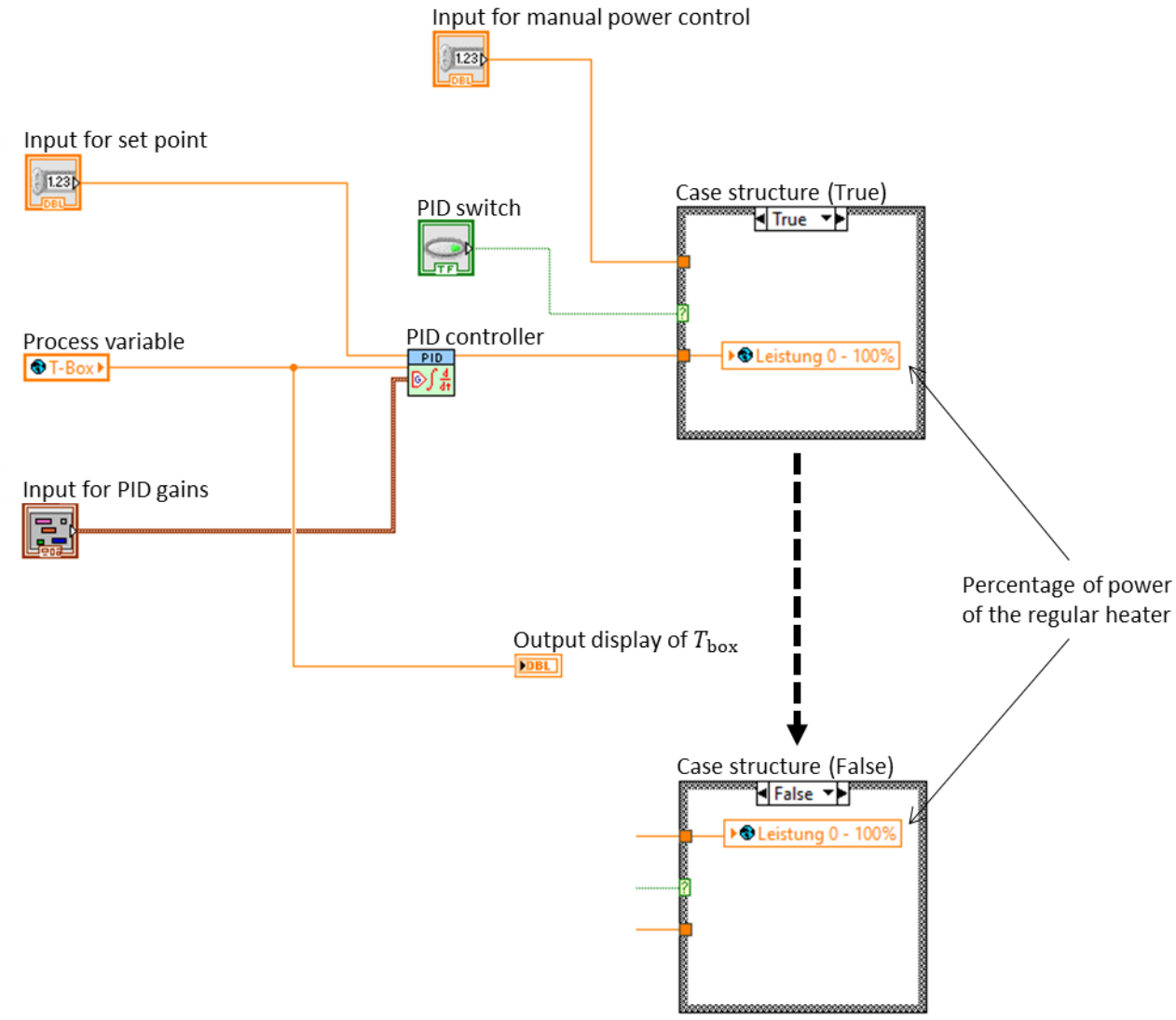

Figure C-1: Block diagram for the implementation of the PID controller. The PID switch is used to control the case structure. When the switch is on, the case structure is true, which means that the percentage of power of the regular heater is adjusted by the PID controller. When the PID switch is off, the case structure is false, which means that the percentage of power of the regular heater is adjusted by the manual control.

LabVIEW Block Diagram for Implementing the Heat Flux Sensor

Figure C-2 shows the block diagram for calculating and saving the heat flux through a measurement sample from the voltage reading of the heat flux sensor.

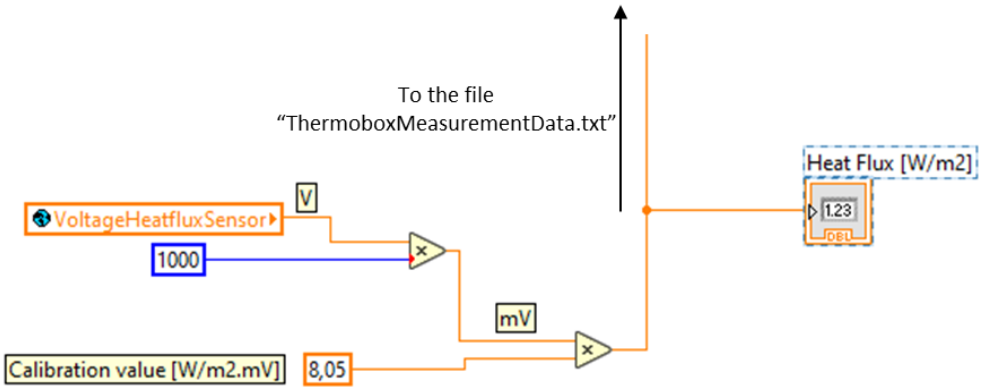

Figure C-2: Block diagram for calculating the value of heat flux from the measurement of the heat flux sensor. The voltage (in volts) measured by the sensor, V_{th}, is converted to millivolts, and then is multiplied by the calibration coefficient, c (8.05 W/m2.mV). This leads to the heat flux through the sample, which is then sent to the output to be saved in the file "ThermoboxMeasurementData.txt".

D Temperature Profile of the Measurement Samples

Figure D-1 shows the steady-state temperature profiles of the MDF sample without insulation and the MDF sample with inside insulation during primary steady-state measurements.

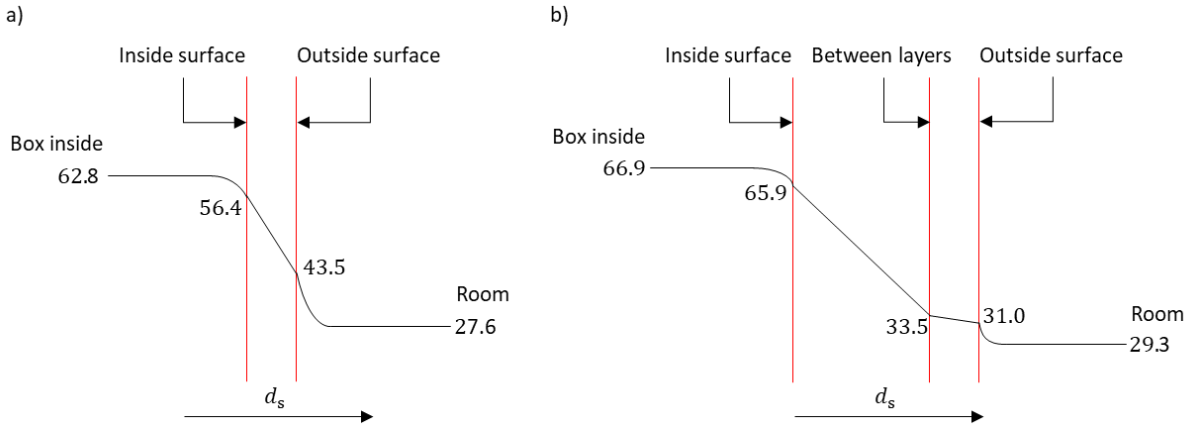

Figure D-1: Steady-state temperature profile of a) MDF without insulation and b) MDF with inside insulation

Figure D-2 shows the steady-state temperature profiles of the transparent samples during primary steady-state measurements.

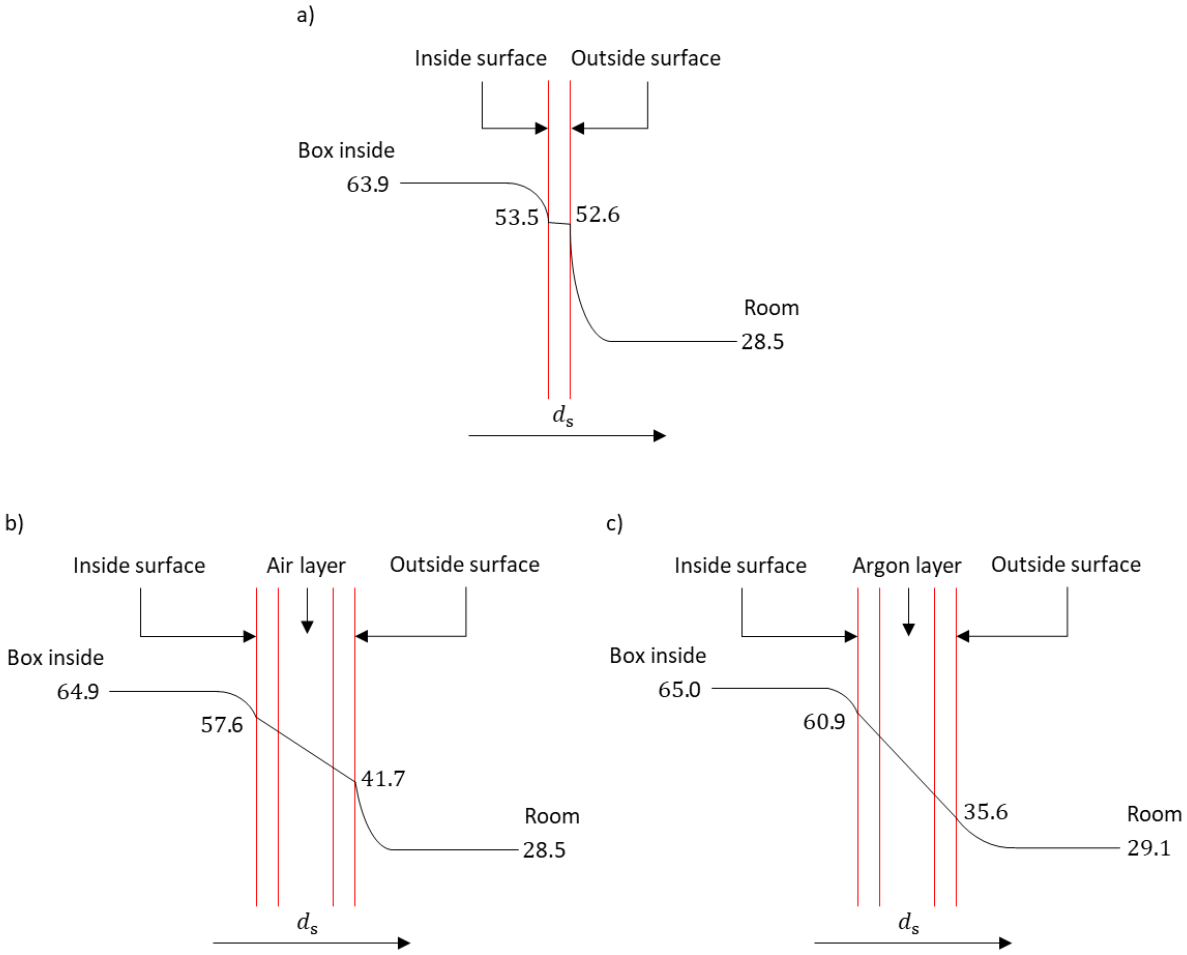

Figure D-2: Steady-state temperature profile of a) single glass, b) double glazing with air and c) double glazing with argon

E Steady-state Measurement Results

This section contains tabular presentations of the results of the steady-state measurements with the Thermobox.

Results from the Primary Steady-state Measurements

Table E-1 presents the experimental and the reference values of thermal conductance and the experimental thermal transmittance values from the primary steady-state measurements.

Table E-1: Thermal conductance and thermal transmittance values of measurement samples from primary steady-state measurements with $h_o = 7.69$ W/m²K

Measurement sample	k_s (W/mK)			Experimental U_s (W/m²K)
	Reference	Experimental	Deviation of k_s from reference (%)	
MDF without insulation	0.16	0.15	0	3.48
MDF with inside insulation	0.025-0.030	0.022	-12.4	0.36
UHPC without insulation	1.8-2.2	2.06	0	5.06
UHPC with outside insulation	0.031-0.032	0.052	62.5	0.78
Single glass	0.95	0.88	-7.6	5.23
Double glazing with air	0.042	0.15	266.3	2.79
Double glazing with argon	0.029	0.045	55.7	1.34

Results from the Steady-state Measurements after the Thermobox Modifications

Table E-2 presents the measurement results from the steady-state measurements after applying the modifications to the Thermobox.

Table E-2: Thermal conductance and thermal transmittance values of measurement samples from steady-state measurements after modifications with $h_o = 7.69$ W/m²K

Measurement sample	Reference k_s (W/mK)	Side insulation and black paint			Inverting fan direction		
		Experimental k_s (W/mK)	Deviation of k_s from reference (%)	Experimental U_s (W/m²K)	Experimental k_s (W/mK)	Deviation of k_s from reference (%)	Experimental U_s (W/m²K)
MDF without insulation	-0.16	0.16	0	3.5	0.16	0	3.68
MDF with inside insulation	0.025-0.030	0.039	31.5	0.63	0.028	0	0.47
UHPC without insulation	1.8-2.2	2.09	0	4.98	2.27	3.3	5.34
UHPC with outside insulation	0.031-0.032	0.066	107.5	0.99	0.069	116.3	1.04
Single glass	0.95	0.90	-5.6	5.28	1.05	10.4	5.68
Double glazing with air	0.042	0.17	305.3	2.98	0.18	317.6	3.14
Double glazing with argon	0.029	0.059	101.9	1.65	0.059	104.6	1.72

Steady-state Measurements at Different T_{box} with Heat Flux Method

Table E-3 presents the experimental values of k_s at three different set values of T_{box} calculated by the heat flux method and the reference values, along with the calculated U_s values.

Table E-3: Reference and experimental k_s and U_s values of the measurement samples at different set values of T_{box} calculated by the heat flux method

Measurement sample		MDF without insulation	MDF with inside insulation	UHPC without insulation	UHPC with outside insulation	Single glass	Double glazing with air	Double glazing with argon
Reference k_s (W/mK)		0.16	0.025-0.030	1.8-2.2	0.031-0.032	0.95	0.042	0.029
$T_{box} = 50$ °C	**Experimental k_s (W/mK)**	0.17	0.037	2.60	0.049	1.05	0.19	0.059
	Deviation from reference (%)	7.3	23.9	18.3	52.4	10.1	351.8	103.9
	Experimental U_s (W/m²K)	3.82	0.61	6.47	0.75	6.70	3.42	1.75
$T_{box} = 60$ °C	**Experimental k_s (W/mK)**	0.17	0.035	3.00	0.048	1.32	0.20	0.068
	Deviation from reference (%)	7.3	17.6	36.2	49.3	39.2	377.6	135.7
	Experimental U_s (W/m²K)	3.86	0.57	6.83	0.72	7.02	3.52	1.97
$T_{box} = 70$ °C	**Experimental k_s (W/mK)**	0.17	0.036	3.05	0.045	1.46	0.21	0.07
	Deviation from reference (%)	7.3	19.5	38.5	41.3	53.9	399.2	142.5
	Experimental U_s (W/m²K)	3.93	0.58	6.87	0.69	7.19	3.58	2.00

Table E-4 presents the experimentally calculated values of h_o and h_i for the measurement samples, obtained from the heat flux method measurements at different set values of T_{box}.

Table E-4: Calculated values of h_o and h_i for the measurement samples from the heat flux method at different set values of T_{box}, both in W/m^{2}K

Measurement sample	**Experimental values at $T_{box} = 50$ °C**		**Experimental values at $T_{box} = 60$ °C**		**Experimental values at $T_{box} = 70$ °C**	
	h_o	h_i	h_o	h_i	h_o	h_i
MDF without insulation	7.90	25.81	8.04	24.18	8.31	24.61
MDF with inside insulation	8.69	33.02	8.23	28.68	7.35	26.30
UHPC without insulation	8.97	27.00	9.63	26.81	9.84	25.82
UHPC with outside insulation	6.47	29.51	5.59	25.45	5.90	19.59
Single glass	8.85	30.78	9.37	30.70	9.77	29.49
Double glazing with air	8.10	23.36	8.34	22.65	8.41	21.98
Double glazing with argon	8.39	22.20	8.72	23.54	8.78	22.04

Steady-state Measurements at Different T_{box} with Temperature Method

Table E-5 presents the experimental values of k_s at three different set values of T_{box} calculated by the temperature method and the reference values, along with the calculated U_s values.

Table E-5: Reference and experimental k_s and U_s values of the measurement samples at different set values of T_{box} calculated by the temperature method with $h_o = 7.69$ W/m²K

Measurement sample		MDF without insulation	MDF with inside insulation	UHPC without insulation	UHPC with outside insulation	Single glass	Double glazing with air	Double glazing with argon
Reference k_s (W/mK)		0.16	0.025-0.030	1.8-2.2	0.031-0.032	0.95	0.042	0.029
$T_{box} = 50$ °C	**Experimental k_s (W/mK)**	0.16	0.033	2.23	0.058	0.91	0.18	0.054
	Deviation from reference (%)	0	9.7	1.4	81.2	-4.3	328.7	86.9
	Experimental U_s (W/m²K)	3.72	0.54	5.54	0.89	5.82	3.24	1.61
$T_{box} = 60$ °C	**Experimental k_s (W/mK)**	0.16	0.033	2.39	0.066	1.09	0.19	0.06
	Deviation from reference (%)	0	9.9	8.8	105.5	14.3	340.3	107.9
	Experimental U_s (W/m²K)	3.7	0.54	5.45	0.99	5.77	3.25	1.74
$T_{box} = 70$ °C	**Experimental k_s (W/mK)**	0.16	0.038	2.38	0.059	1.15	0.19	0.062
	Deviation from reference (%)	0	25.1	8.2	84	21.1	340.3	112.3
	Experimental U_s (W/m²K)	3.64	0.6	5.37	0.89	5.66	3.28	1.75

F Measured Temperature Differences and Heat Fluxes From the Sensitivity Analysis Measurements

Table F-1 presents the measured temperature differences between different measurement points of the Thermobox and the measurement from the heat flux sensor for the five steady-state measurements performed with the MDF sample for the sensitivity analysis. The measured values of T_{box} are also presented.

Table F-1: Measured temperature difference and heat flux value, as well as the temperature inside the Thermobox, for the sensitivity analysis steady-state measurements on the MDF sample without insulation

Measurements	T_{box} (°C)	Temperature difference (K)				Heat flux (W/m²)
		$T_{\mathrm{box}} - T_{\mathrm{w,i}}$	$T_{\mathrm{w,i}} - T_{\mathrm{w,o}}$	$T_{\mathrm{w,o}} - T_{\mathrm{room}}$	$T_{\mathrm{box}} - T_{\mathrm{room}}$	
Measurement 1	60.0	5.3	12.1	16.7	34.1	131.4
Measurement 2	60.1	5.2	11.7	16.7	33.6	122.9
Measurement 3	60.1	5.4	12.2	16.6	34.2	132.2
Measurement 4	60.0	5.3	12.0	16.7	34.1	130.1
Measurement 5	60.0	5.3	11.9	16.7	33.9	128.1